January 2014

Theoretical And Experimental Investigation Of Water And Nanofluid Flow In Channels With Sudden Area Change

Emmanuel Hitimana

THEORETICAL AND EXPERIMENTAL INVESTIGATION OF WATER AND
NANOFLUID FLOW IN CHANNELS WITH SUDDEN AREA CHANGE

By

Emmanuel Hitimana

Bachelor of Arts, William Penn University, 2011

A Thesis

Submitted to the Graduate Faculty

of the

University of North Dakota

in partial fulfilment of the requirements

for the degree of

Master of Science

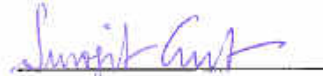Grand Forks, North Dakota

December

2014

The Thesis, submitted by Emmanuel Hitimana in partial fulfillment of the requirements of the Degree of Master of Science from the University of North Dakota, has been read by the faculty advisory committee under whom the work has been done and is hereby approved.

Clement Tang

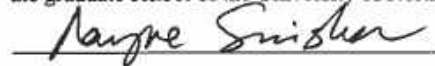Dr. Clement Tang, Chairperson

NSGrewal
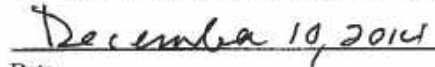
Dr. Nanak Grewal, Committee member

Surojit Gupta

Dr. Surojit Gupta, Committee member

This, thesis meets the standard for appearance, conforms the style and format requirements of the graduate school of the University of North Dakota and is hereby approved.

Wayne Swisher

Dr. Wayne Swisher, Dean of School of Graduate Studies

December 10, 2014

Date

ii

PERMISSION

Title   Theoretical and Experimental Investigation of Water and Nanofluid Flow in Channels with Sudden Area Change

Department   Mechanical Engineering

Degree   Master of Science

In presenting this thesis in partial fulfillment of the requirements for a graduate degree from the University of North Dakota, I agree that the library of this University shall make it freely available for inspection. I further agree that permission for extensive copying for scholarly purposes may be granted by the professor who supervised my thesis work or, in his absence, by the chairperson of the department or the dean of the School of Graduate Studies. It is understood that any copying or publication or other use of this thesis or part thereof for financial gain shall not be allowed without my written permission. It is also understood that due recognition shall be given to me and to the University of North Dakota in any scholarly use which may be made of any material in my thesis.

Emmanuel Hitimana

November 18, 2014

TABLE OF CONTENTS

LIST OF FIGURES

LIST OF TABLES

ACKNOWLEDGEMENT

ABSTRACT

Sudden area expansions and contractions in channels are encountered in numerous engineering applications such as pipeline, cooling systems, and heat exchangers. Over the last several decades, numerous studies have been done on this subject. However, there is still a lack of proper investigations, especially on quantifying the viscous pressure loss at the singularity as a function of flow rate along the channel with abrupt area expansion or contraction.

In this study, the investigation was done on the behavior of static pressure of water and 9.58% volume concentration silicon dioxide nanofluid in channels with sudden area expansion and contraction. The main parameters studied are area ratio ($\sigma = 0.0625$ and 0.140), axial length of the channel, static pressure, pressure loss at the singularity, and loss coefficient. These parameters were analyzed at various mass flow rates ranging from 5 to 30 g/s.

The static pressure data were measured and were used to compute the pressure drop and loss coefficient. Results proved that static pressure and pressure drop increase with increasing mass flow rate for sudden expansion and contraction. For sudden area expansion with water, the loss coefficient increases with increasing mass flow rate and reaches an optimum value. The opposite trend was observed for sudden expansion with nanofluid and sudden area contraction with both fluids. In this case, loss coefficient decreases with increasing mass flow rate.

Because loss coefficient varies with the flow rate, the conventional Carnot equation for sudden expansion/contraction could not be used to predict the results. For this reason, new expressions were derived and used to quantify the loss coefficients.

The comparative study between the behavior of water and nanofluid showed that the pressure drop due to sudden expansion or contraction increases as a result of addition of nanoparticles in water. However, the percentage increase in pressure drop is greatly reduced at higher flow rates as a result of the increase in turbulence. For the area ratio of 0.0625 at 7.92 g/s, nanofluid pressure drop due to sudden area change is approximately 129% higher than water pressure drop. This percentage drops to approximately 16.5% at 25.7 g/s.

For nanofluid, the increase in the area ratio showed an impact on the pressure drop. For sudden area expansion, the pressure drop decreases with increasing area ratio; whereas it increases with the increasing area ratio for sudden area contraction. The behavior of the pressure drop, in channel with sudden area contraction with respect to the area ratio, was attributed to the decrease in the corrected dynamic pressure, which is the subtractive term in the overall sudden area contraction pressure drop.

For practical applications, it is recommended that this type of nanofluid be used for systems that require higher flow rates (turbulent flow).

There are number of ways by which this work can be improved in order to make sure, that the subjects covered meet well intended practical applications. In order to gain more insight on silicon dioxide nanofluid thermal performance, there is a desire to investigate heat transfer in channels with sudden area change. The results of the heat transfer investigation can be compared with the results of pressure drop provided by this work. Moreover, silicon dioxide nanofluid with lower nanoparticles concentration should be experimented in order to understand more the effect of nanoparticles addition on fluid flow in complex geometry.

NOMENCLATURE

A   Flow area $[m^2]$

C_C Vena-contracta coefficient

COP   Coefficient of performance

d   Diameter of the channel [m]

d_p Diameter of nanoparticles [m]

$\frac{dT}{dy}$ Temperature gradient [K/m]

f   Friction factor

g   Gravitational acceleration $[m/s^2]$

h   Convective heat transfer coefficient $[W/m^2.K]$

K   Loss coefficient

K_e Loss coefficient due to sudden area expansion

K_c Loss coefficient due to sudden area contraction

K_d Momentum correction factor

K_{th} Thermal conductivity [W/m .K]

k_s Pipe roughness [m]

$\dot{m}$ Mass flow rate [g/s]

m   Mass [kg]

Nu   Nusselt number

P   Pressure [pa]

$\dot{P}$ Pumping power

P_{nf} Prandtl number for nanofluid

ΔP_e Pressure drop due to sudden expansion [pa]

ΔP_{eo} Pressure drop due to sudden expansion at singularity [pa]

ΔP_c Pressure drop due sudden contraction [pa]

ΔP_{co} Pressure drop due to sudden contraction at singularity [pa]

Re   Reynolds number

s   Sutherland's constant [K]

T   Temperature [^{0}C]

U   Velocity [m/s]

$\dot{U}$ Volumetric flow rate [m^3/s]

u_d Diameter uncertainty

u_{ke} Loss coefficient uncertainty for sudden area expansion

u_{kc} Loss coefficient uncertainty for sudden area contraction

u_m Mass flow rate uncertainty

$u_{\Delta p}$ Pressure drop uncertainty

u_v Velocity uncertainty

V   Volume [m^3]

Q   Quantity of heat [W]

$\dot{Q}$ Thermal energy [W]

Greek Symbols

σ Area ratio

ρ Density [Kg/m^3]

$\emptyset$ Particles concentration

τ Shear stress [pa]

μ	Dynamic viscosity [pa s]
υ	Kinematic viscosity [m^2/s]
γ	Flow Characteristic [1/s]

Subscripts

1	Smaller channel
2	Bigger channel
c	Contraction
e	Expansion
o	Initial
nf	Nanofluids
p	Particles
w	Water

CHAPTER I

I. INTRODUCTION AND THEORETICAL STUDY

1.1. Thermo-physical Properties of the Fluid

Fluids have countless applications in various domains. Many engineering systems designed and built for a specific purpose use some sort of fluid in one way or the other. For instance, fluids are used for power generation, for cooling, for biomedical purposes, and so on. Among all the fluids, water is more commonly used. For decades, water has been useful in engineering systems, especially for heat transfer purposes. Although it is cost effective, it is difficult to achieve desired thermal performance when a big amount of heat has to be transported. This is due to low thermal conductivity of water compared to other heat transfer fluids.

Modern electronic devices generate a considerable amount of heat which not only has a negative impact on the device performance, but also damage may occur if a designated range of temperature is exceeded. For this reason, a coolant or a heat transfer fluid is incorporated into most electronic and thermal systems in order to regulate the temperature and ensure optimum performance.

Researchers made effort to find a more efficient heat transfer fluid that can unravel cooling problems and boost thermal performance efficiency. One of the pioneers in this research is Choi (1995) at Argonne National Laboratory. He discovered a potential new kind of heat transfer medium called nanofluid. Nanofluids are made by a mixture of highly thermal conductive nanoparticles of metals with a conventional fluid such as water or air.

1

Although nanofluids have high potential to improve heat transfer compared to water, more pumping power is required in order to achieve a desired flow rate. This is due to the fact that nanoparticles which are used to make nanofluids are weighty. It is important to understand certain fluid properties that are essential for thermal performance. Such properties are primarily density, viscosity, and thermal conductivity.

1.1.1 **Density**

Density of a fluid is defined as a ratio of the mass to the volume, which it occupies.

$$\rho = \frac{m}{V} \quad\text{...} (1)$$

Density of liquid is higher than the density of gas for the same quantity of the fluid, because gases are more elastic than liquid and therefore tend to occupy the maximum space (volume). Nanofluids exhibit higher density compared to conventional fluid such as water. It is not easy to establish a direct comparison between densities of the two fluids, since density of nanofluids depend on the concentration of the nanoparticles.

Density of nanofluids is usually calculated by using Park and Cho (1998) Equation:

$$\rho_{nf} = \emptyset\rho_p + (1 - \emptyset)\rho_w \quad\text{..} (2)$$

Density of fluid decreases with increasing temperature and increases with increasing pressure. It is an important property of the fluid. Based on the density, the flow of the fluid can be classified as either incompressible or compressible.

For incompressible flow, the density of the fluid is constant; whereas for compressible flow the density changes with respect to the temperature and pressure of the fluid.

1.1.2 **Viscosity**

Viscosity is a vital property of the fluid, because it is the principal parameter used to measure viscous effects of the fluid. Viscous effects cause energy loss, drag force, flow separation, and so on.

An unbalanced shear force causes deformation of the fluid; viscosity quantifies the fluid resistance to flow due to unbalanced shear force. Absolute or dynamic viscosity is determined from Newton's law of viscosity which is defined in Equation (3).

$$\tau = \mu \frac{dU}{dy} \quad \text{……………………………………………………………………………} \quad (3)$$

where,

$\frac{dU}{dy}$ is the velocity gradient or rate of shear strain of the fluid. Velocity gradient is depicted in Figure 1, whereby the fluid is forced to move between two parallel plates. The bottom plate is stationary, whereas the top plate is moving at a constant velocity.

The fluid always moves at the same velocity as the object in contact. This is called no slip condition. This condition can well be explained by Figure 1 whereby the fluid velocity is maximum at the top and zero at the bottom.
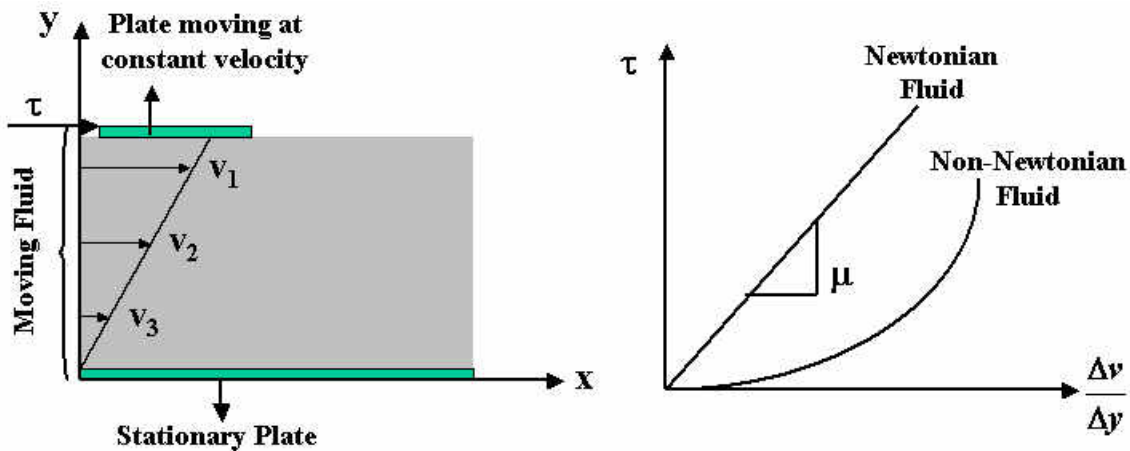
Figure 1. *Fluid flow in two parallel plates (L), Newtonian and non-Newtonian fluid (R), Bear (1972)*

Viscosity can be used to distinguish Newtonian from non-Newtonian fluids. When viscosity remains constant with respect to shear stress and rate of shear strain, the fluid is Newtonian. In this case the relationship between shear stress and rate of shear strain is linear. Newtonian fluids include many common liquids and gases such as water and air.

Fluids are designated non-Newtonian when the Equation (3) is not linear or viscosity is not constant. Examples of non-Newtonian fluids include heavy fluids such as paint.

There exist two types of viscosity, dynamic (μ) and kinematic (υ). While dynamic viscosity is the property that measures viscous effects of the fluid, kinematic viscosity combines viscous and mass characteristics of the fluid. It is numerically defined as the ratio of dynamic viscosity to density:

$$v = \frac{\mu}{\rho} \quad\text{...} \quad (4)$$

One of the parameters that greatly influences viscosity is temperature. When the liquid temperature increases, the intermolecular forces weaken. This renders the viscosity to decrease.
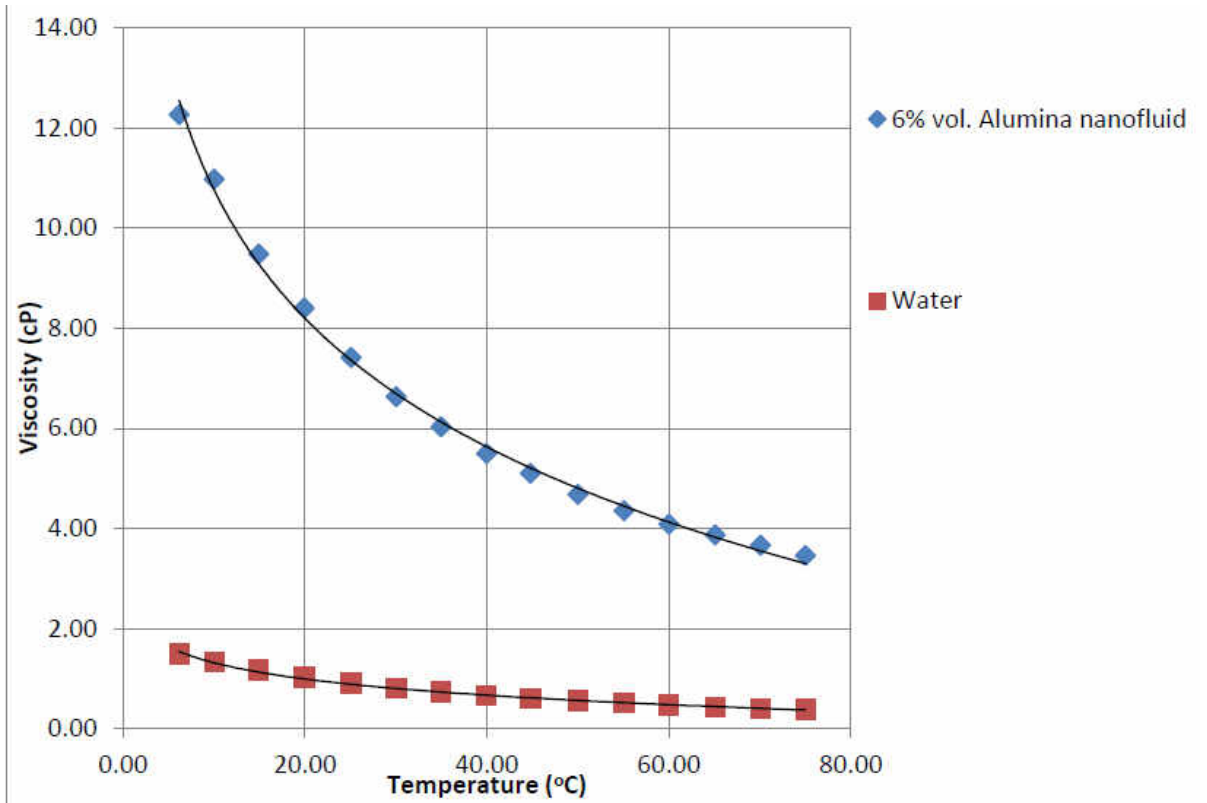
Figure 2. *Viscosity of water and aluminum oxide nanofluid as a function of temperature, Tiwari (2012)*

Equation (5) is used to calculate dynamic viscosity at various temperatures.

$$\mu = Ce^{\frac{b}{T}} \quad\text{...}\quad (5)$$

where, C and b are empirical constants that require viscosity data at two temperatures for evaluation.

Unlike liquids, viscosity of gases increases with increasing temperature. When the gas temperature is increased, molecules in random motion gain a higher momentum. This increases the gas resistance to motion as the temperature increases. Viscosity of gases is usually calculated from Sutherland's Equation (6).

$$\frac{\mu}{\mu_0} = \left(\frac{T}{T_0}\right)^{\frac{3}{2}} \frac{T_0+s}{T+s} \quad\text{..}\quad (6)$$

5

For complex fluid such as nanofluids, viscosity is hard to quantify, because many factors are involved such as the nature and concentration of nanoparticles mixed with the base fluid. In Chapter III, Section 3, different correlations used to calculate viscosity of nanofluids will be presented.

In fluid mechanics, several dimensionless parameters which are used to dynamically characterize the fluid are derived from viscosity. Such parameters include Reynolds, Stanton, Nusselt, and Prandtl numbers. Reynolds number is a dimensionless number defined as a ratio of inertial to viscous forces.

$$Re = \frac{Inertia\ forces}{Viscous\ forces} = \frac{U\rho d}{\mu} \dots\dots\dots\dots\dots\dots\dots\dots\dots\dots\dots\dots\dots\dots (7)$$

Reynolds number is used to classify the flow regimes. For pipes, the flow is laminar when Re is less than 2300. For Re between 2300 and 4000, the flow is transitional; and Re greater than 4000, the flow is turbulent. Figure 3 shows laminar and turbulent flow. For laminar regime, the flow is stable; whereas turbulent flow is characterized by the formation of vortices and large eddy currents.
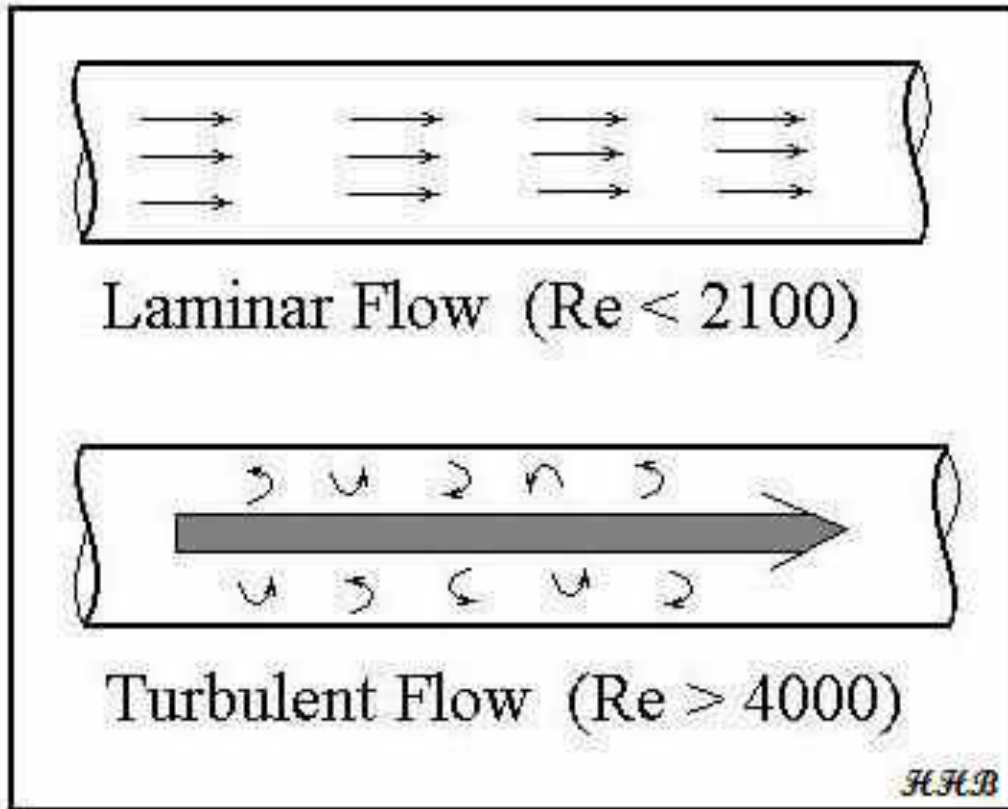
Figure 3. *Laminar and turbulent flow regimes in straight pipes,*
Bengtson and Stonecypher (2010)

The Reynolds number at which the transition for laminar to turbulent flow occurs also known as critical Reynolds number (Re_{crt}) can also vary depending on the nature of the being studied. The delay in transition from laminar to turbulent can be observed for non-Newtonian fluids. This delay is caused by shear thinning. Non-Newtonian fluids can also exhibit suppression of turbulent fluctuations and drag reduction at higher Reynolds numbers, Pinho and Whitelaw (1990), Rudman et. al (2002).

Earlier in this section, it is mentioned that viscous effects cause energy loss of the fluid. Fluid energy loss is often quantified in term of pressure drop. The following section presents pressure drop of the fluid and its impact on the performance of the system.

1.1.3 Pressure Drop

Pressure drop or differential pressure is the difference in static pressure between two location points of the fluid flow. Many factors influence the fluid pressure drop. The major factor is frictional force that originates from the fluid resistance to flow. The most important parameters that influence fluid frictional forces are velocity and viscosity. The Darcy-Weisbach Equation (8) is used to calculate the pressure drop for a straight channel.

$$\Delta P = \frac{f \, L \, \rho \, U^2}{2d} \qquad\qquad (8)$$

where,

f is the Darcy friction factor. For laminar flow regime, f is calculated from Equation (9).

$$f = \frac{64}{Re} \qquad\qquad (9)$$

In turbulent flow regime, the Colebrook Equation (10) is used. Because of the increased shear forces in turbulent regime, the roughness (k_s) of the pipe is considered.

$$\frac{1}{\sqrt{f}} = -2 \log\left(\frac{\frac{ks}{D}}{3.7} + \frac{2.51}{Re\sqrt{f}}\right) \qquad\qquad (10)$$

The Moody diagram that is depicted in Figure 4 can alternatively be used to find the friction factor.
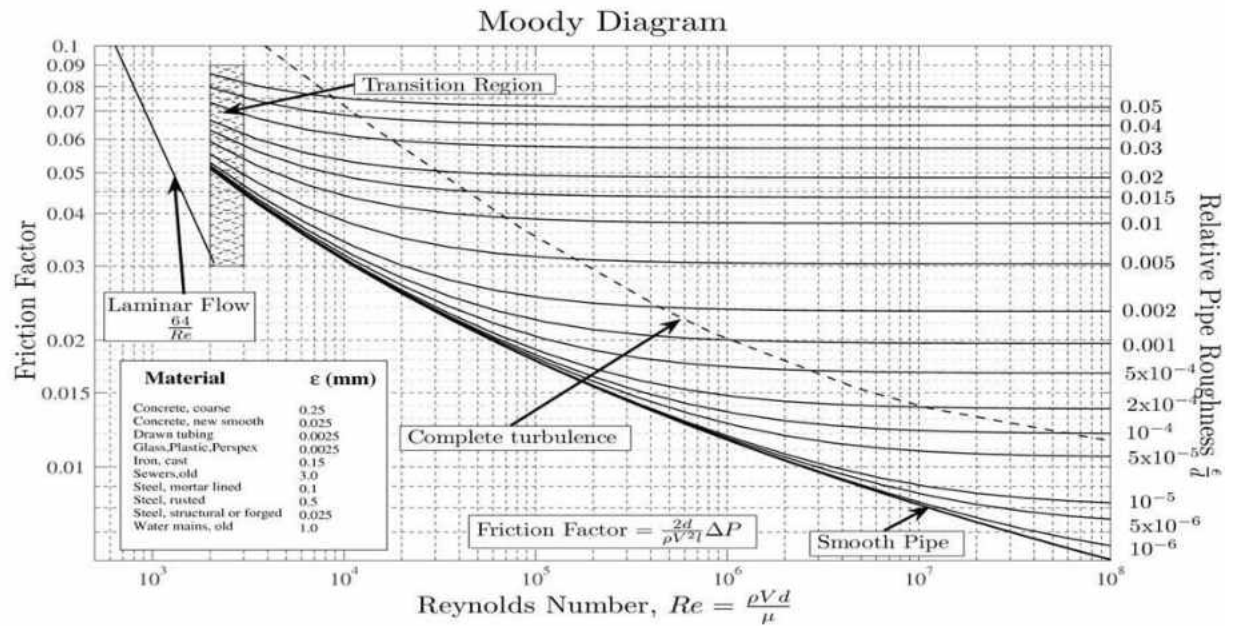
Figure 4. *The Moody diagram: Friction factor versus Reynolds number, Casey and Klepter (2013)*

Darcy-Weisbach Equation (8) doesn't count for the other pressure losses such as those caused by the channel geometry. Such channel geometries include sudden area change, bending, threaded pipe fittings, and so on. Equation (11), a version of Darcy-Weisbach equation, combines frictional losses or major losses and losses caused by the channel geometry. Losses caused by the channel geometry are also called minor losses because they are small compared to major losses. However, for smaller channels and high flow rates such losses are very significant.

$$\Delta P = \frac{f\, L\, \rho\, U_1^2}{2d} + \frac{K \rho U_1^2}{2} \quad\text{...} \quad (11)$$

1.1.4. Thermal Conductivity

Thermal conductivity is an important thermo-physical property of the fluid that quantifies its ability to conduct heat. Numerically, thermal conductivity is the measure of heat (Q) flow per unit area (A) in a direction of the temperature gradient (dT/dy). For a one dimensional flow, thermal conductivity is calculated from Equation (12).

$$\frac{Q}{A} = K_{th}\frac{dT}{dy} \dots\dots\dots\dots\dots\dots\dots\dots\dots\dots\dots\dots\dots\dots\dots\dots\dots\dots\dots\dots \quad (12)$$

Although it is a property characteristic of the fluid, thermal conductivity of the fluid changes with temperature and material composition of the fluid. Due to increase in electrons drift, thermal conductivity of fluids increases with increasing temperature. Although at very high temperature, thermal conductivity may decrease due to phase change. Single phase fluids such as air and water exhibit low thermal conductivity compared to complex fluid such as nanofluids. Nanofluids are merely a mixture of highly thermal conductive material with a single phase fluid such as water.
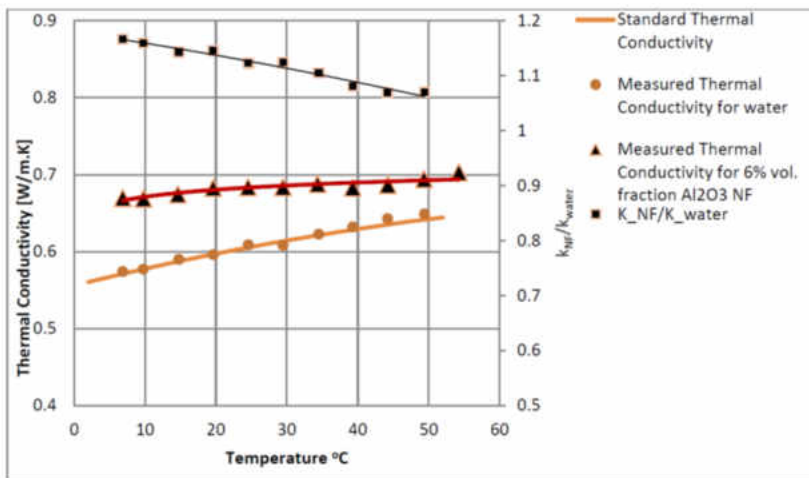
Figure 5. *Thermal conductivity vs. temperature for water and Nanofluids.*
A plot for the thermal conductivity ratio vs. temperature is also shown.
Tiwari (2012)

For heat transfer applications, both conduction and convection of the fluid are considered. Hence, the Nusselt number (Nu) is introduced. Nu is defined as the ratio of thermal resistance to convective thermal resistance of the fluid. Nusselt number is used to characterize convection boundary layer which is necessary to understanding convective heat transfer between a surface and a fluid flowing past it.

$$Nu = \frac{hD}{K_{th}}$$ …………………..…………………………………………………...…………….. (13)

1.2 Nanofluids

Over years, researchers were challenged to find a convenient way to convey heat without clogging flow channels, eroding pipelines and causing severe pressure drops. Because conventional single phase fluids such as water, air, oil, lubricants, and refrigerants would only transfer a small amount of heat. Also, the mixture of Micro/mill-size particles with a fluid was found to improve thermal properties of base fluid, but with many flow problems such as eroding and clogging pipes.

Micro/mill-size particles settle rapidly, clog flow channels, erode pipelines and cause severe pressure drops. For this reason, it was not recommended to use these types of mixtures in micro-channels, Cheng (2009).

Nanofluids were coined by Choi (1995), after realizing mixing nanoparticles (1-100 nm) with a base fluid enhances heat transfer. Materials commonly used as nanoparticles include chemically stable metals (e.g. gold, copper), metal dioxides (e.g., alumina, silica, zirconia, titania), dioxide ceramics (e.g. Al_2O_3, CuO), metal carbides (e.g. SiC), metal nitrides (e.g. SiN), carbon in various forms (e.g., diamond, graphite, carbon nanochannels, fullerene) and functionalized nanoparticles, Cheng (2009).

1.2.1 Nanofluids Preparation Techniques

The key to understanding the specialty of this kind of heat transfer fluid is knowing how they are prepared and produced. Numerous studies have been done regarding nanofluids preparation methods. Based on the ability to efficiently produce stable nanofluids and in mass, each method has its pros and cons.

Stability of nanofluids is an important criterion for quality nanofluids, because if nanoparticles are not stable or evenly dispersed unevenly in the base fluid, negative consequences such as settlement and clogging of flow channels can occur. This also affects nanofluids properties, particularly by decreasing the thermal conductivity.

Two methods are widely used for preparing nanofluids: one step and two steps methods. Two steps method is more popular than one step method. It is called two steps method, because a dry powder of nanoparticles is prepared in one step by using physical or chemical methods. In a separate step, the dry powder of nanoparticles are dispersed into the base fluid and the mixture is stirred by using techniques such as magnetic force agitation, ultrasonic agitation, high-shear mixing, homogenizing and ball milling.
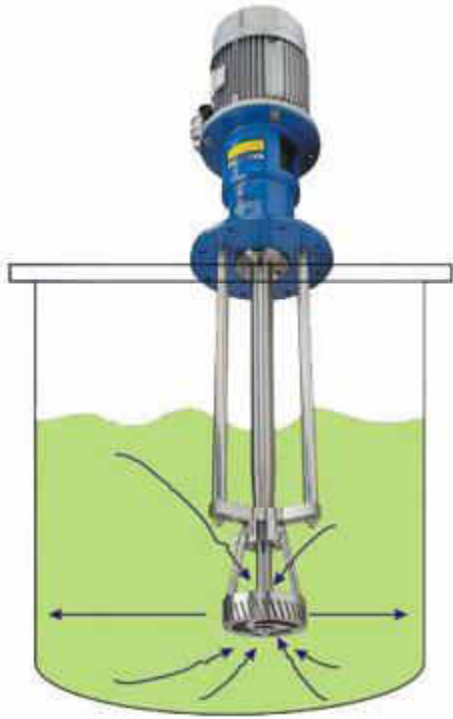
Figure 6. *High shear batch mixer designed and manufactured by BP Systems Company (http://bpsystems-eu.com/batch-mixers/)*

Two step method offers the advantage of massively producing nanofluids at low cost. However due to nanoparticles agglomeration, nanofluids prepared by using this method are not stable.

Contrarily to two step method, nanofluids prepared by using one step method are stable. In one step method, both nanoparticles and nanofluids are prepared in one step. With this method, it is possible to achieve high stability of nanofluids, but it is not cost effective to produce great quantity of nanofluids by using this method.

Table 1. Comparison of one step and two step methods.

	Pros	Cons
One step method	High Nanofluids stability	It is expensive and difficult to prepare nanofluids in large Scale.
Two step method	Nanofluids can be prepared in large scale.	Instability caused by nanoparticles agglomeration is high.
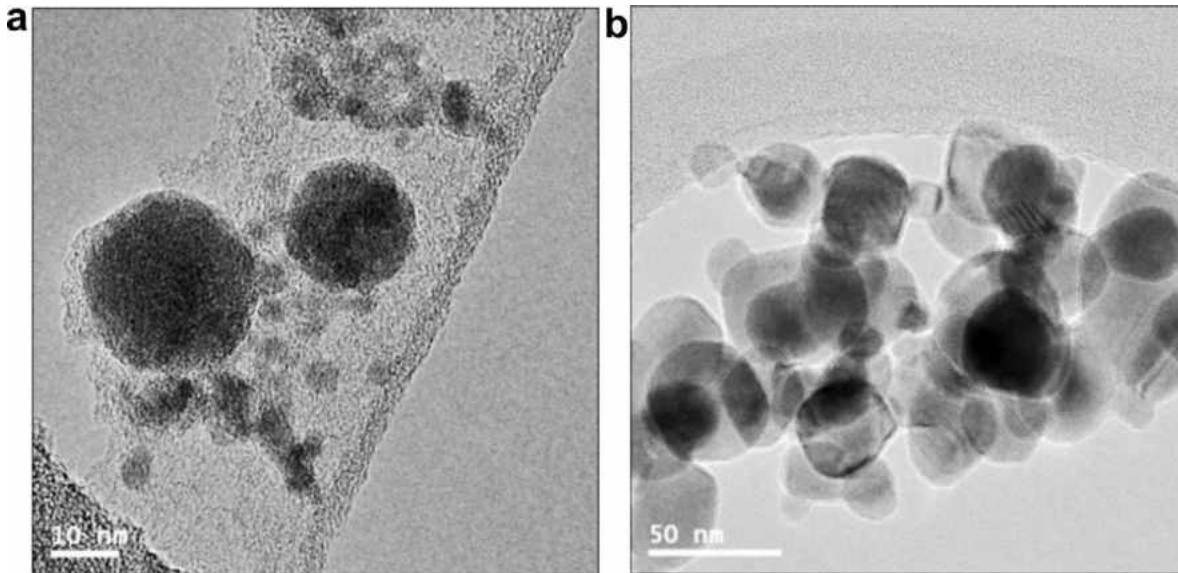
Figure 7. *(a) CuO/water nanofluid is prepared by using one step method,*
(b) two step method, Haddad et al. (2014)

The above microscopic view shows that nanoparticles in Figure 7a are evenly distributed throughout the base fluid. However nanoparticles in Figure 7b are settled at the bottom of the container, therefore rendering nanofluids less sTable and less useful.

1.2.2 Nanofluids Applications

Nanofluids have been regarded by numerous researchers as heat transfer fluids that could replace conventional fluids such as water, air, oil for numerous applications.

- Heat Transfer Applications:

    o Industrial cooling

    o Smart fluids

    o Extraction of geothermal power and other energy sources

    o Heat pipes

- Automotive applications

  o Nanofluid as a coolant

- Electronic applications

  o Cooling of microchips and micro electro-mechanical devices

- Biomedical applications

1.2.3 Silicon Dioxide or Silica Nanofluid

Silicon dioxide is the powder product of silicon oxidation. It is a highly conductive metal dioxide with high thermal energy storage capacity. Physical properties of silicon dioxide would vary depending on the conditions of temperature, pressure, and crystalline forms. Because all experiments of this study were performed at constant temperature and pressure, the density of the powder used to make this nanofluid was taken as 2360 kg/m^3.

1.3. Sudden Area Change in Channels

Numerous engineering systems require the flow of fluid in channels. Key examples include heat exchangers, oil and natural gas pipelines, air conditioning and refrigeration, and electronic systems. Such as systems don't always use straight channels; it comes to the point where an area change is required in order to meet design specifications. Sudden expansion occurs, when an area of a channel abruptly changes from small to large; whereas for sudden contraction, the area abruptly changes from large to small. Figures 8 and 9 show solar pool heat exchanger designed by Northern Lights Solar Solutions Company and is capable of handling high secondary flow in pools.

Figure 8. *Three dimensional view of Northern Lights Solar Solutions
Company solar pool heat exchanger,*
(http://www.solartubs.com/solar-pool-heat-exchanger.html)
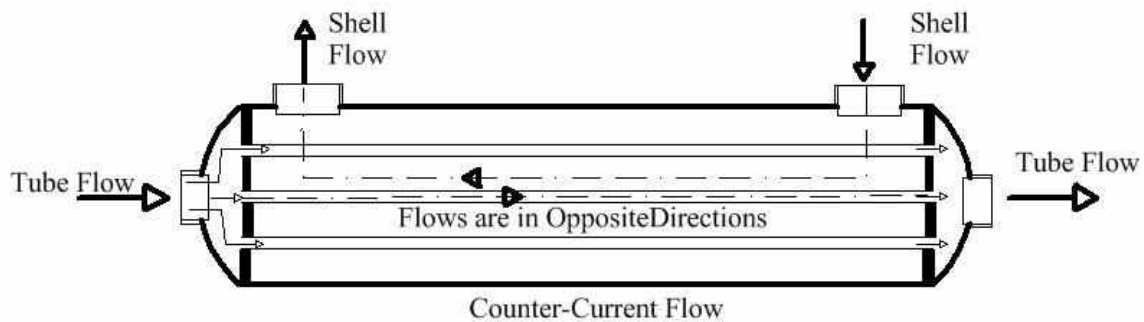
Figure 9. *Two dimensional view of Northern Lights Solar Solutions
Company solar pool heat exchanger,*
(http://www.solartubs.com/solar-pool-heat-exchanger.html)

A close look at Figure 9 shows a sudden expansion at the flow inlet and sudden contraction at exit. When the fluid flow encounters a sudden area change, not only faces velocity fluctuation but also static pressure downstream decreases significantly. This is a big problems for engineering systems that require such flow, because greater pumping power is required to compensate the mechanical energy lost by the fluid. It is therefore necessary to study the mechanism of the flow through systems with sudden area change in order to optimize the efficiency.

In the following section an attempt was made to derive equations that quantify pressure drop and loss coefficient for sudden area expansion and contraction.

1.3.1 Sudden Expansion

The fluid flow through a passage with abrupt area expansion is accompanied by a mechanical energy loss. This mechanical energy is easily understood when quantified in form of viscous pressure loss. Abrupt area expansion is not the only factor that contributes to mechanical energy loss of the fluid. The length, shape, and roughness of the channel can also cause pressure losses.

Many engineering fluid mechanic textbooks define major and minor losses. Major losses are pressure losses due viscous forces along the channel, whereas minor losses are those that are due to sudden area change of the channel. This research focuses primarily on minor losses due to sudden expansion and contraction of the channel.
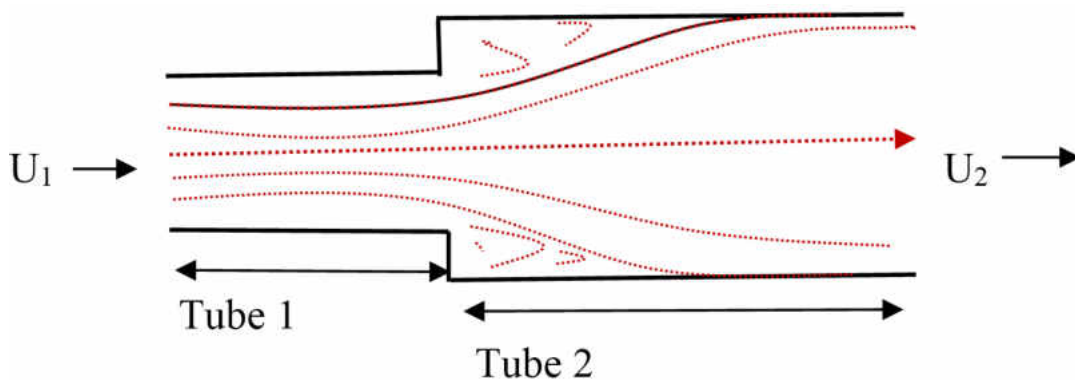
Figure 10. *Flow through sudden area expansion*

Equations (14) and (15) define pressure drop due to sudden expansion and contraction respectively, they can be derived by applying one-dimensional momentum and conservation of energy Equations.

$$\Delta P_e = \frac{1}{2}K_e U_1^2 \rho \quad \dots\dots\dots\dots\dots\dots\dots\dots\dots\dots\dots\dots\dots\dots\dots\dots\dots\dots\dots\dots\dots\dots\dots\dots \quad (14)$$

$$\Delta P_c = \frac{1}{2}K_c U_1^2 \rho \ \text{………………………………………………} \ (15)$$

Over decades numerous researchers have developed expressions for quantifying the loss coefficient due to sudden expansion K_e and sudden contraction, K_c. Borda-Carnot equation is one of the simplest expressions.

$$K_e = (1 - \sigma^2) \ \text{………………………………………………} \ (16)$$

Carnot derived his equation based on the fact, that the velocity is uniformly distributed upstream and downstream of the flow channel. Schutt (1929) has experimentally verified Carnot Equation for fully turbulent flow at Reynolds numbers great than 10 000.

Kays (1949) proved that loss coefficient does not only depend on area ratio of the flow channels. In fact, momentum distribution and magnitude of the velocity ahead of the expansion also affect the loss coefficient. In his research, Kays (1949) developed correlations for sudden expansion pressure drop and loss coefficient.

In the following section, formulation of pressure drop and loss coefficient Equations for a single phase flow with sudden expansion will be detailed. This will later be handful during the analysis of the experimental data.

Equations Derivation

Momentum-force analysis is used to predict the behavior of the fluid through sudden expansion. This can be achieved by applying the second law of Newton which is defined based on one directional momentum Equation.

$$\frac{K_{d2} \, \rho \, U_2^2 A_2}{g} - \frac{K_{d1} \, \rho \, U_1^2 A_1}{g} = P_2 A_2 - P_1 A_1 \ \text{………………………………} \ (17)$$

By assuming incompressible flow and rearranging terms in Equation (17) and using continuity Equation, the differential pressure Equation across the flow passage can be derived. This pressure drop comes from momentum loss that results in pressure gradient across the flow passage.

$$\Delta P_{eo} = \frac{\rho\, U_1^2}{2} \left(\sigma\, K_{d2} - \sigma^2 K_{d1} \right) \dots\dots\dots\dots\dots\dots\dots\dots\dots\dots\dots\dots\dots\dots\dots\dots\dots \quad (18)$$

where $\sigma = A_1 / A_2$.

Figure 11 demonstrates pressure gradient in passage with sudden expansion for a single phase flow. Zero location is the singularity or the region where the cross section changes abruptly. It is important to notice the impact of sudden expansion on the fluid, as it slows down near the construction.
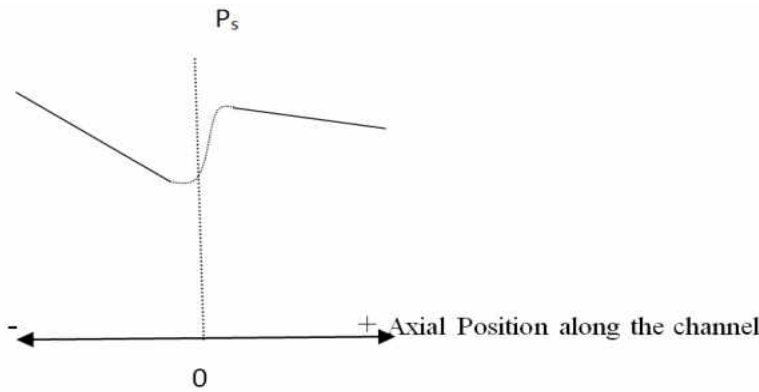
Figure 11. *Pressure profile in sudden area expansion*

Furthermore, the velocity varies along the channel depending on the type of flow being experimented. This is due to the sudden area change which becomes a disturbing barrier for the flow. For this reason, the velocity distribution coefficient, K_d is introduced in order to account for the velocity fluctuation downstream and upstream of the test section. K_d is defined as the ratio of the actual momentum rate to the momentum rate based on the average bulk velocity.

$$K_d = \frac{1}{A\,U_{avg}^2} \int_0^A U^2 \, dA \quad \text{..(19)}$$

In order to derive the expression of loss coefficient, the ideal pressure drop Equation is first defined. The ideal pressure drop is the total differential pressure obtained by assuming a frictionless flow and uniform velocity distribution.

$$\frac{\Delta P_{ideal}}{\rho} = \frac{U_2^2}{2g} - \frac{U_1^2}{2g} = \frac{U_1^2}{2g}\,(1 - \sigma^2) \quad \text{...(20)}$$

The ideal pressure drop includes momentum and expansion losses.

$$\Delta P_{ideal} = \Delta P_e + \Delta P_{eo} \quad \text{...(21)}$$

Rearranging Equation (21) and utilizing the ideal pressure drop Equation (20), the total expansion losses can be numerically defined as follow:

$$\Delta P_e = \Delta P_{ideal} - \Delta P_{eo} = \rho \frac{U_1^2}{2}\,(1 - \sigma^2) - \Delta P_{eo} \quad \text{.............................(22)}$$

Substituting (20) into (22) gives

$$\Delta P_e = \rho \frac{U_1^2}{2}\,[\,1 - 2\sigma K_{d1} + \sigma^2\,(2K_{d2} - 1)] \quad \text{.............................(23)}$$

In fluid mechanic, pressure loss due to sudden area expansion is defined as

$$\Delta P_e = K_e\,\rho\,\frac{U_1^2}{2} \quad \text{...(24)}$$

Comparing Equations (23) with (24), it yields an expression for the loss coefficient

$$K_e = 1 - 2\sigma K_{d1} + \sigma^2\,(2K_{d2} - 1) \quad \text{.......................................(25)}$$

In cases where uniform velocity distribution is assumed upstream and downstream of the singularity, $K_{d1} = K_{d2} = 1$. However due to the flow disturbance as the flow approaches the construction, K_{d2} becomes greater than one in order to account for the non uniform velocity distribution. For the channel downstream of the singularity ($K_d = 1$), in view of the strong mixing that results from the flow disturbance.

20

The momentum coefficient K_d in the upstream channel can depend on the fluid flow regime. $K_d = 1$ for turbulent flow (Re >2300) and $K_d = 1.33$ for laminar flow (Re < 2300), Abdelall et al. (2004).

I.3.2 **Sudden Contraction**

In sudden area contraction, the channel area abruptly decreases or contracts. This abrupt area contraction engenders a local hydraulic resistance that causes a mechanical energy loss to the fluid. As a result of mechanical energy loss, the velocity profile near the singularity becomes non-uniform and local static pressure downstream decreases significantly.
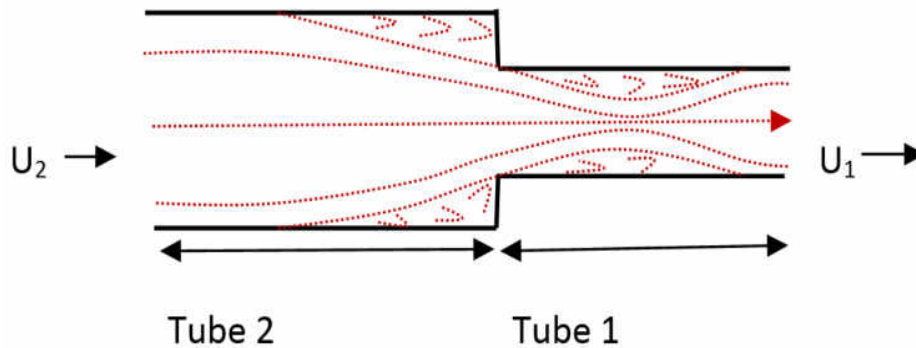
Figure 12. *Flow through sudden area contraction*
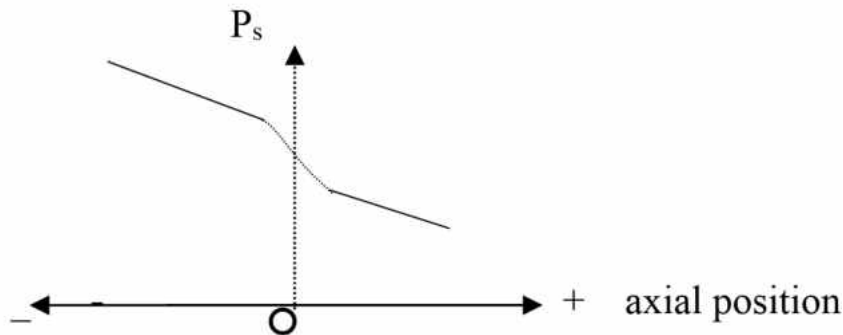
Figure 13. *Pressure profile for sudden area contraction*

Figure 12 depicts the flow through sudden area contraction. The region where the fluid stream is minimum and velocity is maximum is known as vena contracta. Local static pressure at vena contracta is minimum, as a result the velocity becomes maximum and differential pressure is increased. Vena contracta coefficient, C_c is often used to describe vena contracta.

$$C_c = \frac{A_c}{A_1} \quad \ldots\ldots\ldots\ldots\ldots\ldots\ldots\ldots\ldots\ldots\ldots\ldots\ldots\ldots\ldots\ldots\ldots\ldots\ldots\ldots\ldots\ldots\ldots \quad (26)$$

As the flow approaches the singularity, separation may occur and eddy zones can develop at the front of transitional cross section. The contracted flow forms itself into a small jet flow pattern with the narrowest cross section of the jet being called vena-contracta which is located immediately after the transition cross section, Chen et al. (2008).

For single-phase flow through a sudden flow area contraction, it is usually assumed that the flow up to vena-contracta point is isentropic, and pressure loss takes place during the deceleration of the fluid downstream the vena-contracta point, Chalfi and Ghiaasiaan (2008).

The effect of the sudden area contraction decreases gradually downstream of the vena contracta and eventually becomes negligible. This phenomenon is called relaminarization, and the distance from the relaminarization point to the construction is designated as relaminarization length. Beyond relaminarization length, mechanical energy losses are almost entirely friction losses and are directly proportional to the length of the channel.

It is crucial to understand and quantify the losses due sudden area contraction. Common equation for quantifying pressure drop due to sudden area contraction is derived from continuity and momentum equations.

$$\Delta P_c = K_c \rho \frac{U_1^2}{2} \quad\text{...(27)}$$

In the following section, equations for calculating loss coefficient of a channel with sudden area contractions will be derived.

Sudden Area Contraction Loss Coefficient

Similarly to sudden expansion, necessary Equations are derived by doing momentum analysis. An assumption is made, that velocity distribution at vena contracta is uniform. Based on this assumption, kinetic energy correction factor in channel 1 is one ($K_{d1} = 1$). The velocity distribution in channel 2 may not be uniform; the reason why the kinetic energy correction factor K_{d2} is introduced. The loss coefficient therefore becomes:

$$K_c = \frac{1 - K_{d2}\, \sigma^2 C_c^2 - 2C_c + C_c^2\ 2K_m}{C_c^2} - (1 - \sigma^2) \quad\text{..(28)}$$

By assuming a flat velocity upstream of the singularity and downstream of the vena-contracta ($K_m = K_{d2} = 1$), Equation (28) reduces to Equation (29).

$$K_c = (1 - \frac{1}{C_c})^2 \quad\text{..(29)}$$

The jet contraction ratio, C_c is often defined in term the area ratio. Geiger (1964) developed an expression for jet contraction ratio based on his doctor of philosophy dissertation results.

$$C_c = 1 - \frac{1 - \sigma}{2.08\,(1 - \sigma) + 0.5371} \quad\text{...(30)}$$

Chisholm (1983) proposed an equation similar to Geiger's equation for jet contraction ratio.

$$C_c = \frac{1}{[0.639(1 - \sigma)^{0.5} + 1]} \quad\text{...(31)}$$

1.4 STATEMENT OF THE PROBLEM AND RESEARCH OBJECTIVES

The problem to be addressed is pressure drop in horizontal channels with sudden area expansion and contraction for single phase flow. Also the flow of complex fluid will be considered. In order to approach the problem, an experimental investigation of water as a single phase fluid and silicon dioxide-water nanofluid at 9.58% volume concentration as a complex fluid will be performed. In addition, theoretical Equations will be derived and utilized to quantify the minor loss coefficients. The following keys questions will be addressed:

1. How does static pressure at upstream compare with static pressure at downstream of singularity? Does static pressure vary with mass flow rate?

2. How do static pressures for sudden area expansion compare with static pressures for sudden area contraction?

3. How does pressure drop caused by sudden area expansion compare with pressure drop caused by sudden area contraction? How does pressure drop vary with mass flow rate for both sudden area changes?

4. How do loss coefficients for sudden area expansion compare with loss coefficient for sudden area contraction? How do they vary with mass flow rate and area ratio? Is there any difference between loss coefficient for water and for nanofluid for the same flow conditions?

5. How do loss coefficient results compare with those reported in textbooks or theoretical calculations?

In order to answer these questions, the experimental investigation will consist of the measurements of static pressure along two test sections ($\sigma = 0.0625$ and 0.140) for various mass flow rates ranging from 5 to 30 g/s. These data will be used to determine pressure drops and loss coefficients. All experiments will be performed at ambient conditions of temperature and pressure. A comparative study between experimental and theoretical results is also considered.

1.5 OUTLINE OF THE STUDY

This study provides experimental methodology for measuring static pressure for water and silicon dioxide nanofluid flowing in channels with sudden area contraction and expansion. Also expressions and methodology for quantifying pressure drops and loss coefficients are detailed. Chapter I introduces some of the key parameters which are investigated. Fluid parameters that are addressed include density, viscosity, pressure drop, and thermal conductivity. Chapter II emphasizes on literature review. Previous works on sudden area change and nanofluid are presented. Chapter III describes instruments of the flow loop and the methodologies that were used to acquire data for this study. In addition uncertainty analysis is done. Chapter IV presents and discusses the results of water and silicon dioxide nanofluid flow. Chapter V draws a conclusion based on experimental and theoretical results. Also this chapter includes a recommendation for potential applications.

CHPAPTER II

LITTERATURE REVIEW

2.1 Sudden Area Expansion

Sudden area expansion is not a new concept. Over decades, several researchers have shown interest in sudden area expansion subject due its numerous applications in engineering systems. Most of studies available emphasize on single phase flow and gas-liquid or steam-liquid or two gases mixture flow.

Kays (1949) developed Equations for evaluating loss coefficients in channels with sudden area contraction and expansion for single and multitudes systems. He applied momentum analysis by taking into consideration the velocity distribution downstream and upstream of the singularity. The results of Kays' analysis were validated for Reynolds numbers between 500 and 20,000.

Mendler (1963) measured the static pressure variation along three test sections with sudden area expansion in single and two phase flow at various flow rates. Test sections utilized have area ratios of 0.145, 0.264, and 0.493. The measured static pressure was then utilized to quantify pressure drop and loss coefficient for both flow phases. The study concluded that fully developed flow model provides a better prediction of flow behavior in sudden area expansion especially for area ratios of 0 to 0.5 with pressures ranging from 200 to 600 psi.

Abdelall et al. (2004) utilized the same methodology as Mendler (1963) to quantify single phase and air-water mixture flow pressure drop caused by abrupt area changes in

27

small channels. Larger and smaller channels had internal diameters of 1.6 and 0.84 mm respectively. They found out that with turbulent flow in the smaller channel, approximately constant expansion loss coefficients occurred in experiments with water.
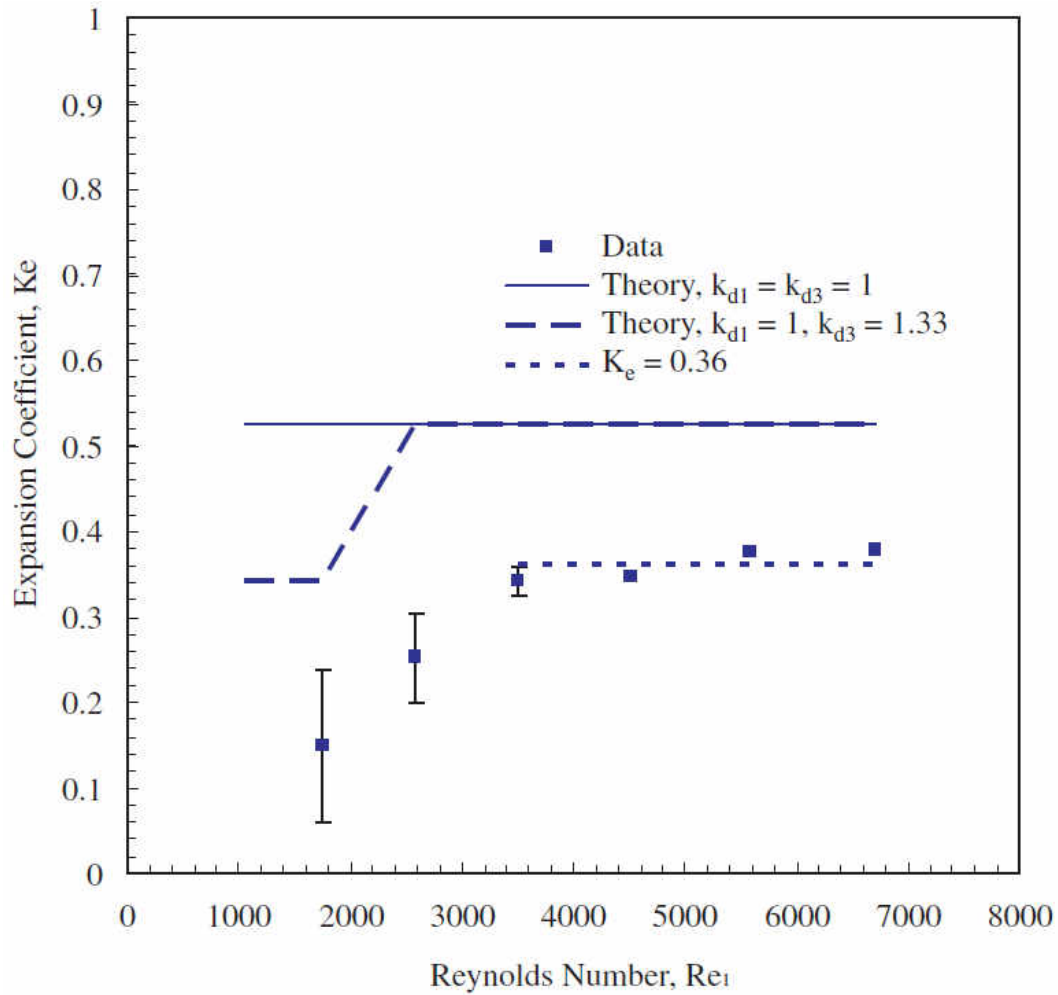
Figure 14. *Expansion loss coefficients obtained from experiments with water, Abdelall et al. (2004)*

2.2 Sudden Area Contraction

Like sudden area expansion, sudden contraction has been extensively studied in the past. Most of the works available in this subject have put an emphasis on single phase or two phase (mostly condensation or boiling) flow.

Geiger (1964) investigated water and steam-water mixture in a vertical channel (area ratios of 0.398, 0.253, and 0.144) with sudden area contraction. He analyzed the fully developed and separated two phase flow models. The separated flow model appeared to underestimate the pressure drop than the fully developed model. His results for single phase flow appeared to agree with theoretical prediction with 11.5 percent error.

Balakhrisna et al. (2010) attempted to understand the behavior of oil–water flow when it encounters a sudden change in cross-section. They used both high viscous and low viscous oils as test fluids in order to note the influence of physical properties on flow and pressure drop characteristics. They found out that the flow patterns are influenced by oil properties. Viscous oils have a tendency to form different types of core annular flow, whereas lighter oils exhibit a wider variety of distribution in water. They also noted that the pressure profiles have been observed to be independent of oil viscosity although the formation of core flow reduces the pressure drop for viscous oils.

Numerous researches reported the pressure profile as a decreasing trend curve along the test channel. However, at the singularity there is an abrupt and significant pressure loss due to sudden area change, Figure 15.
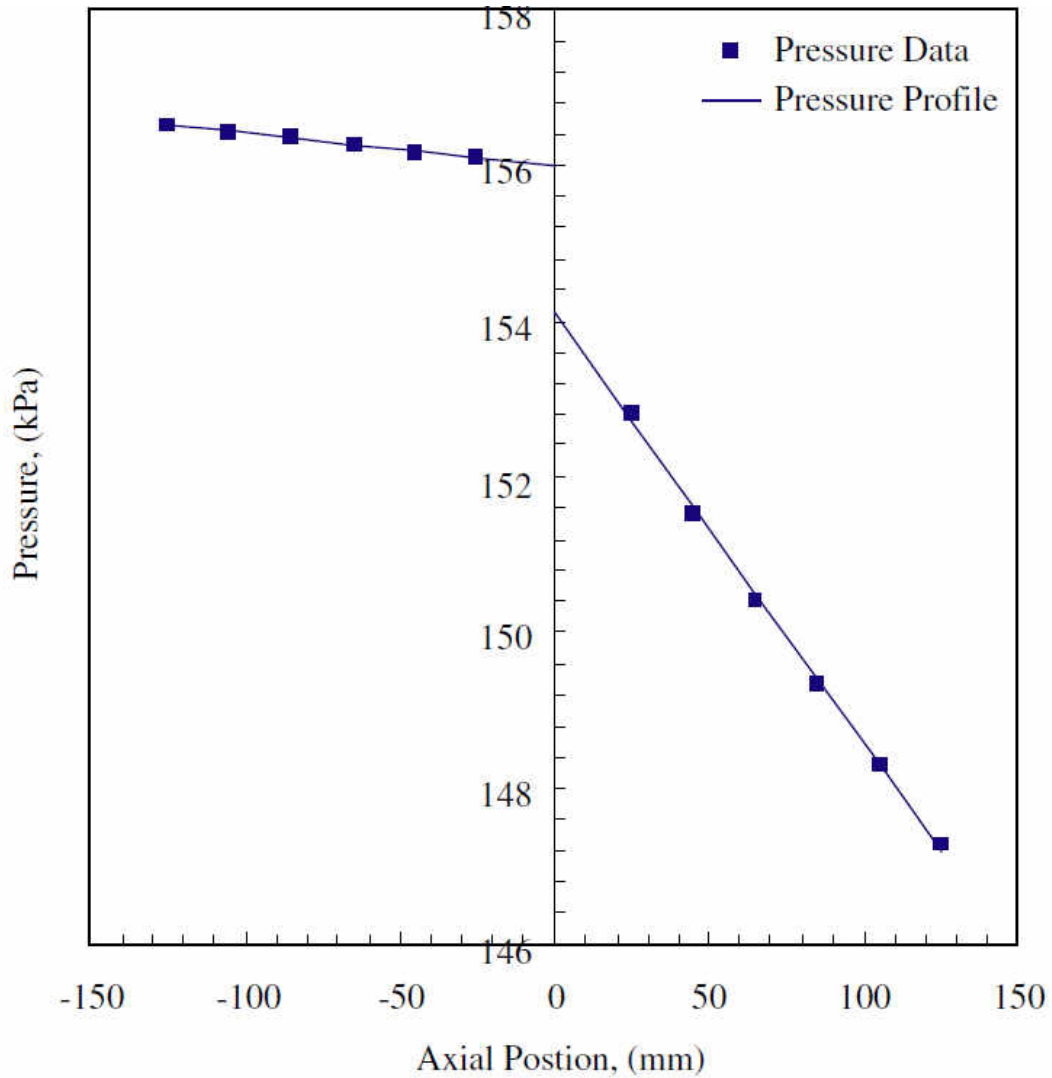
Figure 15. *Measured pressure profile for water flow in small channels with sudden contraction, Abdelall et al. (2004)*

The high demand for micro-electro-mechanical devices has raised dispute on whether or not conventional correlations and theories can be applied to macro-channels can also be applied to micro-channels. Guo et al. (2009) approached this by quantifying the loss coefficient for sudden area contraction in micro-channels. The inside diameters of channels used in their experiments ranged between 0.8 to 2.1 mm with area ratios of 0.274 and 0.284.

They found out that in laminar flow region, when the diameter increases, the experimental results of loss coefficients for the flow in microchannels are much closer to the theoretical results of loss coefficients for the flow in macrochannels. However this was not the case for turbulent flow region. For both flow regions, the loss coefficient decreased as the channel diameter increased.

2.3 Nanofluids

2.3.1 Viscosity

Nanofluids have been reported to exhibit higher viscosity compared to conventional fluids. There has been much interest in studying viscosity of nanofluids due to its influence on other thermal physical properties. One of the challenges that researchers encountered while studying viscosity of nanofluids is to develop a common correlation which can be used to quantify viscosity of different nanofluids. Not only nanofluids differ by the kind of nanoparticles used, but also by their concentration in the base fluid.

Table 2. Review on selected correlations developed
for a variety of nanofluids with water as the base fluid.

Nanoparticle	Author (s)	Applicability	Correlation
Al_2O_3	Park and Cho (1998)	$d_p = 13$ $25 \leq T_b \leq 70$ $1.34 \leq \emptyset \leq 4.33$ $8.5 \leq Pr_{nf} \leq 12.3$	$\dfrac{\mu_{nf}}{\mu_w} = 1.00869 e^{\left(\frac{\emptyset}{1.93595}\right)}$
	Williams et al. (2008)	$d_p = 46$ $21 \leq T_b \leq 80$ $0.9 \leq \emptyset \leq 3.6$	$\dfrac{\mu_{nf}}{\mu_w} = 0.4914 + 0.5255 e^{\left(\frac{\emptyset}{2.453}\right)}$
	Nguyen et al. (2007)	$36 \leq d_p \leq 47$ $25 \leq T_b \leq 55$ $0.2. \quad \leq \emptyset \leq 9.0$	$\dfrac{\mu_{nf}}{\mu_w} = 0.0130 \emptyset^{0.4557} d_p^{1.122}$
CuO and Cu	Nguyen et al. (2007)	$d_p = 29$ $20 \leq T_b \leq 50$ $0.2. \quad \leq \emptyset \leq 9.0$	$\dfrac{\mu_{nf}}{\mu_w} = 1.475 - 0.319 \emptyset + 0.05 \emptyset^2$ $+ 0.009 \emptyset^3$

Studies have shown that nanofluids viscosity increases with increasing nanoparticles concentration. This increase as shown by the correlations in Table 2. Nanofluids viscosity generally decreases with increasing temperature.
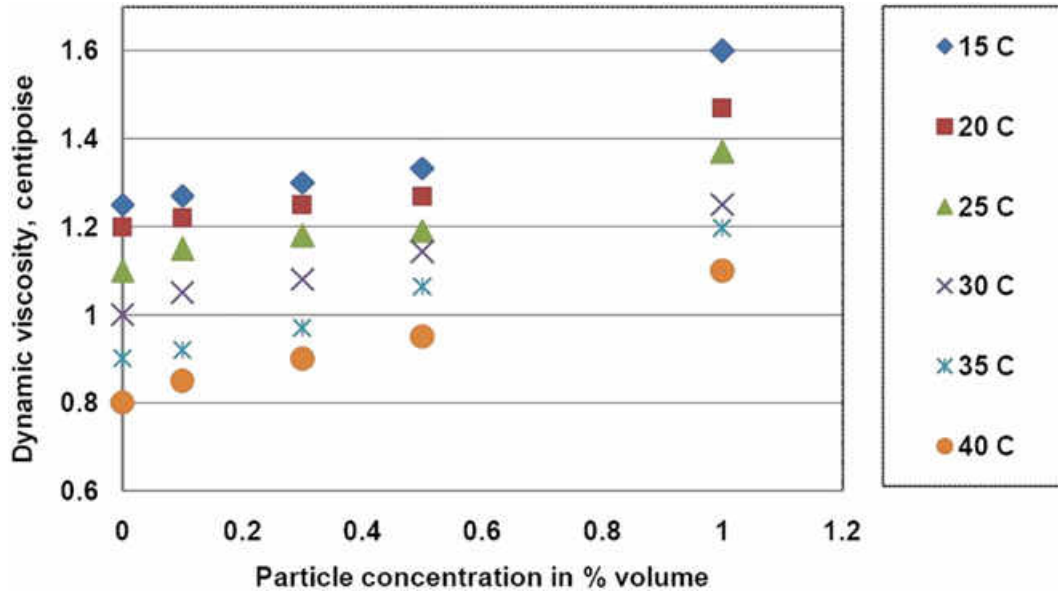
Figure 16. *Variation of Al2O3 viscosity with temperature*
at different nanoparticles concentration,
Sonawane et al. (2011)

In addition to temperature and nanoparticles concentration, shear rate also affects

the viscosity of nanofluids. Viscosity of nanofluids has been reported to decrease with

increasing shear rate. Figure 16 summarizes the results of the viscosity measurements of

nanofluids containing carbon nanochannels.
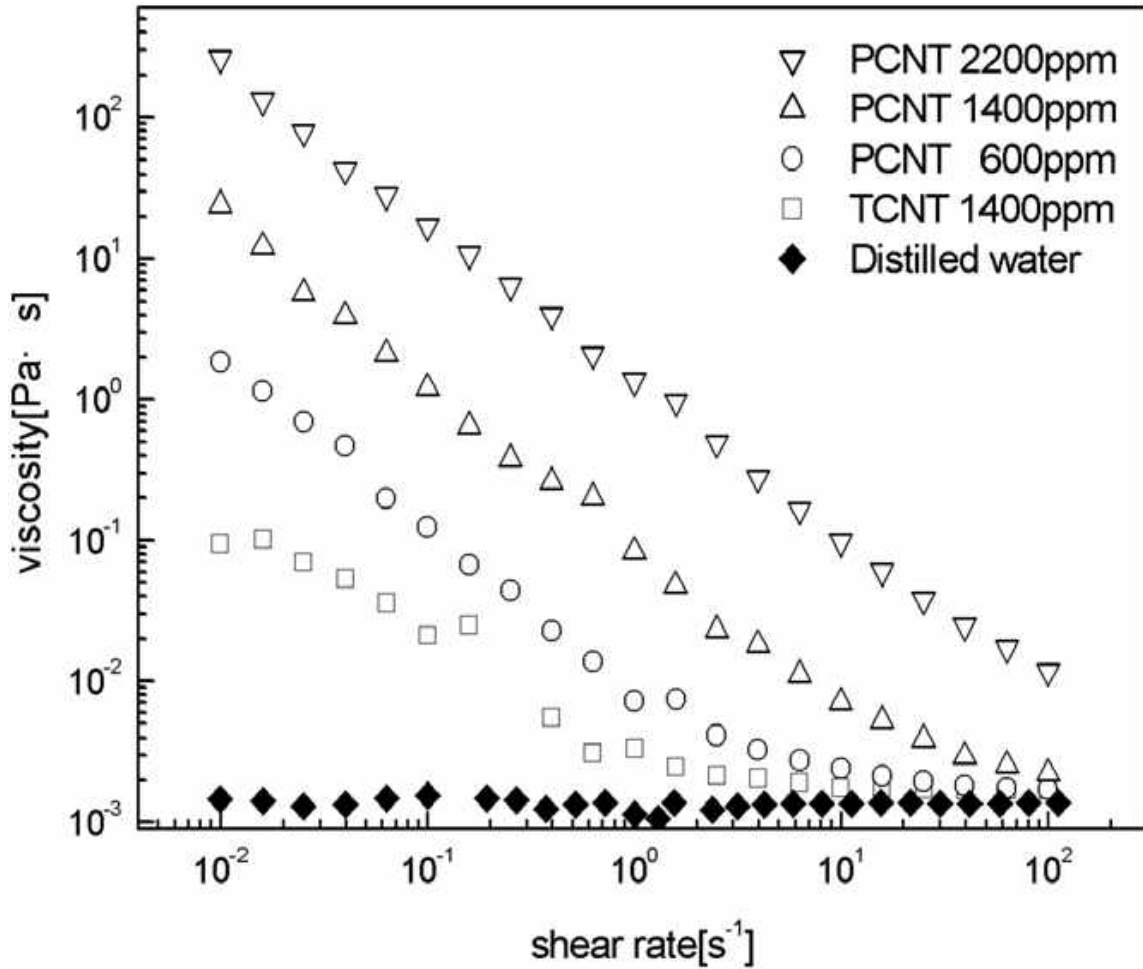
Figure 17. *Viscosity of nanofluids with carbon nanochannels versus shear rate, Heo et al. (2007)*

2.3.2 Pressure Drop

The increase in viscosity of nanofluids causes pressure drop in channels. For this reason, systems that utilize nanofluids as the working fluid require higher pumping power in order to compensate the mechanical energy losses. However for low concentration in nanoparticles, nanofluids have been reported to have little or negligible penalty in pressure drop difference compared to the base fluid.

Duangthongs and Wongwises (2009) studied forced convective heat transfer and flow characteristics of a nanofluid consisting of water and 0.2 vol.% TiO2 nanoparticles. The results of their study confirms (Figure 18) that the pressure drop and friction factor of the nanofluid are approximately the same as those of water in the given conditions. This implies that the nanofluid at very low nanoparticles concentration incurs no much penalty of pump power and may be suitable for practical application. Predictions of the pressure drop with the conventional theory for the base liquid agree well with the measurements at relatively low Reynolds numbers. Deviation occurs at high Reynolds numbers possibly due to the entrance effect, He et al. (2006).
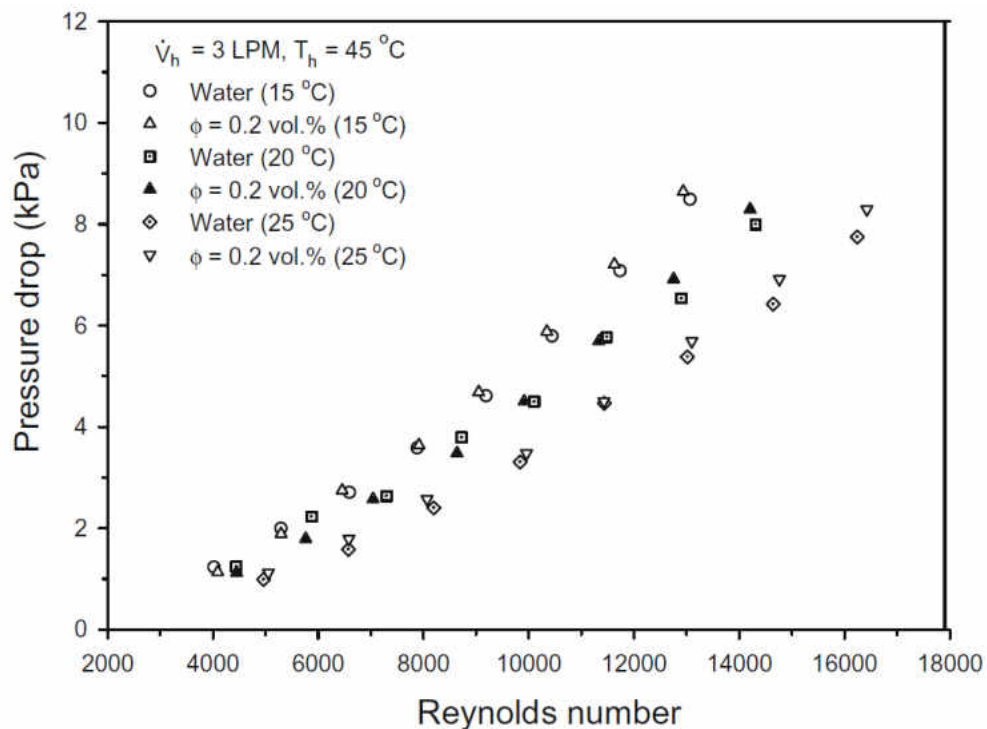
Figure 18. *Comparison of 0.2 vol.% nanofluid pressure drop and water pressure drop, Duangthongs and Wongwises (2009)*

As previously discussed, pressure drop is directly proportional with friction factor. Sahin et al. (2013) experimentally investigated heat transfer and pressure drop of aluminum dioxide nanofluids at volume concentration ranging from 0.5 to 4%. They found out that increased in viscosity caused the increase in friction factor which also increased with increasing of nanoparticles concentration. The concentrations of Al_2O_3 particles higher than 1% volume in the base liquid were not suitable for heat transfer enhancement. The viscosity increase of the nanofluids was much more effective than the thermal conductivity of the nanofluids for the particle volume concentrations higher than 1 vol. % on heat transfer enhancement.
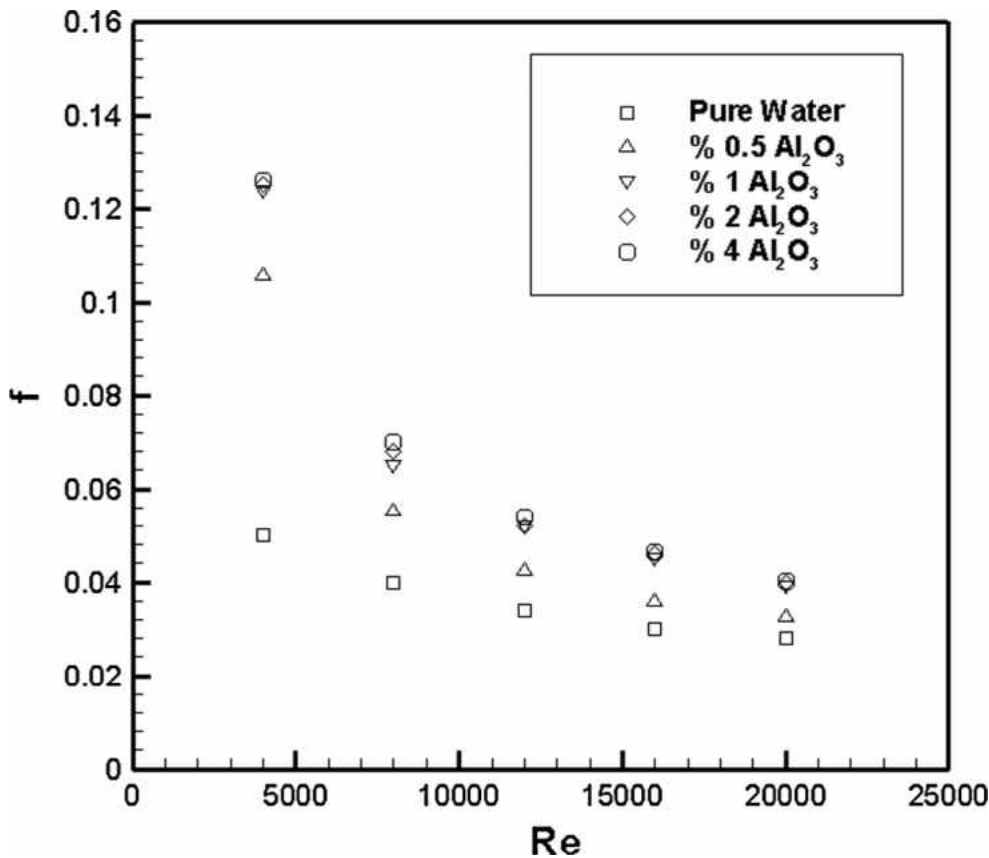
Figure 19. *Effect of nanoparticles concentration on friction factor at various Reynolds number, Sahin et al. (2013)*

Higher pressure drop of nanofluids at higher flow rates is one of the limiting factors for industrial applications, especially in micro and nanochannels. For instance, the small quantity of nanoparticles in microchannel heat sinks make turbulent flows impractical as they would result in large pressure losses across the heat sink, Escher et al. (2011). High pressure drop is not the only potential limitation if nanofluids applications. It has also been reported that for higher Reynolds numbers, some nanofluids show a reduction in heat transfer. This was particularly observed for studies done on silica and carbon nanochannel nanofluids in channel flow.

The enhancement of convective heat transfer due to presence of nanoparticles is observed for the smaller values of Re numbers, where turbulent heat transfer reduction due to additives used is not strong enough to neutralize the enhancement. However, for higher values of Re numbers, the turbulent heat transfer reduction is predominant and stronger than the heat transfer enhancement due to nanoparticles, resulting in over-all reduction in convective heat transfer, Kostic (2013).

2.2.3 Weighing Thermal Performance of Nanofluids

Thermal performance of a fluid is defined as its ability to transport thermal energy with respect to the power required to achieve a certain heat transfer rate. Thermal performance is best quantified by the coefficient of performance which is a ratio of heat transfer rate to the pumping power.

$$COP = \frac{\dot{Q}}{\dot{P}}$$ .... (32)

where,

$$\dot{P} = \Delta P \, \dot{U}$$ .... (33)

The increase in nanoparticles concentration in base fluid increases heat transfer of nanofluids. However, this increases the viscosity of the fluid and therefore rendering the pumping power to increase and thermal performance to decrease. The applicability of nanofluids requires a balance between the heat transfer capability and viscous pressure losses due to the increased viscosity.

Table 3. Collection of several findings of researchers who have experimented heat transfer and viscous pressure drop associated properties of different kinds of nanofluids.

Researchers	Objectives	Nanofluid Types	Findings
1. Sajadi and Hazemi (2011)	Investigation of turbulent convective heat transfer and pressure drop of TiO2/water nanofluid in circular channel	TiO2/Water 0.05%, 0.1%, 0.15%, 0.2%, and 0.25% volume fraction of particles	The pressure drop of nanofluid increased with increasing the volume fraction of nanoparticles. The maximum pressure drop was about 25% greater than that of pure water which was occurred in the highest volume fraction of nanofluid (0.25%) at Reynolds number of 5000.
2. Sahin et al (2013)	Experimental investigation of heat transfer and pressure drop characteristics of Al2O3–water nanofluid	Al2O3/Water Nanofluid, 0.5, 1, 2,3, and 4% volume fraction.	Adding nanoparticles into pure water enhanced heat transfer for the cases in which the particle volume concentrations were lower than 2 vol.%. Up to theparticle volume concentration of 1 vol.%, the Nusselt number increased with the increase of the Reynolds number as well as the particle volume concentration.
3. Chandrasekar et. al (2010)	Experimental Studies on Heat Transfer and Friction Factor Characteristics of Al2O3/Water Nanofluid in a Circular Pipe Under Transition Flow With Wire Coil Inserts	Al2O3/Water Nanofluid, 0.1% concentration	The friction factors of the Al2O3/water nanofluid are almost equal to those of water under the same Reynolds number. Dilute nanofluids will not cause an extra penalty in pump power.

Table 3 continued…

4. Liu et. al (2009)	Performance of Water Chiller System using Nanofluid	MWCNTs/water, 0.1% volume fraction	At the standard rating condition, the introduction of nanofluids gave rise to an increase in the COP by 5.15%, relative to a condition without nanofluids. Furthermore, the pressure drop penalty of the addition of nanofluids was almost negligible.
5. Manay et. al (2012)	Thermal performance Analysis of Nanofluids in Microchannel Heat Sinks	CuO/Water and Al2O3/Water, 0, 0.5, 1, 1.5, and 2% volume fraction	Heat transfer increased with increasing Reynolds number as well as particle volume concentration. CuO-water nanofluid provided higher heat transfer than that of Al2O3. No significant increase in friction factor was observed by the addition of the Nano particles into the pure water.
6. Selvakumar and Suresh (2012)	Convective performance of CuO/water nanofluid in an electronic heat sink	CuO/Water, 0.1 and 0.2% volume fraction	The pressure drop characteristics of CuO/water nanofluids is also studied and rise in pressure drop associated with the inclusion of nanoparticles in deionised water is not much compared to the rise in convective heat transfer coefficient.
7. Xuan and Li (2003)	Investigation of Convective Heat Transfer and Flow Features of Nanofluids	CuO/Water, 0.1, 0.3, 0.5, 0.8, 1.0, 1.2, 1.5, 2.0% volume fraction	Nanofluids are expected to be ideally suited for practical application with incurring little or no penalty in pressure drop because the nanoparticles are so small that the nanofluids behaves like a pure liquid.

Table 3, continued…

8. Ijam et. al (2012)	Cooling of minichannel heat sink using nanofluids	Al2O3/Water and TiO2, 4% volume fraction	Pressure drop increased with increasing mass flow rate and density of the nanofluid (Volume Fraction of the nanoparticles)
9. Duangthongs, Wongwises (2009)	An experimental study on the heat transfer performance and pressure drop of TiO2-water nanofluids flowing under turbulent flow regime	TiO2/Water, 0.2-2% volume fraction	Pressure drop was slightly higher than that of pure water and increases with the increasing volume fraction of Nanoparticles.

CHAPTER III

EXPERIMENTAL SET UP AND METHODOLOGY

The measured data of static pressure are key to the outcome of this research, because the behavior of upstream and downstream pressure determines the results of pressure drop and loss coefficients. In order to accurately measure the static pressure at different mass flow rates, a flow loop and test sections were designed.

This chapter primarily focuses on the flow loop and test section design. Major components will be discussed in details. Furthermore, the methodology and equations for quantifying the pressure drop and loss coefficient will be discussed.

3.1 Test Section

The schematic of the test section is shown in Figure 21. The downstream and upstream channels were machined from a 1 inch diameter aluminum rod, and then flanged. For the purpose of this study, it is crucial to maintain the isothermal condition of the fluid. In order to maintain the incompressible flow, properties of the fluids (specifically density) should remain constant or don't change significantly.

The interior and exterior views of the assembled test section are shown in Figures 20 and 21, respectively.

Figure 20. *The exterior view of the test section*

Five pressure taps, located at one inch apart from each other, are connected to the upstream and downstream channels. Each channel insert of pressure tap is made out of brass and is 1/8 inch outside diameter and 1 inch long. Because it is very important not to disturb the flow, channel inserts do not have a direct contact with the flow, they are rather fed by thin holes as shown in Figure 20.

Location of tube inserts for pressure taps   **Flange**   **Singularity**   **Flow channels**
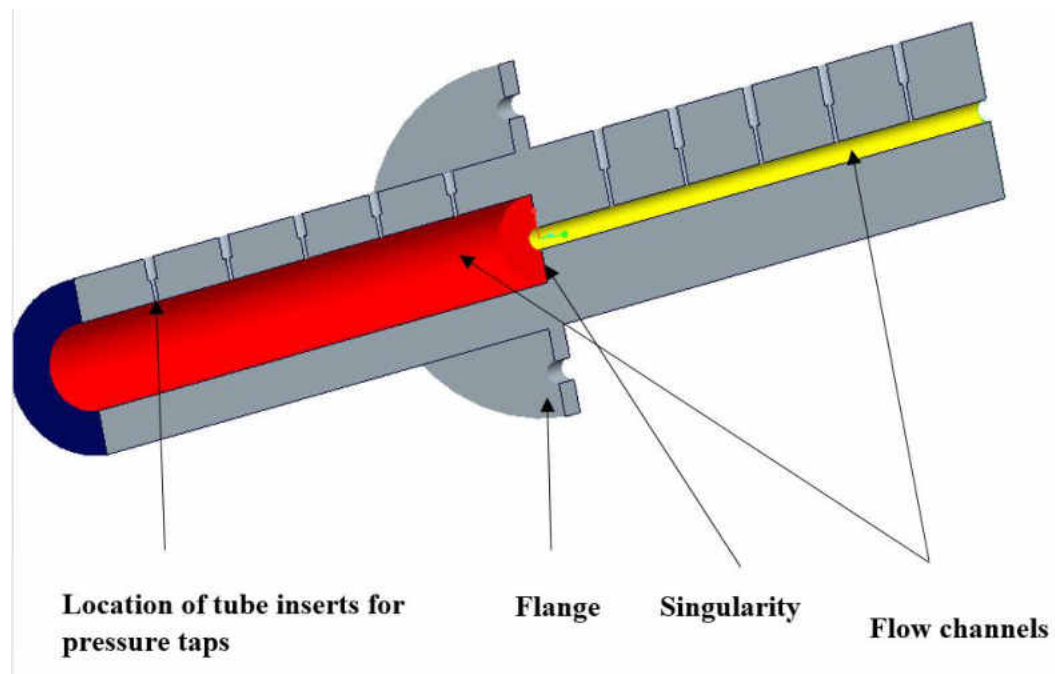
Figure 21. *The interior view of the test section*

Some of the biggest issues for low viscosity fluid measurements are channel leakage and formation of bubbles in fluid. In order to prevent the leaking, tube inserts were glued to the connectors by using the silicon epoxy.

3.2. Flow Loop

The diagram in Figure 22 depicts the closed loop used for conducting differential and static pressure measurements. The primarily components of the loop are the fluid storage tank, gear pump, heat exchanger, flow meter, pressure transmetters, static pressure probe, DC power supply, data acquisition system, and pipes network used to connect major componentes of the loop. The pipes network consists of ¼ inch stainless steel tubing, flexible PVC tubing, and 1/8 inch brass channel for pressure taps.
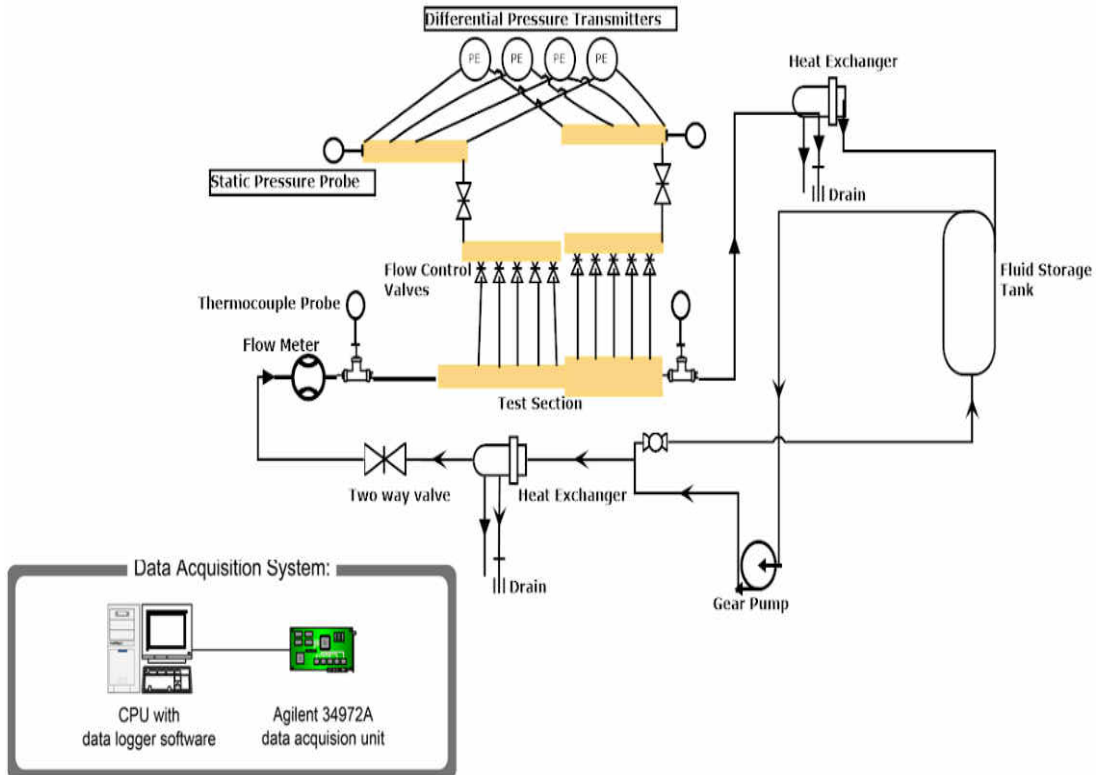
Figure 22. *Closed flow loop for conducting pressure measurements*

The fluid storage tank is the starting point of the fluid circulation through the loop. The fluid is pumped by the gear pump and passes through the counter flow heat exchanger which primary role is to regulate the fluid temperature. The fluid losses its gained heat from the pump by passing through the heat exchanger, and therefore the fluid temperature is regulated. The flow meter indicates the mass flow rate of the fluid entering the test section. Next to the flow meter is the thermocouple which is used to measure the inlet temperature of the fluid. Four differential pressure transmitters were calibrated for different pressure range and are used to take the pressure drop readings. There are two manifolds incorporated into the loop to support the fluid flow control. One manifold is connected to the pressure taps from the upstream channel and the other one is connected to pressure taps from the downstream channel. The inlet and outlet static pressure probes are used to measure upstream and downstream respectively. Because it is important maintain the fluid

44

at nearly isothermal conditions, the second thermocouple is installed at outlet of the test section to measure the exit temperature which is used to determine the temperature drop. The fluid exiting the test section passes through a second heat exchanger for temperature regulation before going back to the storage tank. The data acquisition system is connected to the loop.

3.2.1 Fluid Storage Tank

The tank used for fluid storage is shown is Figure 23. It is cylindrical and made out of PVC material. The tank is 0.25 m diameter, 0.3048 m long, and has the capacity of 15 liters. The tank placed at 1 m above the gear pump in order to reduce the amount of pumping power requirement. The tank is completely sealed in order to prevent any leakage and excessive energy exchange with the surrounding environment. In order to ensure the purity, the fluid is periodically monitored and replaced as deemed necessary.
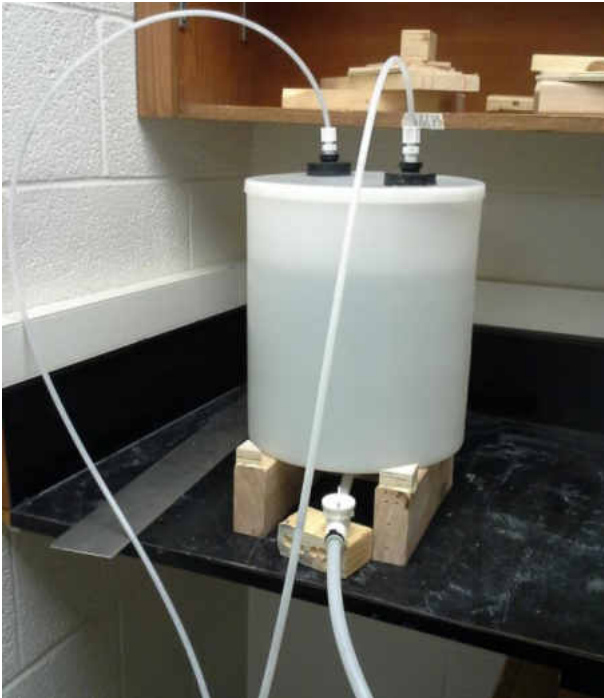
Figure 23. *The fluid storage tank*

3.2.2 Gear Pump

The pump used in this research is a Liquiflo gear pump model 35 F and is pictured in Figure 24. To the left it is connected to the T junction and directly storage tank to the right. It is designated to operate at maximum flow of 12.8 LPM and maximum pressure drop of 100 psi. The pump operates at a wide range of speeds up to a maximum of 1750 RPM and within the ambient temperature range of -20°C and 40°C. The pump performance curves are presented in Figure 25. It has been tested by the manufacturer for water and oil at different differential pressures, flow rates, and pumping power. As opposite to water results, the flow rate drops slowly with increasing differential pressure.

Figure 24. *Liquiflo sealed gear pump, model 35 F*
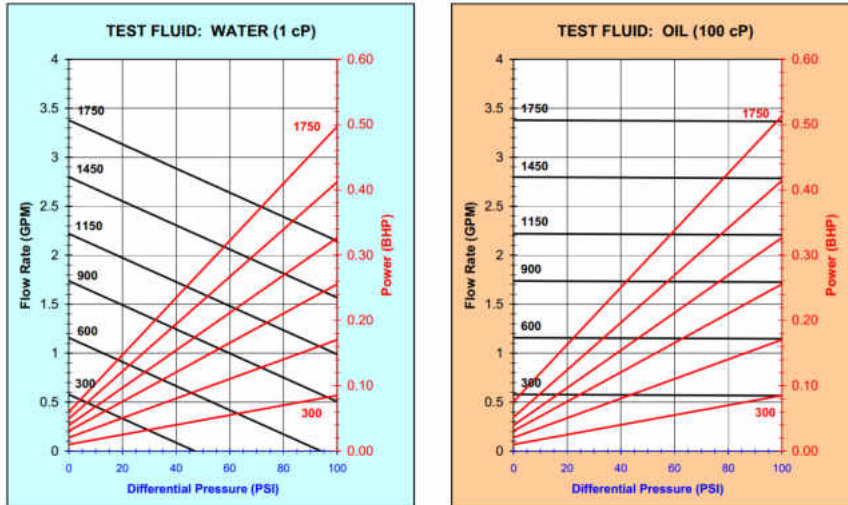
Figure 25. *The liquiflo gear pump performance curves for water and oil,*
(http://www.liquiflo.com/v2/gears/3/35f.htm)

3.2.3 Mass Flow Meter

The flow meter used in the flow loop is pictured in Figure 26. It is a micro mass flow sensor of CMFS010M model and Elite series. The sensor is ±0.05% accurate for mass flow rate and volume and ±1°C for the temperature measurements. It is currently calibrated for a maximum mass flow rate of 30 g/s. Its operation is such that the fluid is passed through a U-shaped channel that vibrates at a given frequency. The angular velocity and inertia of the fluid can cause the U-shaped channel to twist. The twisting of the two legs of the U-shaped channel causes an angular momentum change which is sensed by an electromagnetic sensor.

47

Figure 26. *Mass flow rate meter, model CMFS010M*

3.2.4 Thermocouples

The thermocouples were used to measure the bulk inlet and outlet temperatures of the fluid (see Figure 27). They are manufactured by Omega Company and have model no. TMQSS-020U-6. Such thermocouples are 6 inches long and have 0.02 inch diameter probe and are rated for temperatures up to 220°C.

Figure 27. *Thermocouples, model TMQSS-020U-6, (www.omega.com)*

3.2.5 Pressure Transmitters

Pressure transmitters used in this research are shown in Figures 28 and 29. Pressure transmitter in Figure 28 measures differential pressures. Four differential pressure transmitters were used with capabilities of measuring 300 psi, 30 psi, 9 psi, and 2.5 psi pressure drops. They are all directly connected to the two manifolds.

Each manifold is a converging point for upstream and downstream channels. The pressure transmitter outputs DC current which is directly proportional to the pressure drop. If a pressure drop reading is above the maximum range of a given transducer, the data acquisition unit is programmed to produce an alarm, after which a valve on the pressure transmitter itself allows for the isolation of the particular transmitter. Pressure transmitters are connected in parallel to each other in order to produce independent accurate readings.

Figure 28. *Rosemount 3051S pressure transmitters used to measure pressure drops,*
(http://www2.emersonprocess.com/)

Figure 29. *Omegadyne brand (model PX 409-050G10V) static pressure probe,*
(www.omegadyne.com)

Static pressure transmitter shown in Figure 29 measures static pressure along the

channel. It is rated for 0 to 50 psi and -29 to 85°C temperature range.

3.2.6 Heat Exchangers

For the purpose of this study, two heat exchangers have been incorporated into the loop primarily for controlling the inlet and outlet temperatures of the fluid. They are ½ inch diameter stainless steel tubing with length of 38 inches and fitted coaxially to the ¼ inch tubing in the experimental loop. One heat exchanger is connected between the gear pump and flow control valve in order to regulate the temperature of the fluid, before it enters the flow meter. The other heat exchanger is connected in the loop after the outlet of the test section in order to regulate the temperature of the fluid coming back to the storage tank.

3.2.7 Data Acquisition System

The instrument used for acquiring data for this study is an Agilent data acquisition unit (model 34972A) with a 20 channel multiplexer. It is pictured in Figure 30. The channels of multiplexer are connected to the flow loop measuring instruments (flow meter, pressure transmitters, and thermocouples). These instruments transmit a DC current output signal to the Agilent Data acquisition unit. This output is sensed and converted into output readings for pressure and mass flow rate. The data acquisition unit is connected to the PC via a USB cable. Agilent Benchlink Data Logger 3 is used to program the channels, set the reading time and capture data. Captured data are exported and organized into spreadsheets files for further processing.

Figure 30. *Agilent data acquisition unit (model 34972A)*

3.3 Pressure Transmitters Calibration

Pressure transmitters used for this study were calibrated by using a pneumatic hand pump of Ametek brand model T-970. This pump is rated for 0 to 580 psi pressure range. In addition, digital electronic gages from Dwyer (model DPG-107, range 0–300 psi) and (model DPG-104, range 0–50 psi) were also used in this process. The calibration was done by recording voltage outputs that corresponds to the amount of pressure applied to the hand pump. Before and during calibration, the pump should be checked for any leakage, because it lowers the pressure and thus affects the voltage reading.

The following steps are required for calibration:

1. Connect the digital pressure gauge to the hand pump. Then connect the hand pump to the high pressure side of the pressure transmitter.

2. Apply certain amount of pressure and record the voltage corresponding to the pressure.

3. Increase the applied pressure by the appropriate interval and record the voltage. Repeat this step until the higher range of the pressure transmitter has been reached.

4. Import voltage data for further processing.

Figures 31 through 36 represent the regression analysis that was done for pressure versus voltage in order to obtain the linear regression coefficient (R^2).

Figure 31. *Ametek hand pump for calibration of the pressure transducers.*
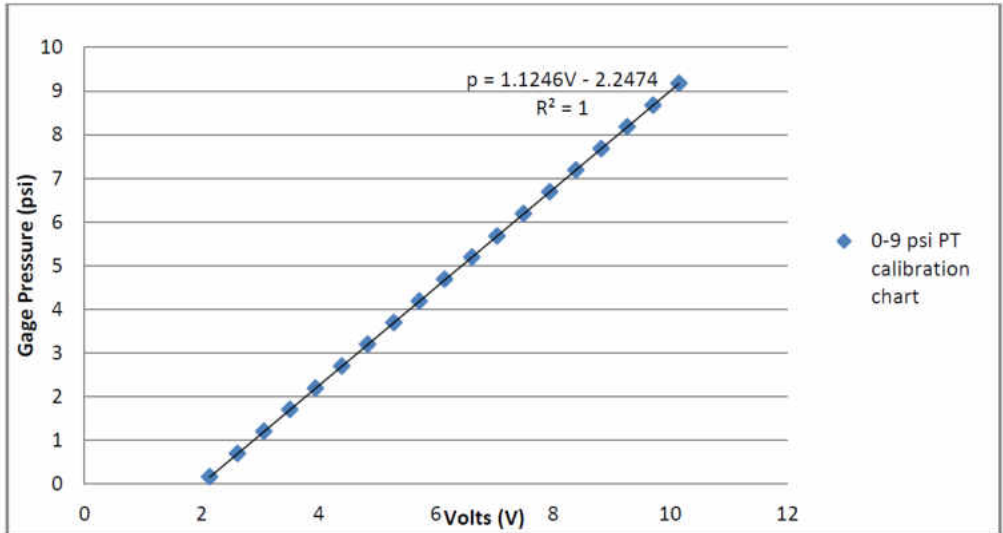
Figure 32. *Calibration graph for 0–9 psi pressure transmitter, Tiwari (2012).*
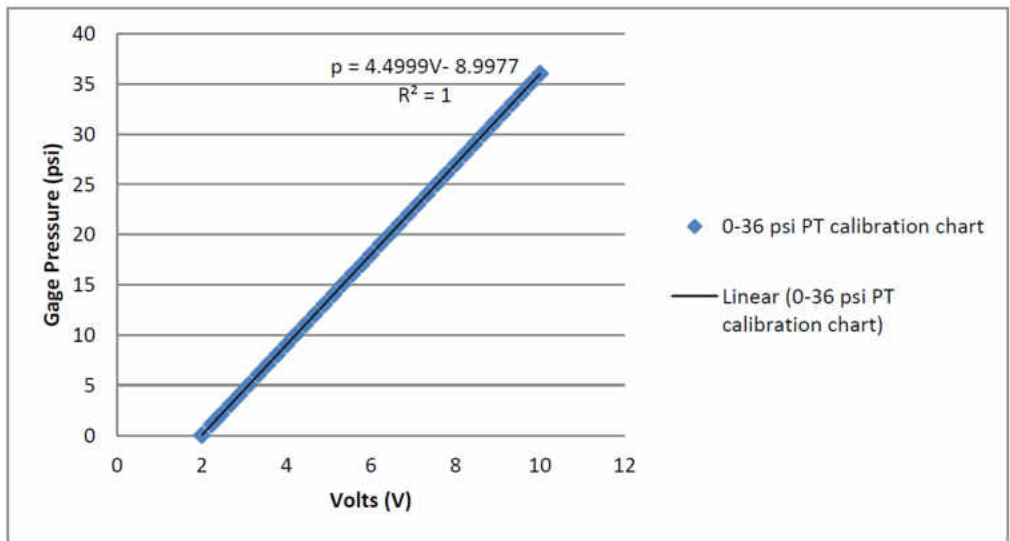
Figure 33. *Calibration graph for 0–30 psi pressure transmitter, Tiwari (2012).*
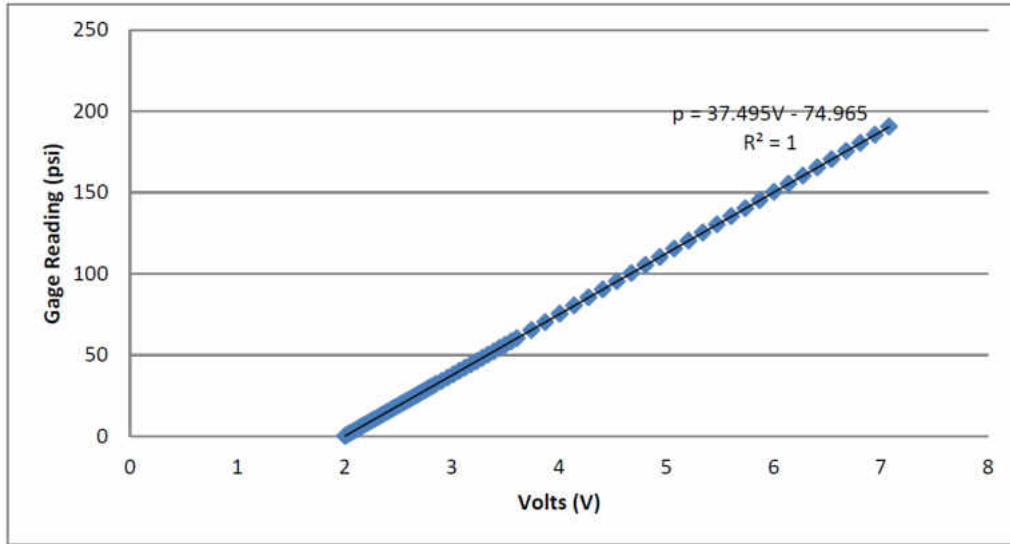
Figure 34. *Calibration graph for 0–300 psi pressure transmitter, Tiwari (2012).*
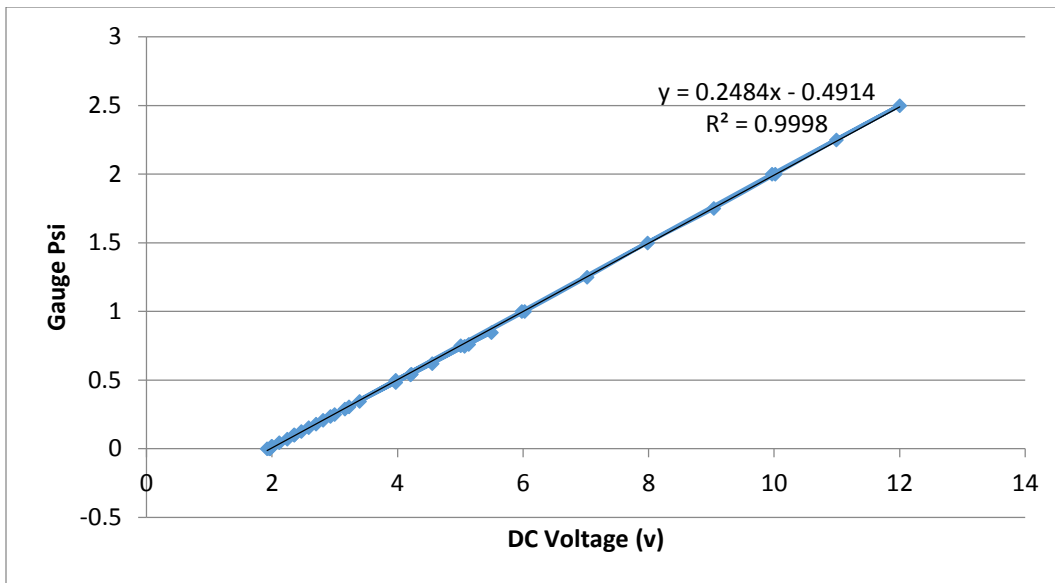
Figure 35. *Calibration graph for 0–2.5 psi pressure transmitter.*

y = 4.973661x + 0.442146
R² = 1.000000
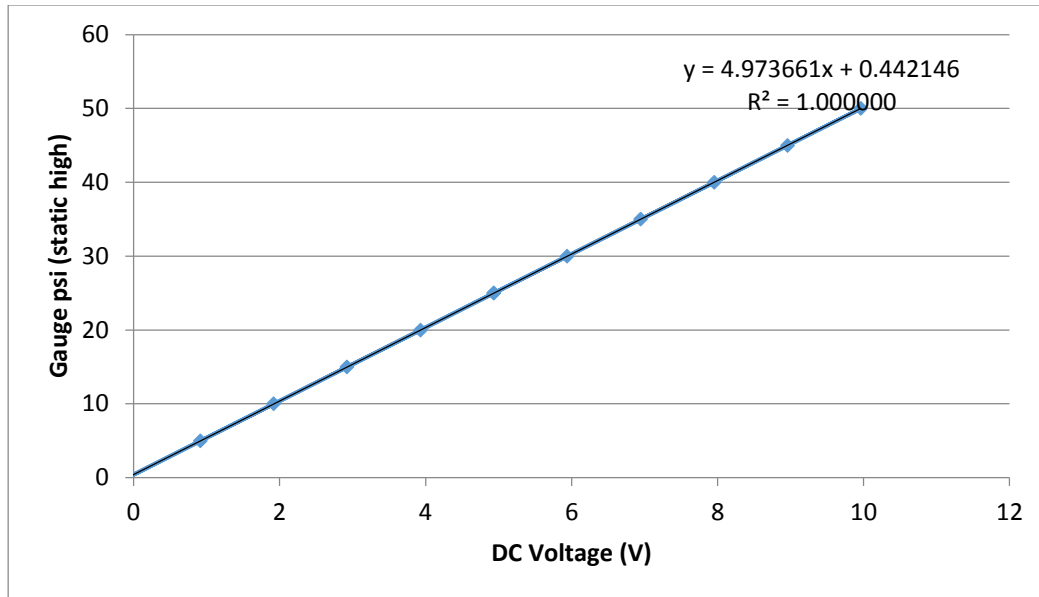
Figure 36. *Calibration graph for static pressure transmitter.*

4.4 Pressure Measurement

For static pressure measurements, Omegadyne static pressure probe was utilized; whereas four transmitters rated for different pressure ranges were used to measure differential pressure. The measurements were done symmetrically with respect to the singularity of the test section. The upstream and downstream channels of the test section have five equally spaced pressure taps.

The following are necessary steps for measuring and acquiring pressure data:

1. Check and make sure that there are no bubbles present in flexible channels that feed pressure transmitters. Bubbles can be eliminated by using the release valve located between the two manifolds that connect upstream and downstream pressure channels.

2. Close all the control valves except the two symmetrical ones that match the location at which you want to take a reading.

56

3. Start up the pump, mass flow meter, data acquisition unit and the pressure transducers.

4. Set the pump speed to match the desired flow rate.

5. Make sure that the bypass valve is open to limit the strain in the pump.

6. Adjust the metering valve to fine tune the flow rate.

7. Check if all the pressure transducers are stable and reading the same or approximately the same values.

8. Wait 5 minutes to allow the system to be in steady state.

9. Start recording the outputs from the mass flow meter, pressure transducers and bulk temperature measuring thermocouples for 3 minutes.

10. See if all the recordings indicate a steady state process.

11. Open the control valves of the desired locations.

12. Once you have taken five readings at five locations of the test section for one flow rate, increase or decrease the flow rate by 2.5 g/s by fine tuning the metering valve or increasing the speed of the pump and repeat the process.

3.5 Experimental Data Processing Methodology and Uncertainty

Bias and precision uncertainties were analyzed for velocity, pressure drop, and loss coefficient at various mass flow rates. Bias uncertainties were calculated based on the instruments accuracies. Instruments used for uncertainty include caliper (accuracy of $\pm$ 0.001 in) for length, mass flow meter (accuracy of 0.05%), and static pressure transmitter (accuracy of 0.08%). Precision uncertainties were calculated from standard deviations of the mass flow rates and static pressures data.

3.5.1 Mean Velocity

The velocity fluctuates in channels, especially in channels with sudden area change wherein the flow is disturbed by the construction of the channel. For the purpose of this study, a mean velocity was used to quantify other parameters such as Reynolds number, pressure drop, and loss coefficient. The velocity was not a direct measureable quantity in this experiment; it was rather calculated by using the measured mass flow rate data. Equation (34) was used to calculate the mean velocity for a specific channel.

$$U = \frac{4\dot{m}}{\pi\rho d^2} \quad\text{...} (34)$$

Mass flow rate and diameter were found to contribute largely to the velocity uncertainty. Because all measurements were taken at nearly constant temperature, density contribution to the velocity uncertainty can be ignored. Equation (35) was used to calculate the velocity uncertainty.

$$u_v = \left[\left(\frac{1}{\dot{m}}u_m\right)^2 + \left(\frac{-2}{d}u_d\right)^2\right]^{\frac{1}{2}} * V_1 \quad\text{...} (35)$$

On average, the overall velocity uncertainty was found to be 2.49 %. The detailed results for velocity uncertainty are compiled in appendix.

3.5.2 Pressure Drop

The pressure drop at singularity was used to calculate the loss coefficients for sudden expansion and contraction. The singularity or construction is defined at the axial zero location along the test section. This is the junction point for upstream and downstream channels. Because there is no direct analytical equation or a measurement method that can be used to find the pressure drop at singularity, an indirect methodology was used. First

pressure profile was obtained by plotting static pressures against pressure taps locations with respect to the singularity. Next the linear equations were obtained from pressure profiles of upstream and downstream flows. From these two linear equations, static pressures at singularity were obtained and used to calculate pressure drop.

The uncertainties of measured static pressures are within 0.144-1.800% range for all mass flow rates for sudden area contraction. This uncertainty range is 0.277-1.507% for sudden area expansion. The static pressure uncertainty for sudden area expansion was a little higher compared to sudden area contraction, because of some fluctuations in static pressure at lower flow rates.

The total uncertainty for pressure drop at singularity was found by doing vectorial addition of bias and precision uncertainties for pressure drop. The bias uncertainty was calculated based on 0.08% pressure transmitter. In order to cover the maximum possible range of error, the maximum standard deviation for all static pressure data was doubled and taken to be used for precision uncertainty of pressure drop at singularity. Based on 95% confidence level analysis, the minimum uncertainty in pressure drop values is $\pm 0.81\%$ while the maximum is $\pm 5.72\%$ for sudden area contraction. The corresponding results for sudden area expansion are $\pm 1.39\%$ for minimum and $\pm 3.39\%$ for maximum.

3.5.3 Loss Coefficient

A) Sudden area expansion

In Chapter I, total pressure loss was introduced and was defined as the sum of pressure drop at singularity (ΔP_e) and losses caused by sudden area change.

Equation (36), which is used to quantify loss coefficient due to sudden area expansion, was derived from Equation (22). Figure 37 demonstrates how ΔP_{eo} is obtained by linear interpolation.

$$K_e = \frac{\Delta P_{eo} - \frac{1}{2}\rho U_1^2(\sigma^2 - 1)}{\frac{1}{2}\rho U_1^2} = \frac{\Delta P_{eo}}{\frac{1}{2}\rho U_1^2} - (\sigma^2 - 1) \quad \dots\dots\dots\dots\dots\dots\dots\dots\dots\dots\dots\dots\dots \quad (36)$$
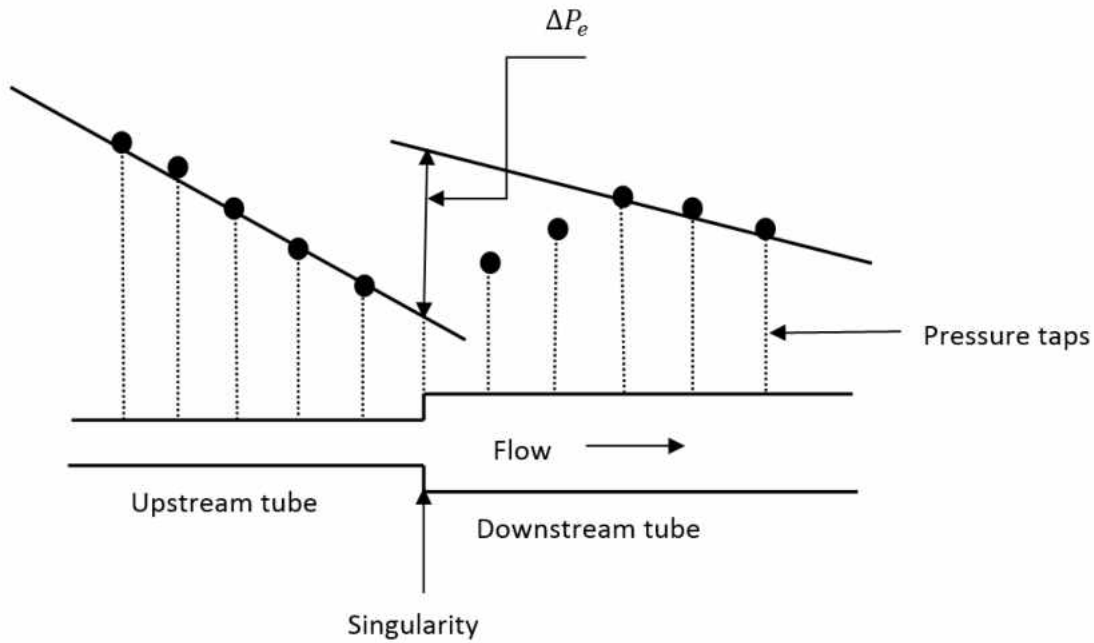
Figure 37. *Depiction of pressure gradient through sudden area expansion and methodology for finding pressure drop at singularity*

Bias and precision uncertainty in loss coefficient values for sudden expansion and contraction were both calculated by using the Equation (37). The main parameters that were considered to contribute to uncertainty are velocity and pressure drop. Area ratio could contribute to uncertainty, but it was not considered because it is calculated based on diameter and diameter uncertainty was considered when calculating velocity uncertainty.

$$u_{ke} = \left[\left(\frac{u_{\Delta pe}}{\Delta P_e}\right)^2 + \left(\frac{-2}{V_1}u_V\right)^2\right]^{\frac{1}{2}} * K_e \quad \dots\dots\dots\dots\dots\dots\dots\dots\dots\dots\dots\dots \quad (37)$$

The bias uncertainties were lower compared to precision uncertainties. The probable cause is the some fluctuation in static pressure that increases standard deviation at lower mass flow rates. This fluctuation was particularly observed at downstream at mass flow rates less than 12.5 g/s. On average bias uncertainty was 3.19%, whereas precision uncertainty was 4.18%. Based on 95% confidence level analysis, the uncertainty in K_e values is estimated to be in ±4.36% to ± 8.10% range.

Figure 38 represents the variation of the percentage of the expansion loss coefficient uncertainty with various mass flow rates. As it is explained in the previous paragraph, it can be observed that the uncertainty increases with decreasing mass flow rate.
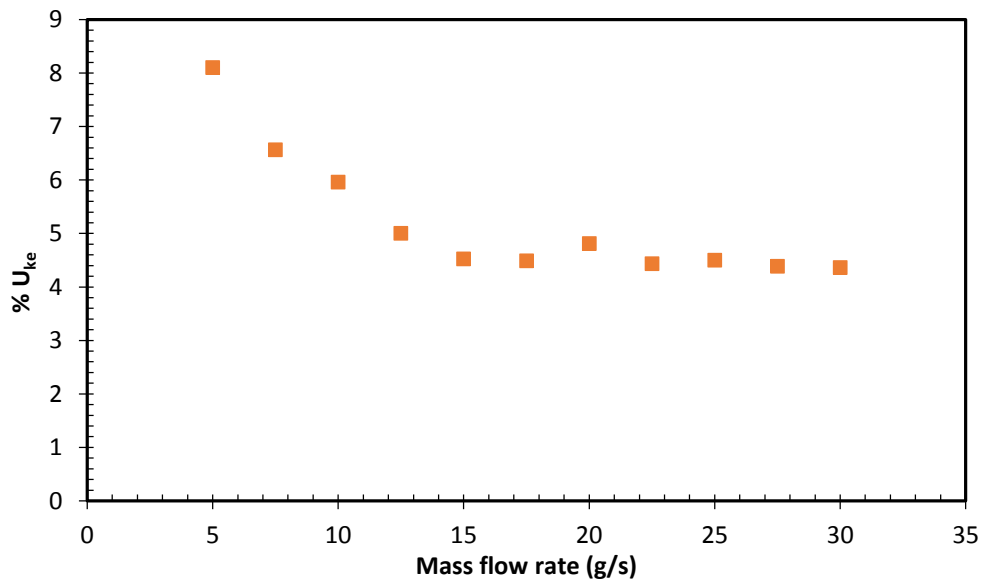
Figure 38. *Variation of total percentage of the expansion loss coefficient uncertainty with mass flow rates*

B) Sudden area contraction

The methodology that was used to quantify loss coefficient and uncertainty for sudden expansion, was also used for sudden area contraction. Because channels of the test sections

were interchanged, the sign of the term that contains area ratio in Equation (36) was also changed; and thus Equation (38) was obtained.

$$K_c = \frac{\Delta P_c + \frac{1}{2}\rho V_1^2(\sigma^2 - 1)}{\frac{1}{2}\rho V_1^2} = \frac{\Delta P_c}{\frac{1}{2}\rho V_1^2} + (\sigma^2 - 1) \quad\ldots\ldots\ldots\ldots\ldots\ldots\ldots\ldots\ldots\ldots\ldots\ldots \quad (38)$$

Similar to sudden expansion, pressure drop at singularity was obtained by linear extrapolation (Figure 39). For sudden contraction, pressure drop at singularity is positive as opposed to sudden expansion, because static pressure in smaller channel (downstream) drops much faster compared to bigger channel (upstream) due to the increase in velocity as the flow diameter is decreased.
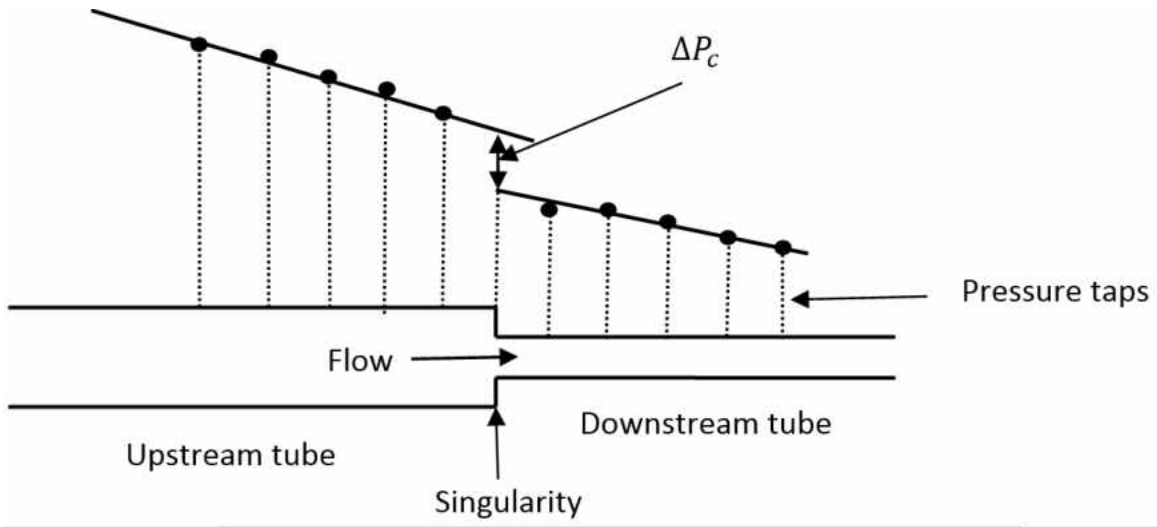
Figure 39. *Depiction of pressure gradient through sudden area contraction and methodology for finding pressure drop at singularity*

Equation (37) remains valid for quantifying uncertainty in loss coefficient values for sudden area contraction.
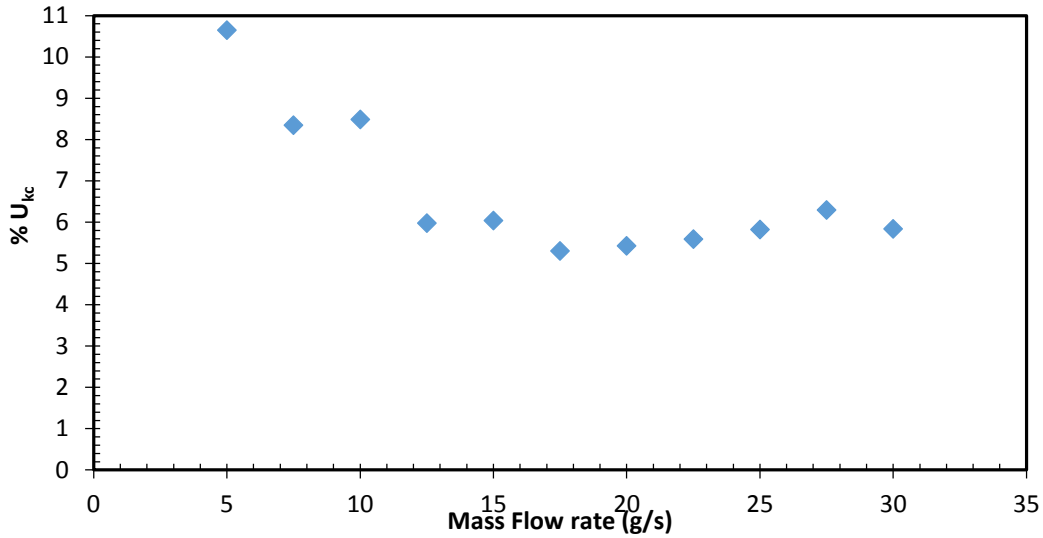
Figure 40. *Variation of total percentage of the contraction loss coefficient uncertainty with mass flow rates*

On average bias uncertainty was 3.43%, whereas precision uncertainty was 4.21%. Based on 95% confidence level analysis, the uncertainty in K_c values is estimated to be in $\pm 5.30\%$ to $\pm 10.65\%$ range. The results are slightly higher compared to the results of sudden area expansion uncertainty analysis; because for sudden contraction pressure drop is high and loss coefficient values are lower.

CHAPTER IV

RESULTS AND DISCUSSION

In this chapter, experimental results will be discussed and compared theoretical results. For the purpose of this study, experimental data of two types of fluids were taken and analyzed. The results of static pressure and loss coefficient for water and 9.58% silicon dioxide nanofluid will be discussed. Experiments using water were performed by using the test section of 0.0625 area ratio. Experiments using nanofluid were performed on two test sections ($\sigma = 0.0625$ and 0.0140).

4.1   Experimental Results with water

4.1.1 Sudden Area Expansion

4.1.1.1 Static Pressure

Static pressure measurements were taken at room temperature of $26 \pm 2^0\text{C}$. The change in temperature was not significant enough to affect the density. Therefore, a unique water density (996.5 kg/m^3) was used for all calculations performed. Static pressure data were taken at five pressure taps locations for upstream and downstream of the singularity. Upstream pressure taps are one inch from each other and symmetrical to downstream pressure taps. In order to gain much insight of how the flow rate affects pressure drop and loss coefficient, various mass flow rates ranging from 5 to 30 g/s with 2.5 g/s increment size were considered.

The final results of static pressure were obtained by averaging several static pressure data measured for a certain mass flow rate. On average, each data point was repeated four times. Figures 41 to 45 present and compare pressure gradients for different mass flow rates. In general, the pressure gradient has been observed to decrease with an increasing flow rate. The flow downstream loses static pressure and would recover some at about 3 inches from the singularity. This pattern is seen for all the flow rates.
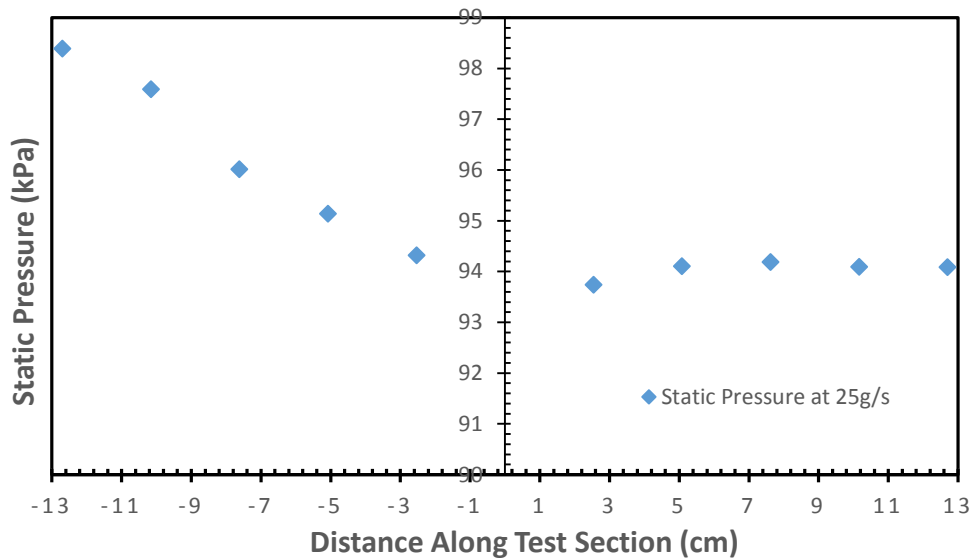
Figure 41. *Variation of water static pressure with distance along test section, $\dot{m}$ = 25 g/s for sudden area expansion (σ = 0.0625)*
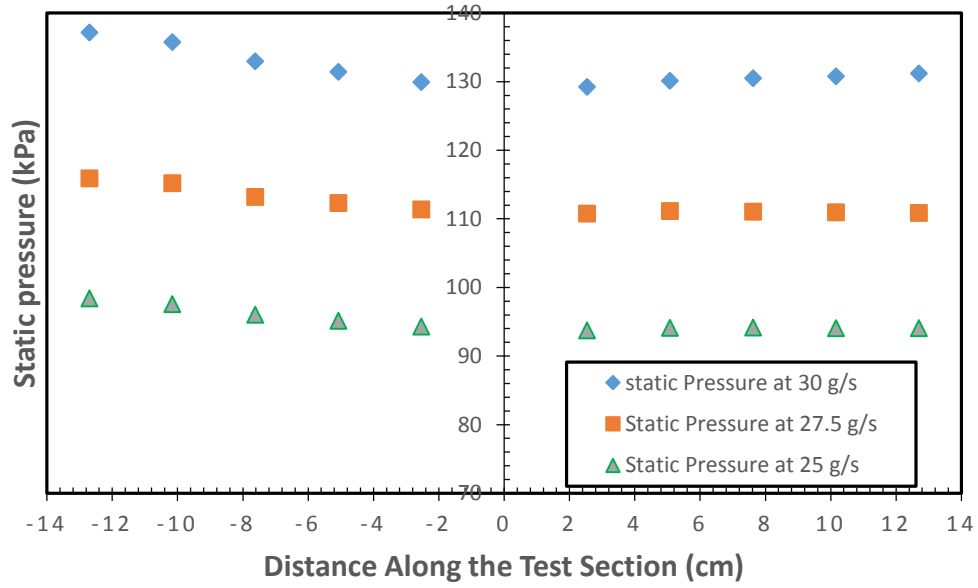
Figure 42. *Variation of water static pressure with distance a long test section and mass flow rate, ṁ= 30, 27.5, and 25 g/s for sudden expansion (σ = 0.0625)*
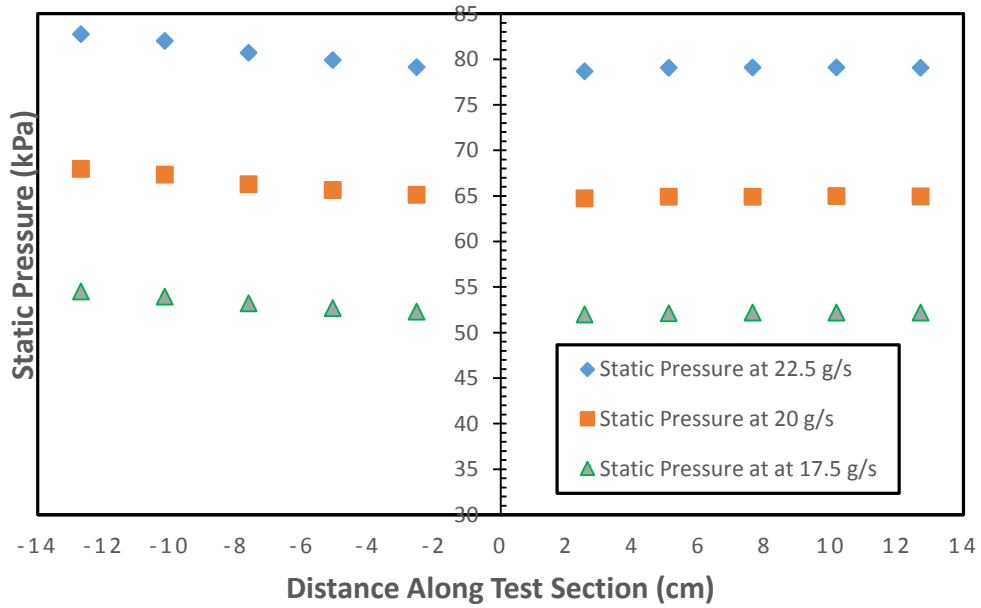
Figure 43. *Variation of water static pressure with distance a long test section and mass flow rate, ṁ = 22.5, 20, 17.5 g/s for sudden expansion (σ = 0.0625)*
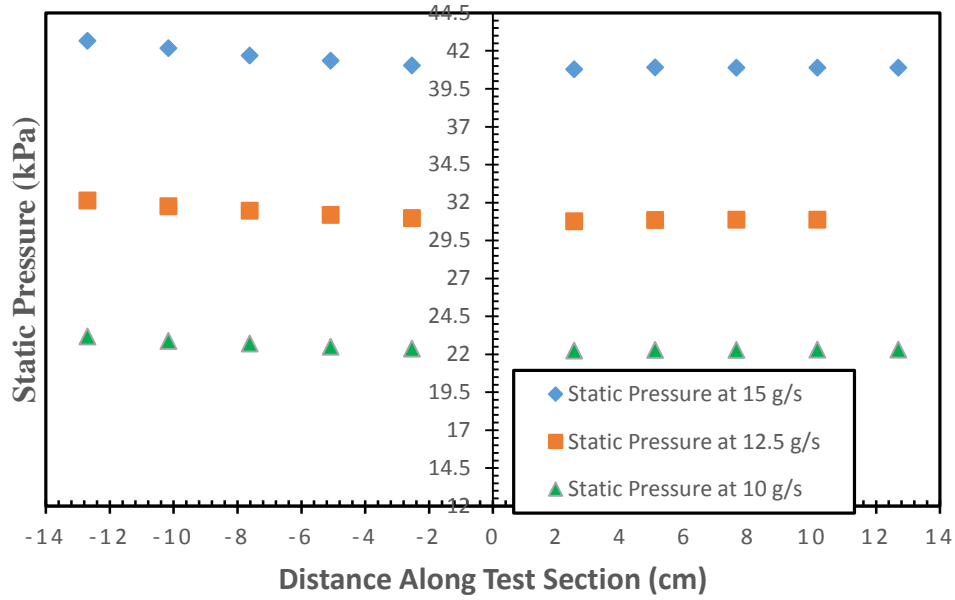
Figure 44. *Variation of water static pressure with distance a long test section and mass flow rate, ṁ = 15, 12.5, and 10 g/s for sudden expansion (σ = 0.0625)*
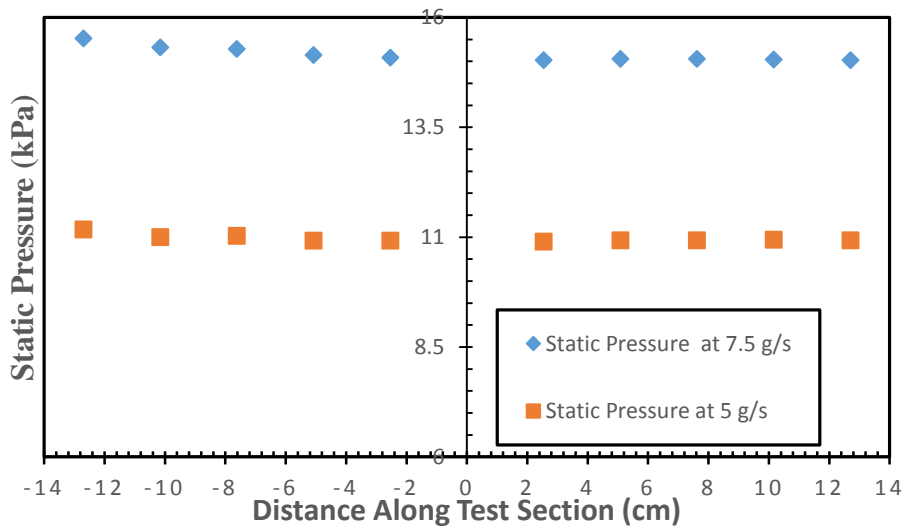
Figure 45. *Variation of water static pressure with distance a long test section and mass flow rate, ṁ = 7.5 and 5 g/s for sudden expansion (σ = 0.0625)*

4.1.1.2 Pressure Drop and Loss Coefficient

Pressure drop at singularity (ΔP_{eo}) was obtained by linearly extrapolating static pressure curve to zero location and by subtracting the upstream from downstream static pressures. The acceleration of the fluid near the singularity causes the upstream static pressure to drop much faster compared to downstream static pressure. At downstream, static pressure drops, and then is quickly recovered and becomes nearly stable at about 2 or 3 inches from the singularity (see Figure 41). This trend, which is observed at all mass flow rates measured, causes the pressure drop at singularity to be negative. The experimental results indicate that the absolute value of pressure drop increases with increasing flow rate.

Table 4. Summary of experimental results of water pressure drop at singularity
for sudden expansion ($\sigma = 0.0625$)

$\dot{m}$(g/s)	U_1(m/s)	Re	ΔP_{eo}(psi)	ΔP_{eo}(pa)
5.01	0.64	2258	-0.01	-68.26
7.49	0.95	3227	-0.01	-88.25
10.00	1.27	4307	-0.01	-102.73
12.49	1.58	5377	-0.02	-162.00
15.01	1.91	6960	-0.04	-248.21
17.49	2.22	8155	-0.05	-355.08
20.00	2.55	9332	-0.10	-495.73
22.49	2.86	10474	-0.09	-655.00
25.00	3.18	11051	-0.11	-730.84
27.49	3.50	12814	-0.13	-903.21
30.02	3.82	13261	-0.17	-1172.11

After obtaining pressure drop results, Equation (36) was then utilized to quantify the loss coefficient due to sudden area expansion, and results plotted in Figure 46. The loss coefficient increases with increasing Reynolds number. Once the flow becomes fairly

turbulent, the change in loss coefficient is significantly reduced. It was predicted that loss coefficient should be constant for all mass flow rate measured. This means that Carnot equation, $K_e = (1-\sigma)^2$, which is widely used to predict loss coefficient, does not work for low Reynolds numbers.
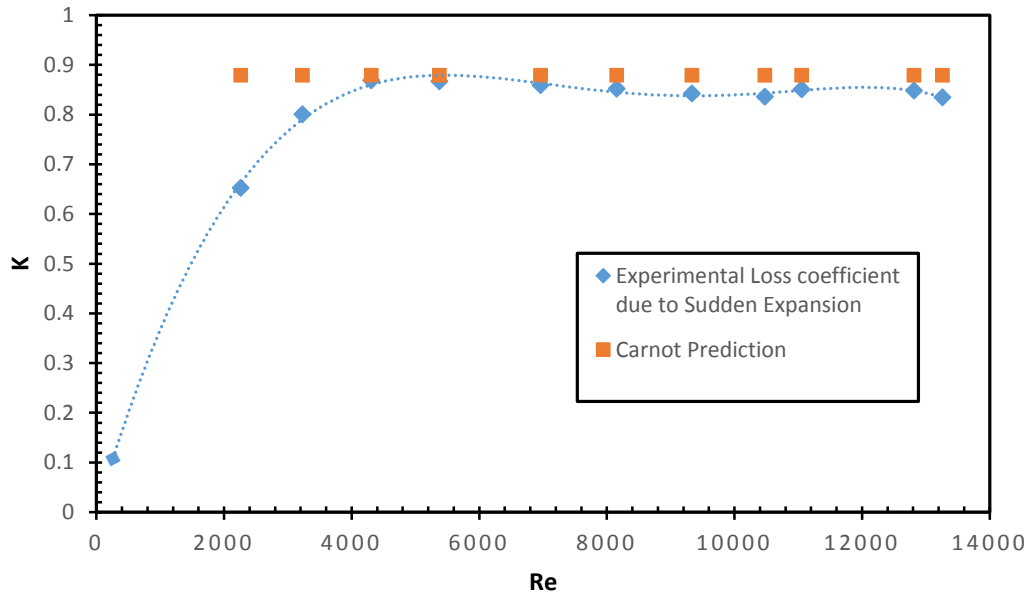
Figure 46.   *Comparison of experimental and theoretical loss coefficients predicted by Carnot equation*

4.1.1.3 Comparative Analysis of Predicted Pressure Drops and Loss Coefficients with Experimental Results

In attempting to predict pressure drop and loss coefficient due to sudden area expansion, a flat velocity profile was assumed upstream and downstream. This renders momentum coefficients for the upstream and downstream channels to be one (K_{d1} =K_{d2} =1). Hence, Equation (25) reduces to Equation (16) of loss coefficient. By substituting Equation (25) into (23) and solving forΔP_{eo}, Equation (39) can be derived.

$$\Delta P_{e0} = \sigma(\sigma - 1)U_1^2 \, \rho \quad \text{...} \quad (39)$$

Equation (39) was utilized to predict the pressure drop at singularity. Because this pressure drop is negative, the magnitude was used to compare experimental with predicted pressure drop at various Reynolds numbers (Figure 47).
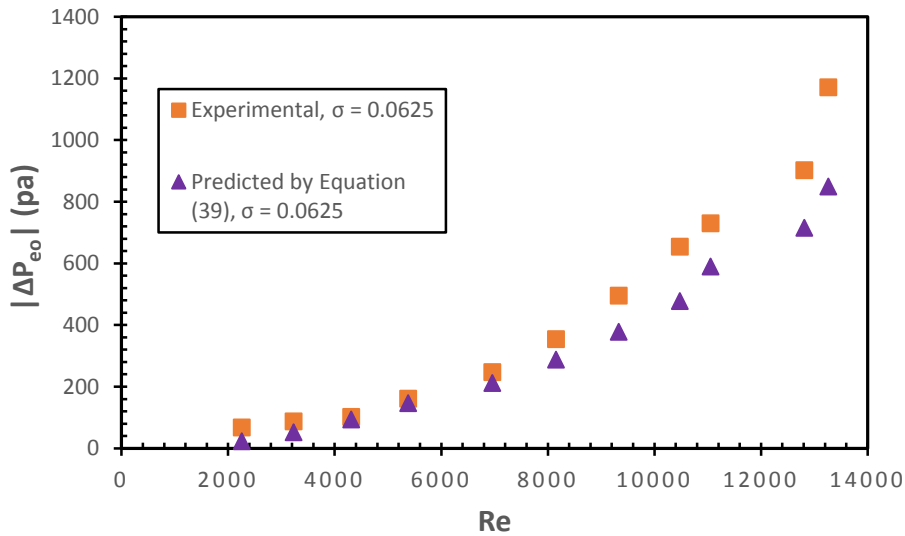
Figure 47. *Comparison of predicted with experimental pressure drop for water flow*

For Reynolds numbers greater than 8000, experimental pressure drop became increasingly high and so did the percentage difference between the two pressures results. This means that Carnot equation which was used to predict loss coefficient does not

quantify well pressure drop. Hence, a different correlation must be developed in order to fairly predict loss coefficient and pressure drop at singularity.

The experimental data show that as the flow increases, the change in downstream static pressure becomes fairly low. This means that, it is reasonable to assume a flat velocity profile at downstream of the singularity ($K_{d2} = 1$). However, it is not very reasonable to assume a flat velocity profile upstream since the static pressure changes with axial distance along the test section. Based on this assumption, Equation (25) reduces to Equation (38)

$$K_e = 1 - 2\sigma K_{d1} + \sigma^2 \ldots\ldots\ldots\ldots\ldots\ldots\ldots\ldots\ldots\ldots\ldots\ldots \quad (40)$$

By solving for K_{d1}, the upstream momentum equation can be calculated from Equation (41)

$$K_{d1} = \frac{1 + \sigma^2 - K_e}{2\sigma} \ldots\ldots\ldots\ldots\ldots\ldots\ldots\ldots\ldots\ldots\ldots \quad (41)$$

In attempting to correlate the momentum coefficient, the momentum coefficient was calculated using Equation (41) and loss coefficient results from various experimental data (area ratios of 0.0625, 0.145, 0.264, 0.2756, and 0.493) with Reynolds numbers ranging from 1746 to 120 000. As the results in Table 5 show, the momentum cannot be assumed to be a unit ($K_{d1} \neq 1$). This is especially true for lower area ratios at low or moderate Reynolds numbers.

Results in Table 5 were utilized to develop Equations (42) and (43) that can be used to predict momentum coefficient for upstream flow.

$$K_{d1} = 2.466 - 0.1185 \ln(R_{e1}) - 0.1689\sigma \ldots\ldots\ldots\ldots\ldots\ldots\ldots \quad (42)$$

$$K_{d1} = 5.5721 - 0.4619 \ln(R_{e1}) - 1.3788\sigma \ldots\ldots\ldots\ldots\ldots\ldots\ldots \quad (43)$$

By substituting Equations (42) and (43) into Equation (40) and rearranging terms, Equations (44) and (44) can be derived.

$$K_e = (1 - \sigma)^2 + 2\sigma[0.4619 \ln(Re_1) + 1.37885\sigma - 4.5721] \ldots\ldots\ldots\ldots \quad (44)$$

If we look closely at Equations (44) and (45), we can realize that the first term is Carnot equation and the second term was added to account for the changing flow rate.

$$K_e = (1 - \sigma)^2 + 2\sigma[0.1185\ln(Re_1) + 0.1689\sigma - 1.4666]\ldots\ldots\ldots\ldots\ldots\ldots \ (45)$$

Although both Equations (44) and (45) predict loss coefficients better than Carnot equation, it is worth noting some limitations. Equation (44) was proven to predict loss coefficient for channels with area ratio less than 0.3 ($\sigma < 0.3$) and Re < 7000. Equation (45) works better for channels with area ratio less than 0.4 ($\sigma < 0.4$) and

7000 <Re < 120 000.

Further steps can be taken and pressure drop at singularity can be predicted by using the newly developed loss coefficients equations. By rearranging terms in Equation (36), Equation (46) can be developed.

$$\Delta P_{eo} = \frac{\rho U_1^2}{2}(K_e - 1 + \sigma^2) \ \ldots\ldots\ldots\ldots\ldots\ldots\ldots\ldots\ldots\ldots\ldots\ldots\ldots\ldots\ldots. \ (46)$$

Figures 48, 49 and 50 show a direct comparison between experimental and predicted pressure drop at singularity at different Reynolds numbers. A tremendous improvement can be achieved by using Equation (46) to predict the experimental pressure drop at singularity and Equations (44) and (45) to predict loss coefficient at appropriate Reynolds numbers.

Table 5. Momentum coefficient as a function of Reynolds numbers and area ratio

σ = 0.0625		σ = 0.2756		σ = 0.145		σ = 0.264		σ= 0.493	
Re	K_{d1}	Re	K_{d1}	Re	K_{d1}	Re	K_{d1}	Re	K_{d1}
2257	2.77	1746	1.69	51234	1.18	26833	1.056	41704	1.060
3227	1.63	2572	1.49	59150	1.13	39082	1.075	55252	1.066
4307	1.08	3501	1.33	71095	1.241	49582	1.092	69596	1.045
5377	1.10	4512	1.32	71526	1.179	56193	1.094	83409	1.06
6960	1.16	5588	1.27	80881	1.269	56777	1.075	96690	1.045
8155	1.22	6714	1.26			61637	1.104	110769	1.051
9332	1.29					71943	1.079	121191	1.050
10474	1.35					86525	1.092		
11051	1.22					97026	1.104		
12814	1.25					97026	1.149		
13261	1.36					97026	1.100		
						110247	1.104		
						122108	1.092		
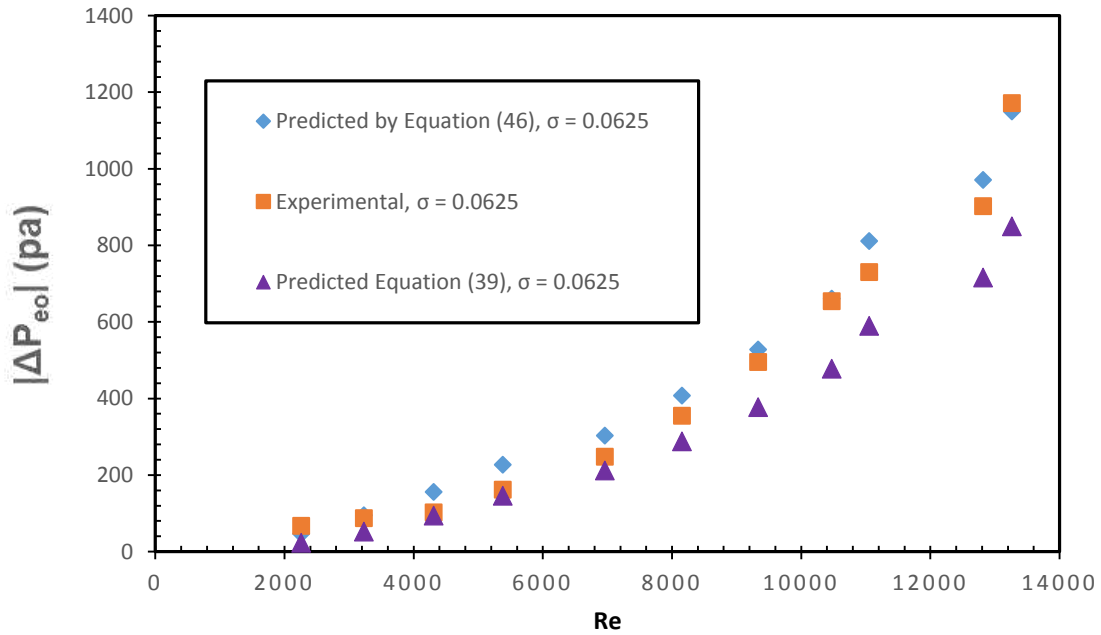
Figure 48. *Comparison between experimental and predicted pressure drop at singularity at different Reynolds numbers*
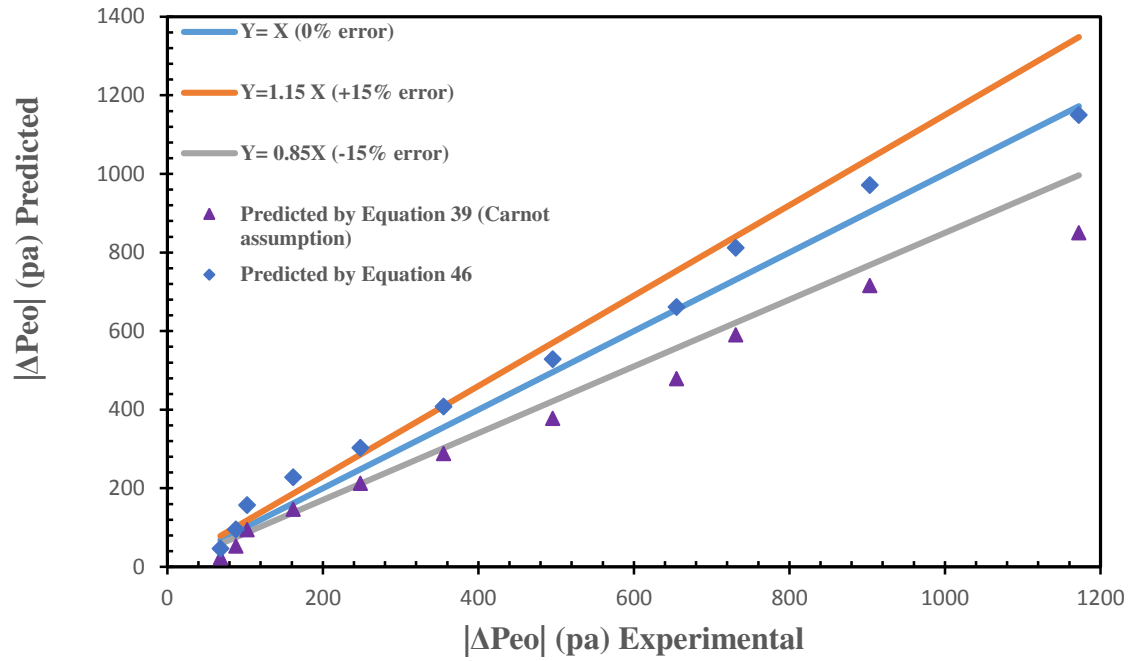
Figure 49. *Comparison between experimental and predicted pressure drop at singularity for sudden expansion, σ = 0.0625*
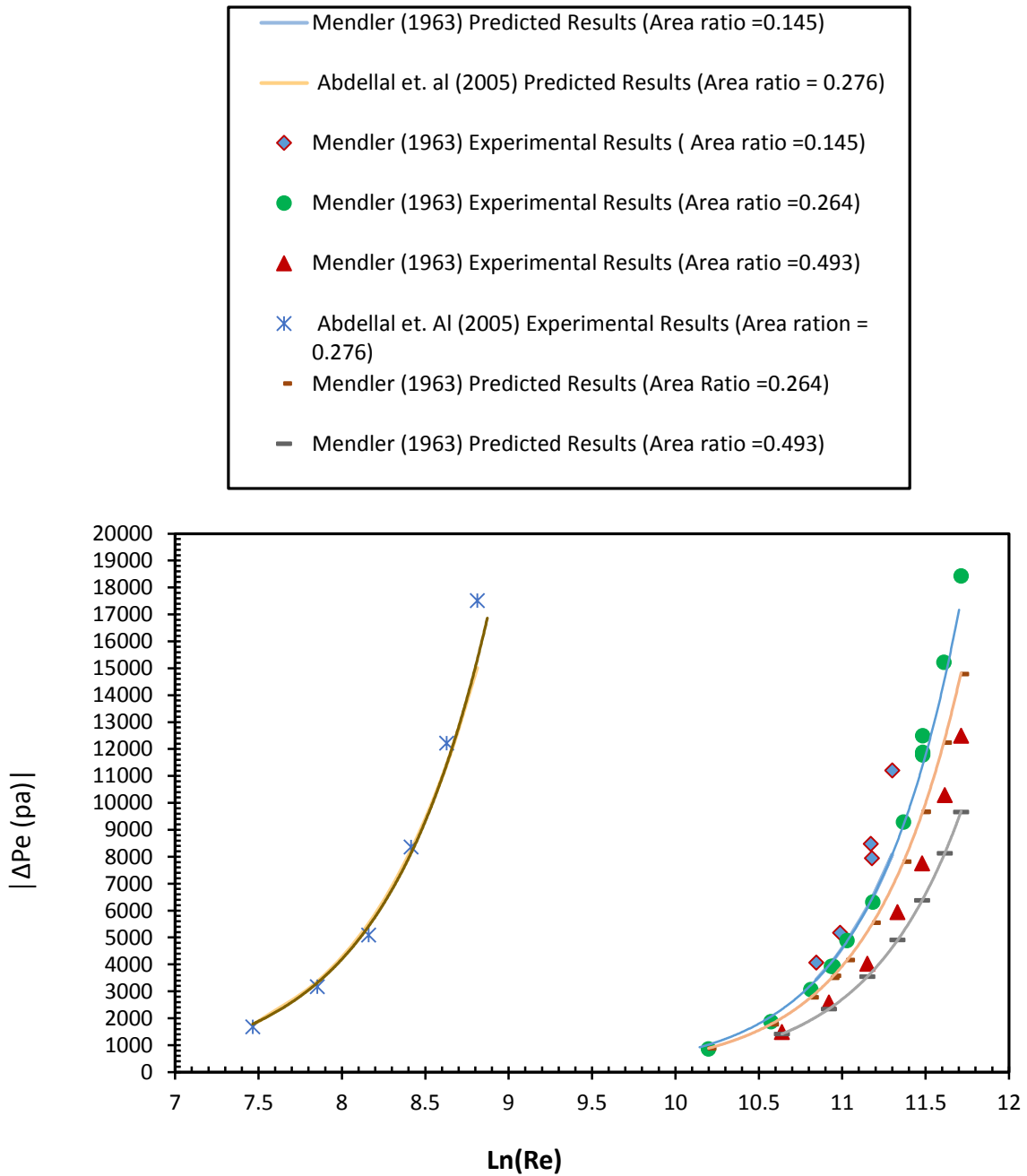
Figure 50. *Comparison between predicted by Equation (46) and experimental pressure drop at singularity results for various area ratios*

Equations (44) and (45) were also used to quantify the loss coefficient due to sudden expansion, and the loss coefficient was used to compute the pressure drop, see Equation (14). The results were plotted in Figure 51 and compared with those obtained when Carnot equation is used for loss coefficient. It is evident, that in this case both results are in good agreement with experimental results. However, at higher Reynolds numbers (Re > 12000) by using Equations (44) and (45) an excellent prediction is achieved.
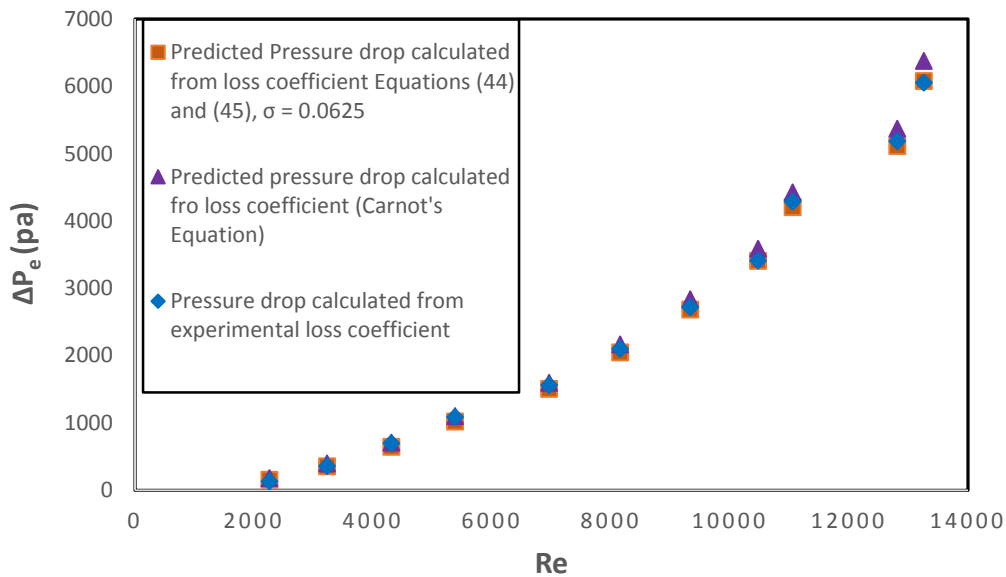
Figure 51. *Comparison of experimental with predicted pressure drop calculated from loss coefficient results for the channel with sudden area change for σ = 0.0625*

4.1.2 Sudden Area Contraction

4.1.2.1 Static Pressure

The same methodology used to measure and acquire static pressure data for sudden area expansion was used for sudden area contraction. The test section was also the same, except that for the upstream channel for sudden expansion is downstream channel for sudden contraction and vice-versa.

The upstream static pressure was found to be nearly constant, whereas it gradually decreases downstream of the singularity. This decreases was very remarkable as the flow accelerated after vena contracta. Although, it is not easy to determine the exact location of vena contracta, for the results of this study show that vena contracta occurred in the neighborhood of 3 inches from the singularity. This trend was observed for all mass flow rates.
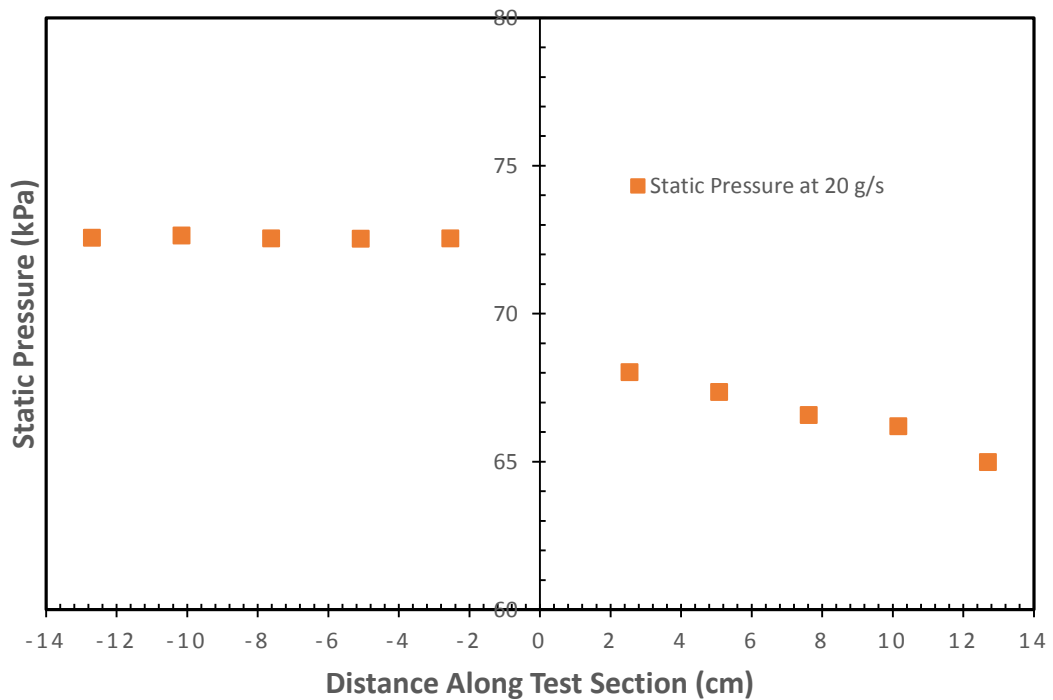
Figure 52. *Variation of water static pressure with distance a long test section*
at ṁ = 20 g/s and σ = 0.0625 for sudden contraction
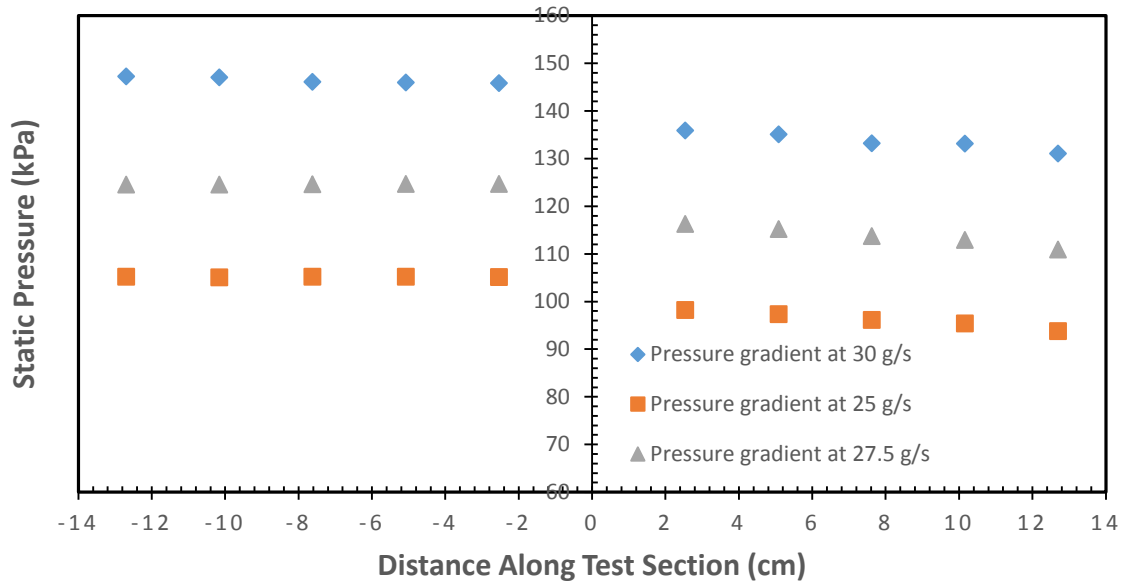
Figure 53.   *Variation of water static pressure with distance a long test section and mass flow rate, $\dot{m}$ = 30, 27.5, and 25 g/s for sudden contraction, σ = 0.0625*
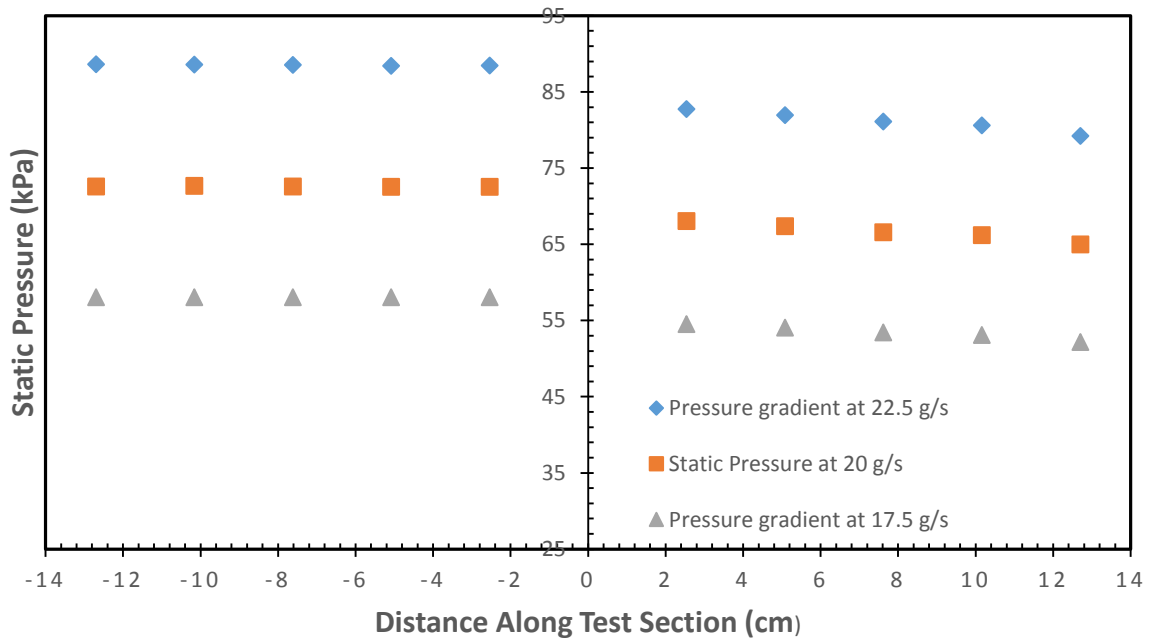
Figure 54.   *Variation of water static pressure with distance a long test section and mass flow rate, $\dot{m}$ = 22.5, 20, and 17.5 g/s for sudden contraction, σ =0.0625*
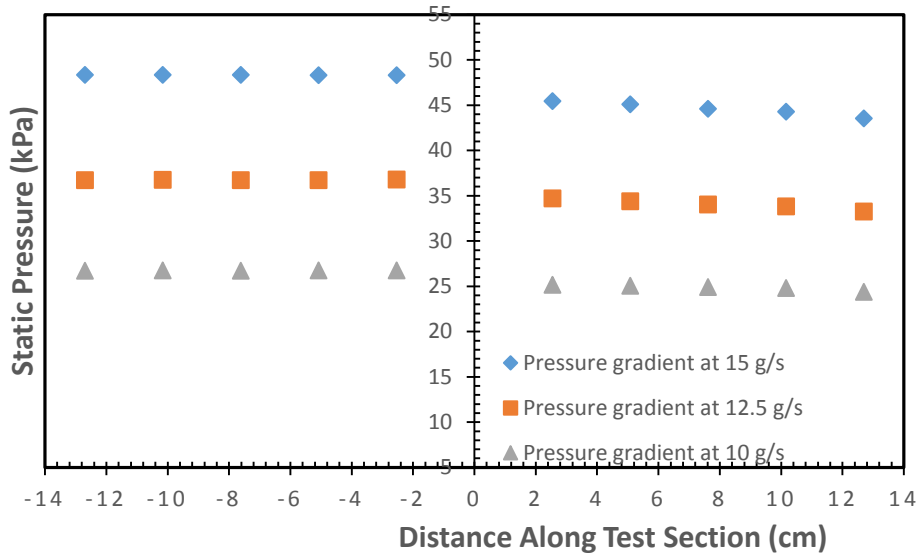
Figure 55. *Variation of water static pressure with distance a long test section and mass flow rate, $\dot{m}$ = 15, 12.5, and 10 g/s for sudden contraction, σ = 0.0625*
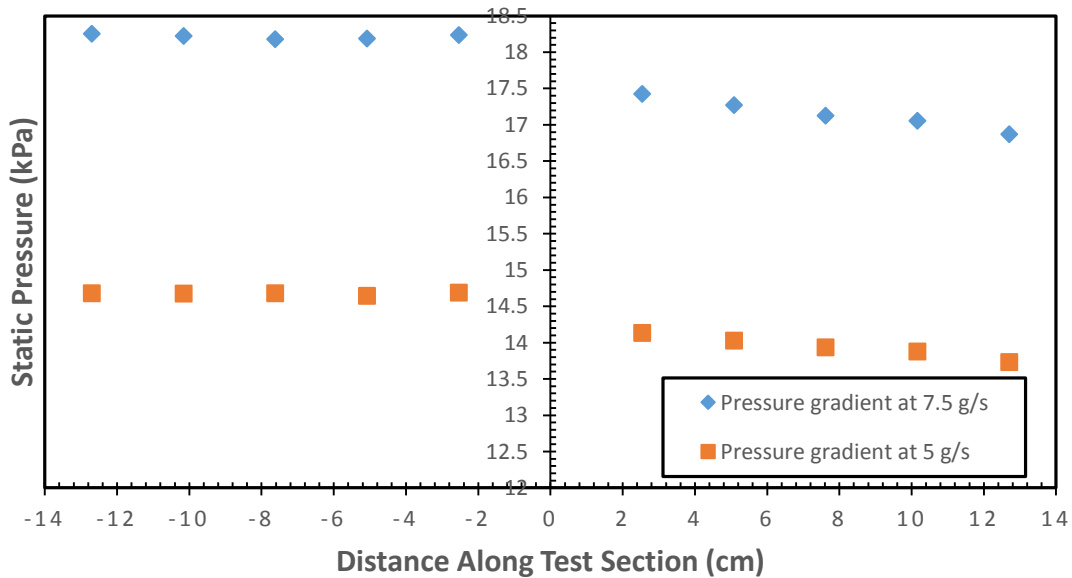
Figure 56. *Variation of water static pressure with distance a long test section and mass flow rate, $\dot{m}$ = 7.5 and 5 g/s for sudden contraction, σ = 0.0625*

As shown by Figures 52 through 56, the static pressure trend is nearly the same for all mass flow rates measured. The trend is such that static pressure increases with increasing mass flow rate.

4.1.2.2 Pressure drop and Loss Coefficient

Earlier in Chapter I, Equation (22) was derived and used for calculating the total pressure drop caused by sudden area expansion. Because channels were interchanged for sudden area contraction, terms in Equation (22) were assigned opposite signs. Hence, Equation (47) is derived.

$$\Delta P_c = \Delta P_{co} - \rho \frac{U_1^2}{2}(1 - \sigma^2) \dots\dots\dots\dots\dots\dots\dots\dots\dots\dots\dots\dots\dots\dots\dots (47)$$

where,

$$\Delta P_c = \frac{1}{2} K_c U_1^2 \rho$$

By substituting expression for ΔP_c into Equation (46) and solving for ΔP_{co}, the pressure drop equation at singularity for sudden area contraction can be derived.

$$\Delta P_{co} = \frac{1}{2} \rho U_1^2 (K_c + 1 - \sigma^2) \dots\dots\dots\dots\dots\dots\dots\dots\dots\dots\dots\dots\dots (48)$$

Theoretical loss coefficient, $(K_c)_{th}$ is calculated from Equation (29). The linear extrapolation method, that was used to obtain the experimental pressure drop at singularity for sudden expansion, was also used for sudden contraction. The results are plotted in Figure 57 along with theoretical prediction results obtained by using Equation (48). The pressure drop trends of experimental and predicted results agreed. It is found that pressure drop at singularity increases with increasing Reynolds number.
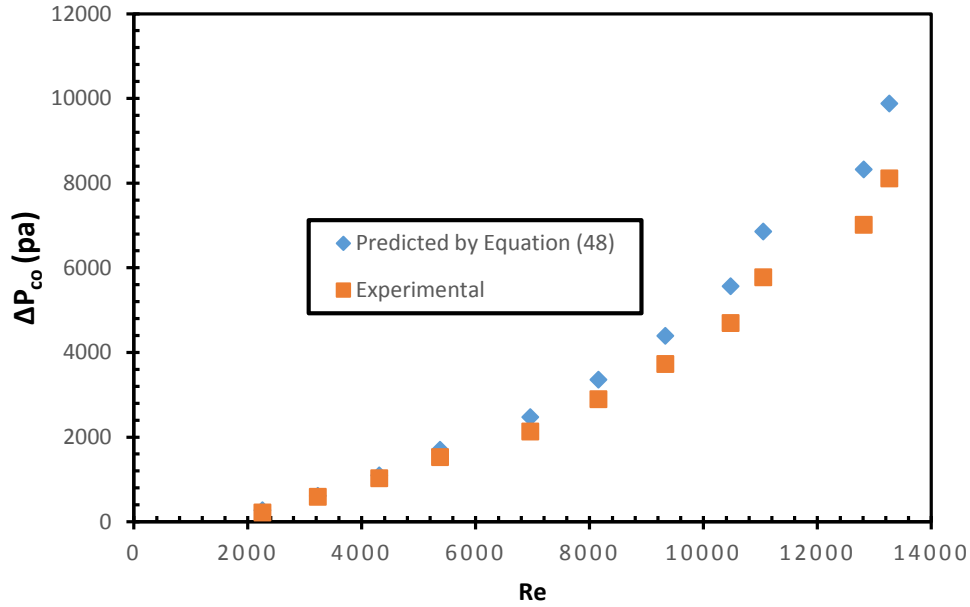
Figure 57. *Comparison of experimental and predicted pressure drop results at singularity for sudden area contraction, σ =0.0625*

The experimental loss coefficient results plotted in Figure 58 show a different trend. Loss coefficient decreases with increasing flow rate and tends to reach an optimum value at higher flow rate. This is best explained by Equation (46) of the total pressure. The value of negative dynamic pressure term increases with increasing flow rate which rends the total pressure to decrease. When the total pressure decreases, the loss coefficient decreases as well, because the two parameters are directly proportional, see Equation (27).

While theoretical loss coefficient values can be obtained from Equation (29), the corresponding experimental values can be quantified by substituting Equation (27) into (44) and solving for K_c. Experimentally, loss coefficient due to sudden area contraction is calculated from Equation (48).

$$K_c = \frac{\Delta P_{c0} - \frac{1}{2}\rho U_1^2 (1-\sigma^2)}{\frac{1}{2}\rho U_1^2} = \frac{\Delta P_{c0}}{\frac{1}{2}\rho U_1^2} - (1-\sigma^2) \dots\dots\dots\dots\dots\dots\dots\dots\dots\dots\dots\dots \text{(49)}$$
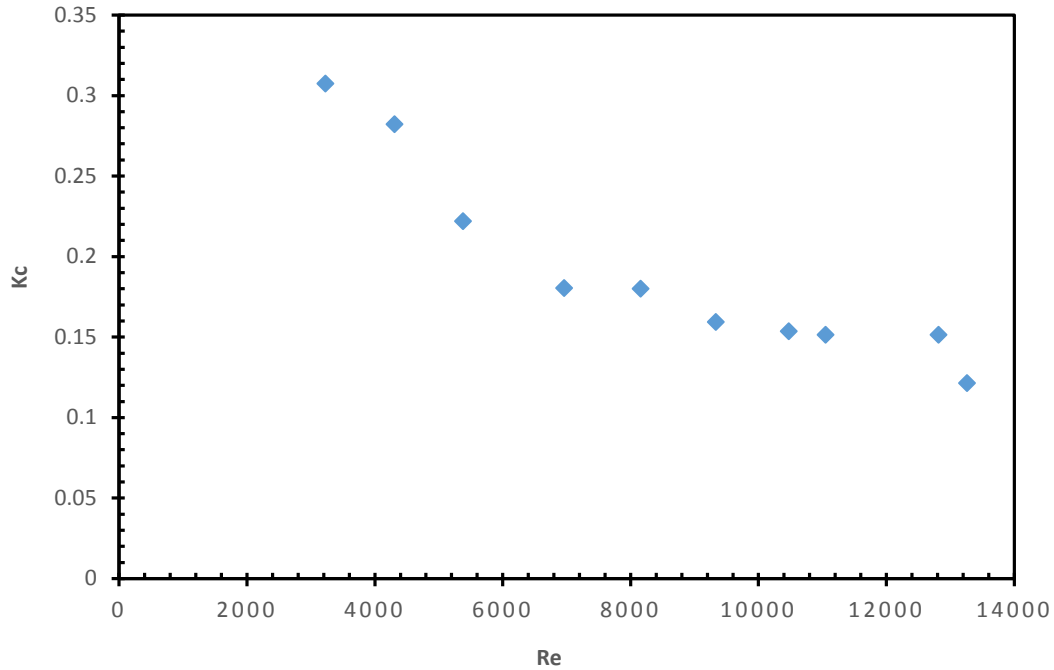
Figure 58. *Variation of experimental loss coefficient with Reynolds number for sudden area contraction, σ = 0.0625*

4.2 Experimental Results with Silicon Dioxide Nanofluid

Experiments were performed for two channels (σ = 0.0625 and 0.140). A 9.58% volume concentration silicon dioxide (silica)/water nanofluid was used as the working fluid for this portion of the study. One of the important parameters for this study is density. The density of silicon dioxide nanofluid is a function of water density, silicon dioxide density, and volume concentration of nanoparticles. It was calculated from Equation (2). Because temperature and pressure were kept nearly constant for all measurements, a single value of density was used throughout. For ambient conditions, density of water and silicon dioxide is 996.5 kg/m^3 and 2360 kg/m^3 respectively. These equate to silicon dioxide nanofluid density of 1127.12 kg/m^3.

The results of the viscosity measurement taken separately show, that the viscosity of non-Newtonian fluids varies with the flow. This means that this particular type of nanofluid, the shear stress versus shear rate function is not linear, (Figure 59).
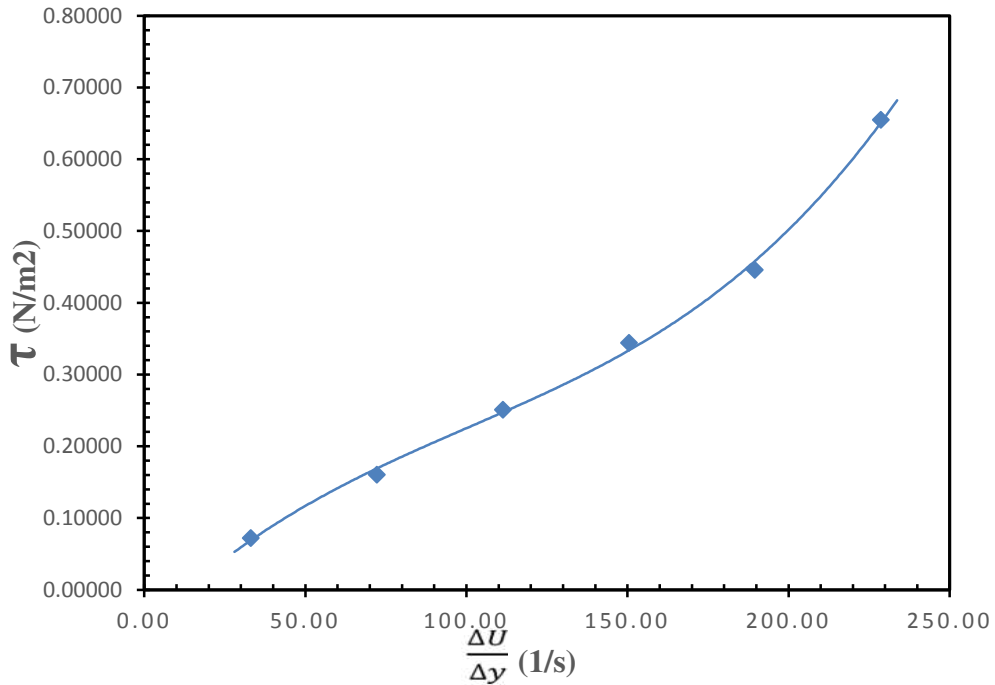
Figure 59. *Variation* of *Silicon Dioxide shear stress with shear rate at T = 20⁰ C*

For a Newtonian fluid such as water, Equation (7) was used to calculate Reynolds number for analyzing parameters that dynamically change. However, further analysis was done, and it was concluded that silicon dioxide nanofluid exhibits a power law behavior. This means that Equation (7) can no longer used as the viscosity changes with the flow rate. A generalized Equation (50) is usually used to quantify the Reynolds numbers for power law fluid at different flow rates.

$$Re = \frac{\rho U_1^{2-n} d^n}{\beta} \quad\dots\dots\dots\dots\dots\dots\dots\dots\dots\dots\dots\dots\dots\dots\dots\dots\dots\dots\dots\dots\dots\dots\dots\dots \quad (50)$$

where, β is defined as the consistency index and n the power law index.

All measurements were done at ambient temperature ($20 \pm 2°C$). For this range of temperatures, the average values of n and β, derived from viscosity data, were found to 0.00124 and 1.1058 respectively. More specifically, Equation (51) is used to quantify Reynolds numbers for a power law fluids flowing in circular channels.

$$Re = \frac{\rho\, U_1 d}{\beta\left(\frac{8U_1}{d}\right)^{n-1}} \dots\dots\dots\dots\dots\dots\dots\dots\dots\dots\dots\dots\dots\dots..\dots\dots\dots\dots\dots\dots\dots (51)$$

where,

$\gamma = \frac{8U_1}{d}$ is the flow characteristic and is directly related to the wall shear stress.

$$\left(\frac{du}{dy}\right)_w = \gamma\, \frac{3n+1}{4n} \dots\dots\dots\dots\dots\dots..\dots\dots\dots\dots\dots\dots..\dots\dots\dots..\dots\dots.. (52)$$

However, due to viscous nature of the type of the nanofluid being studied and the small range of flow rates measured, the results obtained by using Equation (51) have narrow range and do not reflect the increasing flow rate. For this reason, the flow characteristic (γ) was used for all mass flow rates measured which range from 7.92 to 25.70 g/s.

4.2.1 Sudden Expansion

4.2.1.1 Static Pressure

The procedure, that was used to acquire static pressure data for water, is described in Section 3.4. The sample results are presented in Figures 60 and 61 for 10.39 and 21.40 g/s respectively. The effect of sudden area expansion was found to be more important lower area ratio ($\sigma = 0.0625$) compared to $\sigma = 0.140$. This is because, at lower area ratio the fluid upstream velocity is higher and static pressure decreases much faster nearby the singularity as the fluid expands into downstream channel. The flow is disturbed and slowed down at downstream which tends to rise the static pressure until about three inches from the singularity.

After this length the effect of sudden expansion diminishes, and the drop in static pressure is dominantly due to friction between the fluid and the pipe. As rule of thumb static pressure increases with increasing flow rate and area ratio. This trend was observed for all mass flow rates measured. More data about static pressure can be found in Appendix A, Table 6.
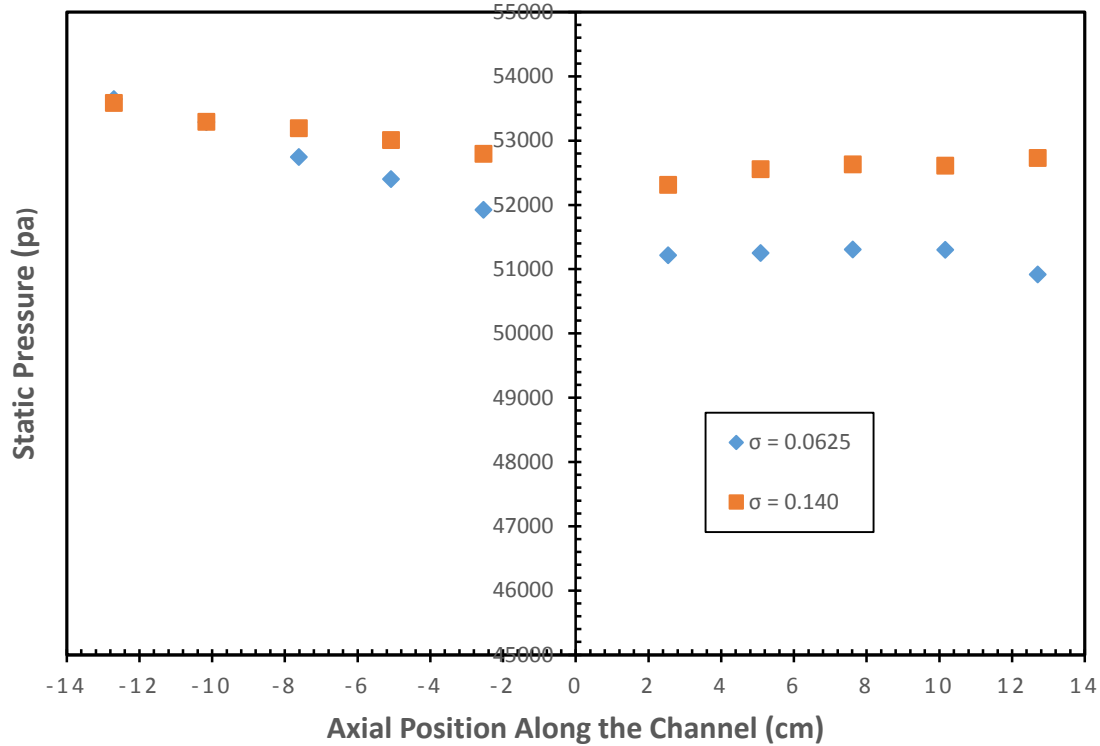
Figure 60. *Comparison of silicon dioxide nanofluid static pressure along the channel with sudden area expansion at 17.24 g/s and different area ratios (σ = 0.0625 and 0.140)*
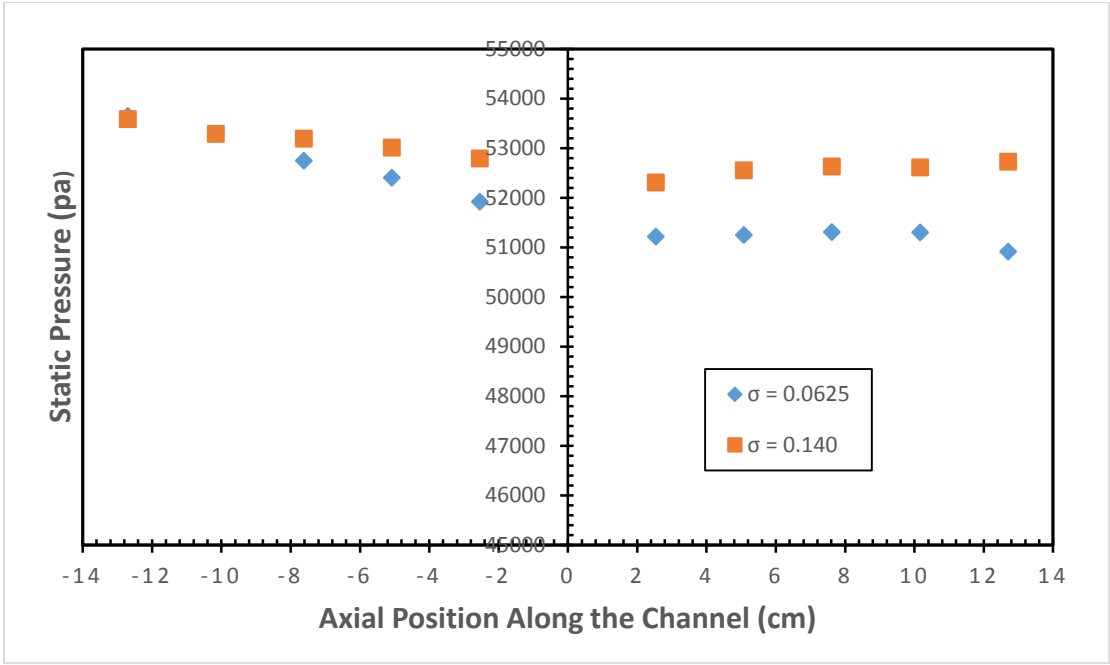
Figure 61. *Comparison of silicon dioxide nanofluid static pressure along the channel with sudden area expansion at 21.339 g/s and different area ratios (σ = 0.0625 and 0.140)*

4.2.1.2. Loss Coefficient and Pressure Drop

The results of loss coefficient were calculated from Equation (36).   The pressure drop at singularity (ΔP_{e0}) is the difference between the extrapolated static pressures from upstream and downstream static pressure curve at singularity. These results and loss coefficient results for water, are plotted in Figure 62.

For nanofluid, loss coefficient decreases with increasing flow characteristic (γ); whereas earlier it was found that sudden expansion loss coefficient for water increases with increasing flow and tends to reach an optimum value. The reveals a very important scientific fact about silicon dioxide nanofluid. At lower flows rates, viscous forces are dominant due to the presence of nanoparticles. However, as the flow increases the fluids gains the momentum from the increasing pumping power and therefore viscous forces start

86

to drop. This can cause the loss coefficient to be higher than water loss coefficient and to drop as the flow increases.

However, as the flow becomes fully turbulent, loss coefficients of nanofluid and water tend to equate. This means that viscous forces have diminished enough for eddy forces to dominate.

A closer look at Figure 62 shows a delayed turbulent for nanofluid, because loss coefficient curve tends to becomes flatter (less change in loss coefficient) at higher flow rates compared to water. This can be a potential defect of silicon dioxide nanofluid applications in channels with sudden area expansions, as it would require much pumping power fully developed flow. Moreover, Figure 62 shows a variation of sudden expansion loss coefficient with area ratio at different γ. Based on the trend of loss coefficient at $\sigma = 0.0140$, it can be predicted that nanofluid loss coefficient would decrease with increasing area ratio. This behavior confirms with the variation of loss coefficient with area ratio for water.
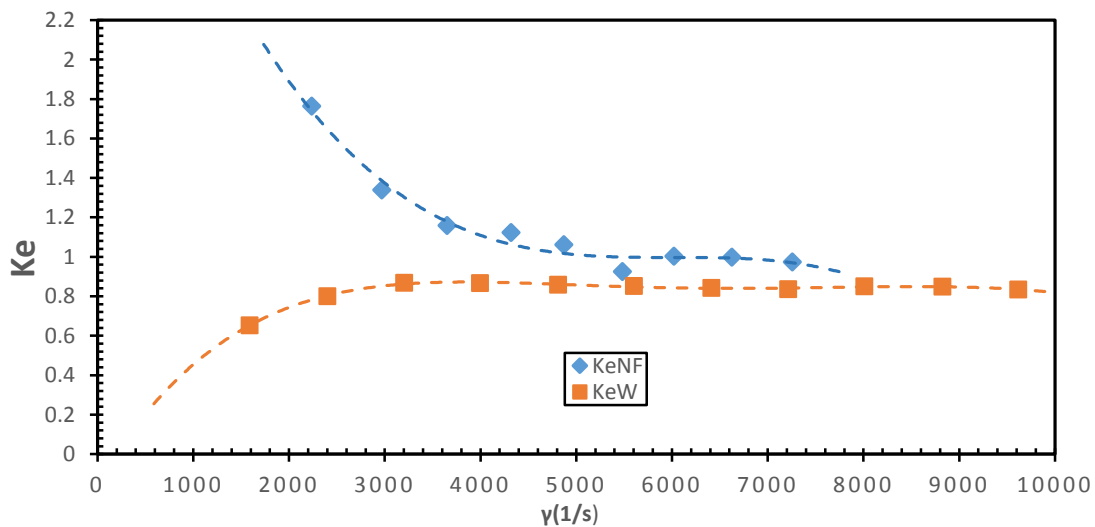
Figure 62. *Comparison of sudden expansion loss coefficient for water and silicon dioxide nanofluid at different γ*
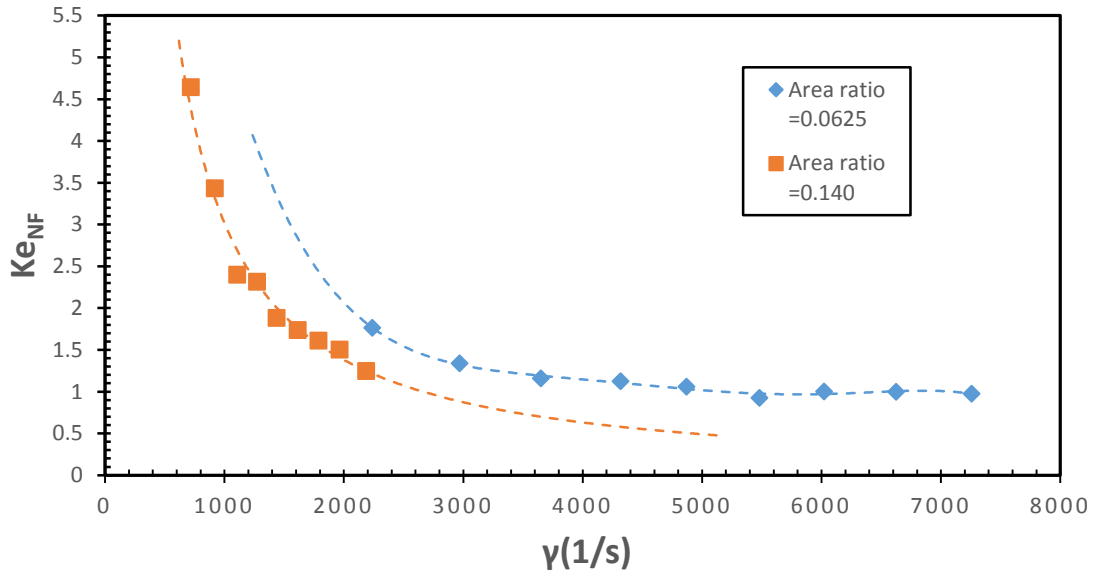
Figure 63. *Variation of sudden expansion loss coefficient*
with area ratio at different γ

In order to gain more insight on the impact of sudden area expansion to the pumping power, pressure drop was calculated at different flow rates. Pressure drop due to sudden area expansion is computed from Equation (8), where U_1 is the average upstream velocity.

The results obtained were plotted against the flow characteristic (Figure 64) and compared with water pressure drop for the same area ratio ($\sigma = 0.0625$). It is found that pressure drop due sudden expansion increases with increasing flow rate for both water and silicon dioxide nanofluid. However, nanofluid pressure drop was to be much higher compared to water pressure drop.

The difference between the two pressures drops decreases exponentially with increasing flow rate. For the range of mass flow rates measured, sudden expansion nanofluid pressure drop is 129% higher than water pressure drop for the lowest flow rate ($\dot{m} = 7.92$ g/s or $\gamma = 2236.5$ 1/s). This percentage continues to drop as the flow rate increases and becomes 16.4% for the highest flow rate ($\dot{m} = 25.7$ g/s or $\gamma = 7255.9$ 1/s) as shown in Figure 64.

These results agree with sudden expansion coefficient results that were discussed at the beginning of this section. It was found that loss coefficient results are higher than water's at lower flow rates. Both results tend to be closer at higher flow rates due to the dominance of eddy forces over viscous forces.

Further analysis done on higher area ratio ($\sigma = 0.140$) shows, that pressure drop decreases with increasing area ratio, see Figure 66. The most valuable cause of this trend is the decrease in upstream velocity, as the area ratio is increased.
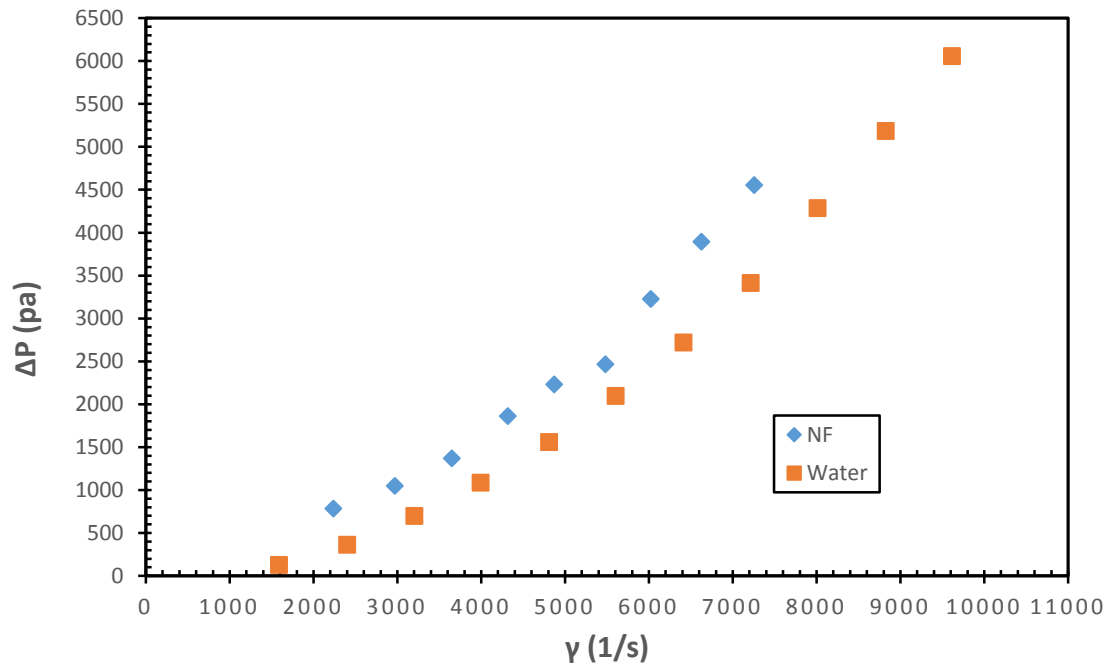
Figure 64. *Comparison of pressure drop calculated from loss coefficient for channel with   sudden area expansion (σ = 0.0625) for water and 9.58 % volume concentration silicon dioxide nanofluid at various γ.*
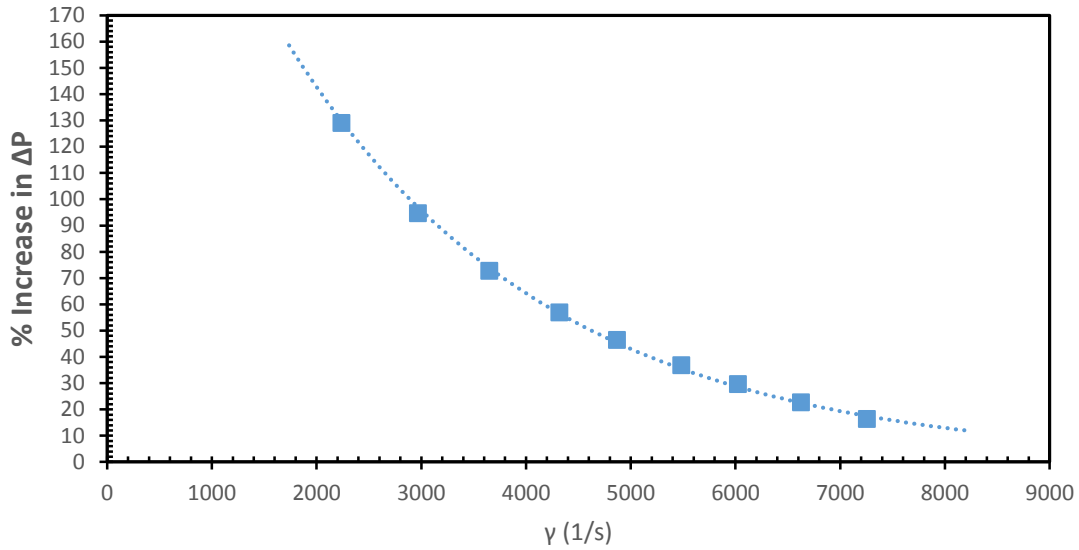
Figure 65. *Variation of percentage increase in nanofluid pressure drop calculated from loss coefficient with γ for sudden expansion, σ = 0.0625*
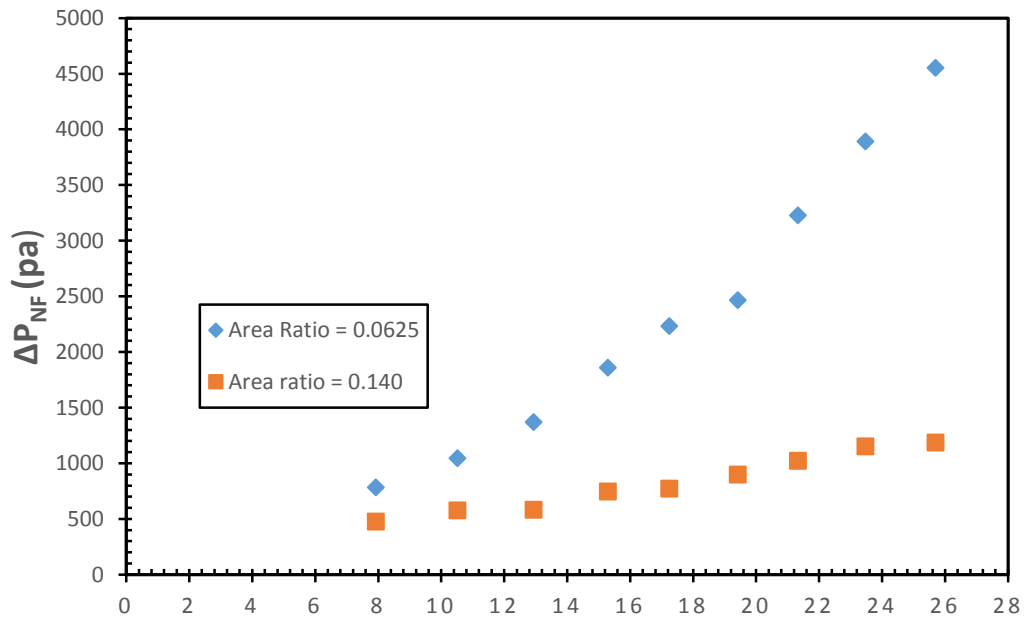
Figure 66. *Comparison of pressure calculated from loss coefficient nanofluid for σ = 0.0625 and 0.140 at various mass flow rates.*

4.2.2 Sudden Contraction

4.2.2.1 Static Pressure

The methodology, which was used for water in channel with sudden area contraction, was also applied in order to acquire static pressure data of 9.58% volume concentration silicon dioxide nanofluid. The two channels ($\sigma = 0.0625$ and 0.140), that were used for sudden area expansion, were also used for sudden area contraction with channels switched. This means that the upstream channel became downstream channel and vice-versa. Sample of the results are presented in Figures 67 and 68 for 10.51 and 25.70 g/s, respectively. The rest of the results are summarized in Appendix B, Tables 10 and 11. The results show that upstream static pressure is not affected by change in area ratio. It is to be recalled that the same channel was used upstream, and the downstream channel internal diameter was changed (from d = 0.126 in. to 0.187 in.) in order to obtain the desired area ratios. This was not observed for sudden area expansion, where the downstream channel was maintained the same. It makes much sense, because for sudden expansion, the flow arrives downstream after losing some momentum from the sudden area change.

Static pressure downstream showed a smooth decrease as the flow moves away from singularity. This trend was observed for the two area ratios and all mass flow rates measured. The downstream static pressure is lower than the upstream static pressure due to the flow acceleration, as it contracts into the smaller channel. The flow continues to accelerate as it moves away from the singularity, and therefore static pressure continues to drop. In addition, the increase in area ratio results in increase in static pressure due to the drop of flow velocity as the channel internal diameter is increased.
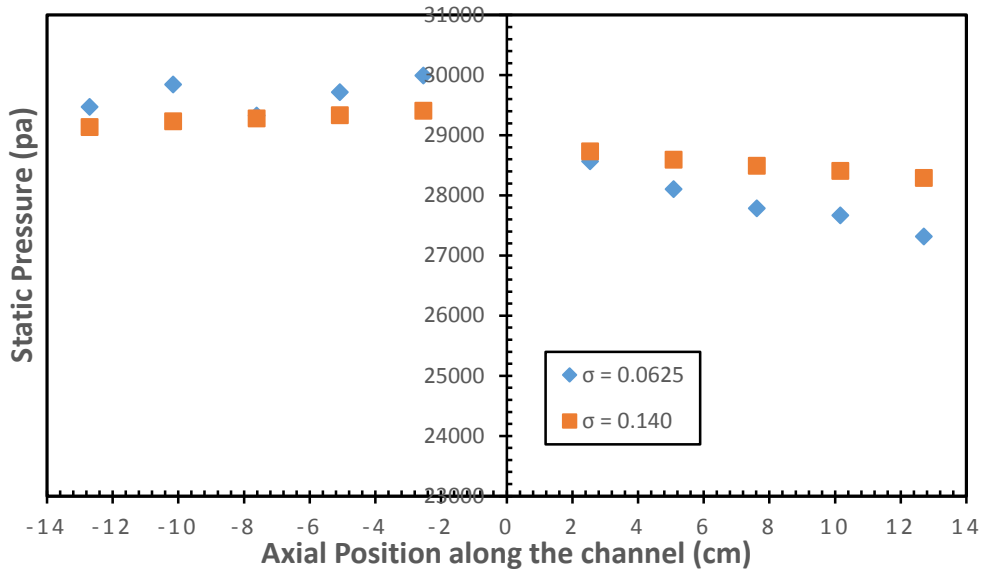
Figure 67. *Comparison of silicon dioxide nanofluid static pressure along the channel with sudden area contraction at 10.515 g/s and different area ratios (σ = 0.0625 and 0.140)*
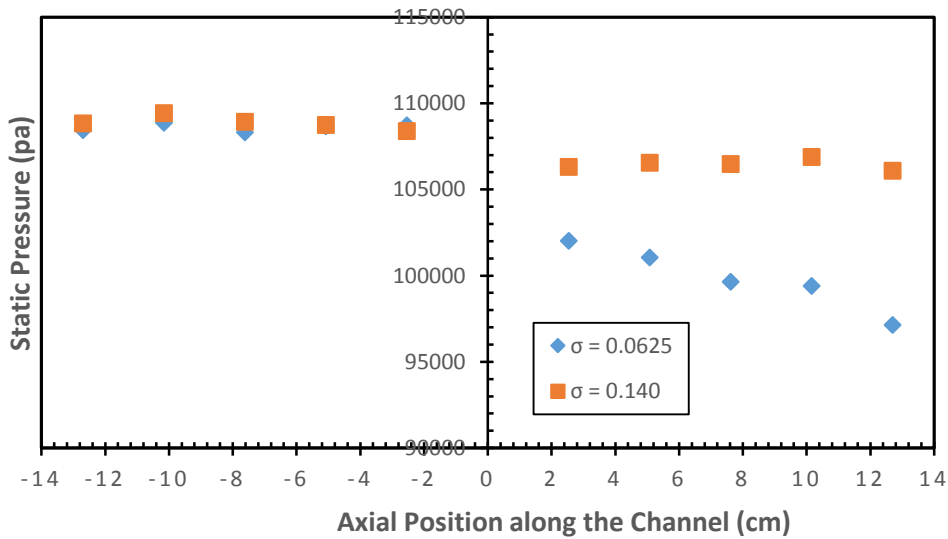
Figure 68. *Comparison of silicon dioxide nanofluid static pressure along the channel with sudden area contraction at 25.70 g/s and different area ratios (σ =0.0625 and 0.140)*

4.2.2. Loss Coefficient and Pressure Drop

The results for loss coefficient due to sudden contraction can be calculated from Equation (48). Pressure drop at singularity (ΔP_{co}) is obtained by doing linear extrapolation methodology that was used for previous analysis. The results plotted in Figures 69 and 70 show that loss coefficient decreases with increasing flow rate and decreasing area ratio. Unlike the results obtained for sudden area expansion, the trend of loss coefficient for sudden contraction shows similarities between water and silicon dioxide nanofluid behavior.

However, for both sudden expansion and contraction, loss coefficients with nanofluid is much higher than loss coefficients with water at lower flow rates. For higher flow rates, the percentage increase in loss coefficient results drops significantly, from 94.38% at 10.51 g/s or γ = 2668.9 1/s to 16.48 % at 25.70 g/s or γ = 7255.9 1/s. As previously explained, the drop in percentage increase is due to the dominance of turbulent eddy viscosity over viscous forces at higher flow rates (Figure 71).
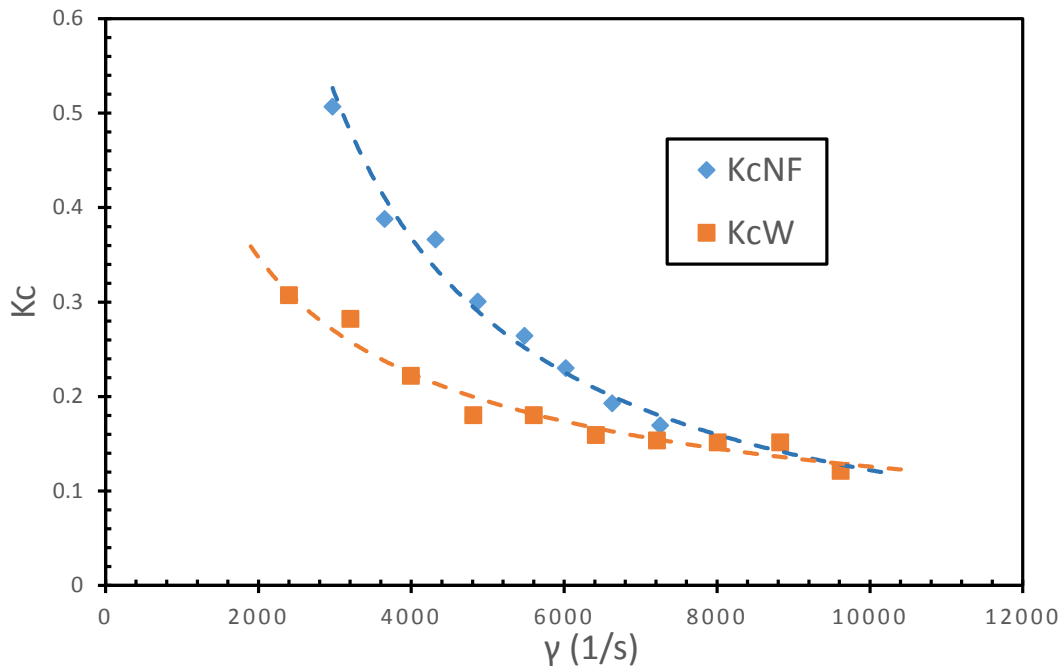
Figure 69. *Comparison of loss coefficient due to sudden area contraction for water and silicon dioxide nanofluid at different γ.*
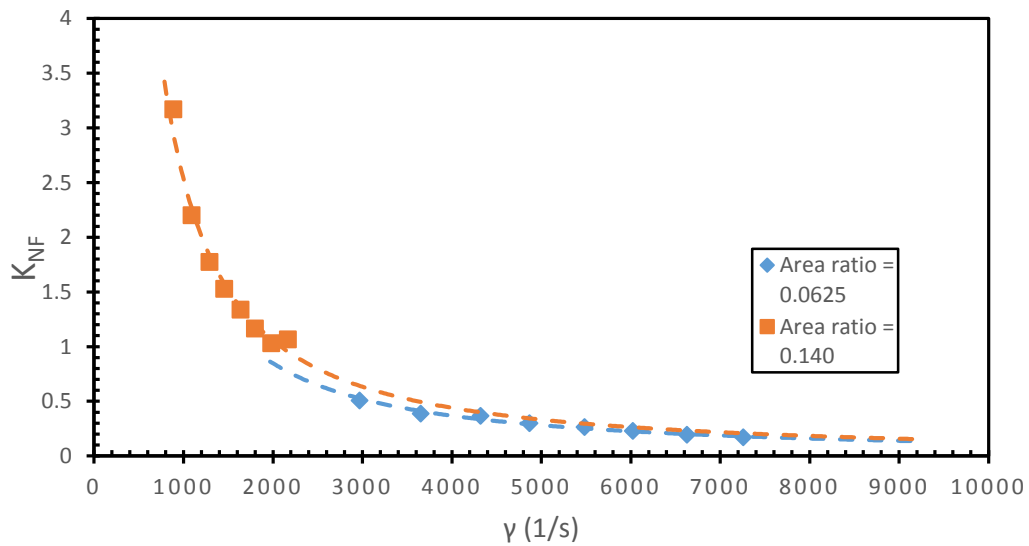
Figure 70 *Representation of the impact of area ratio on loss coefficient due to sudden area contraction*
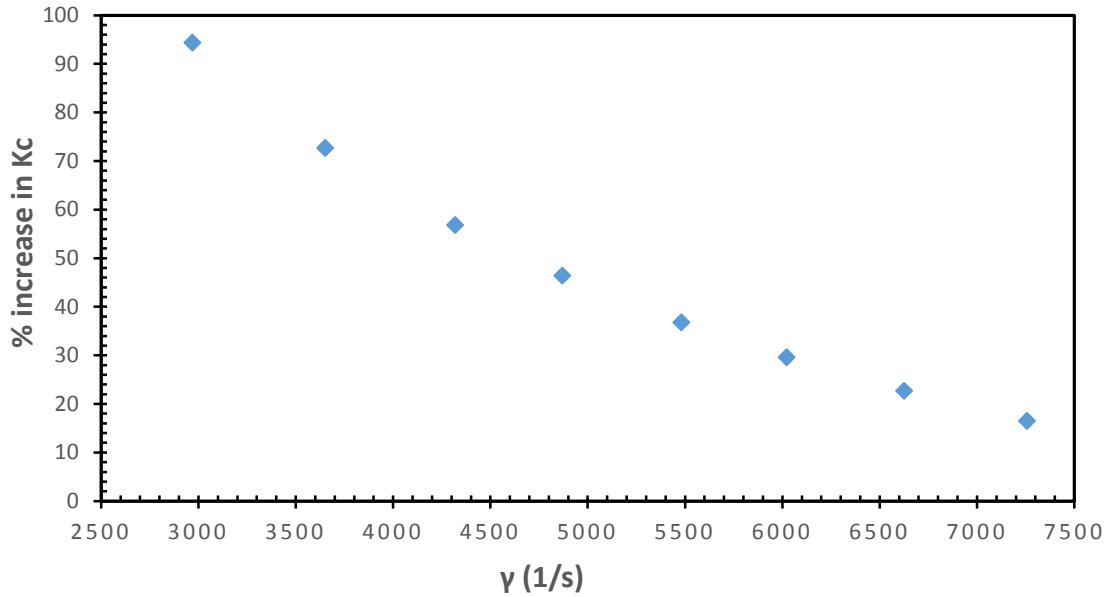
Figure 71. *Variation in percentage increase in sudden contraction ($\sigma = 0.0625$)*
loss coefficient with γ, when silicon dioxide is used instead of water

The results of pressure drop due to sudden area contraction were obtained from Equation (27) and are presented in Figures 72 and 73. Pressure drop increases with increasing flow rate and is higher for nanofluid than water. This is confirmed by the results of loss coefficients.

Unlike sudden area expansion, increasing area ratio would result in pressure drop increase for silicon dioxide flowing in channel with sudden contraction. This can be best explained by using Equation (47). The increase of area ratio requires the increase of downstream inside diameter, and therefore the velocity drastically drops, (Figure 74). The decrease in velocity would result in decrease of corrected dynamic pressure term in Equation (47); hence the overall pressure drop due to sudden contraction would tend to be higher for higher area ratios compared to lower area ratios.
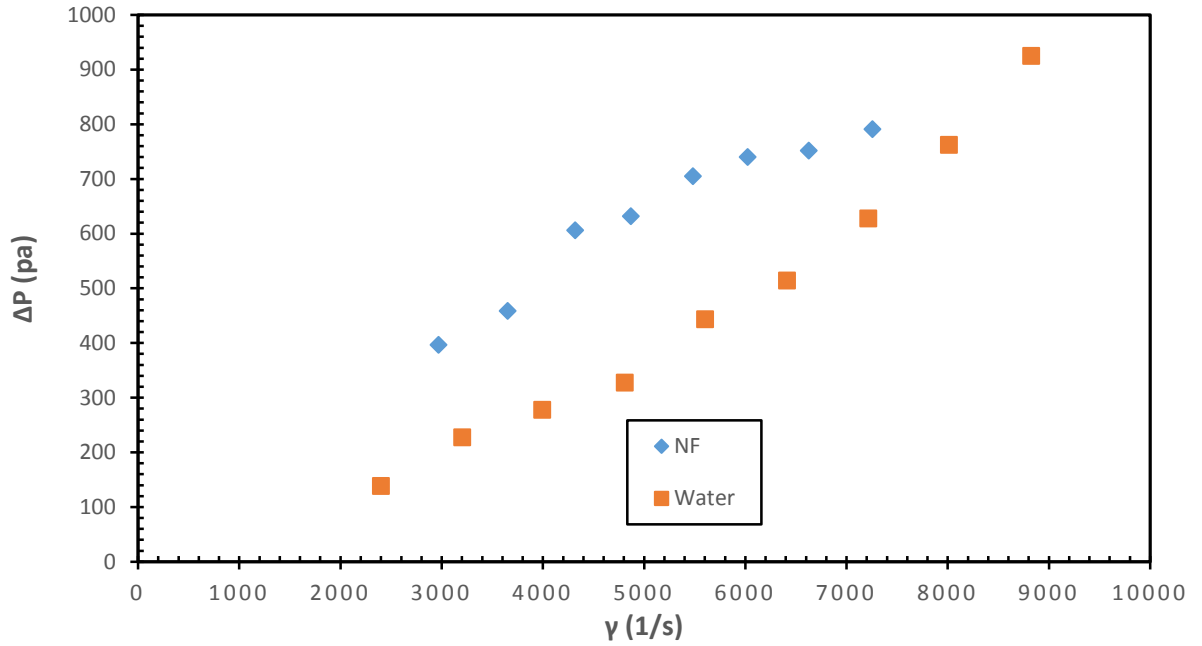
Figure 72. *Comparison of water and silicon dioxide nanofluid pressure drop calculated from loss coefficient results for channel with sudden area contraction (σ = 0.0625)*
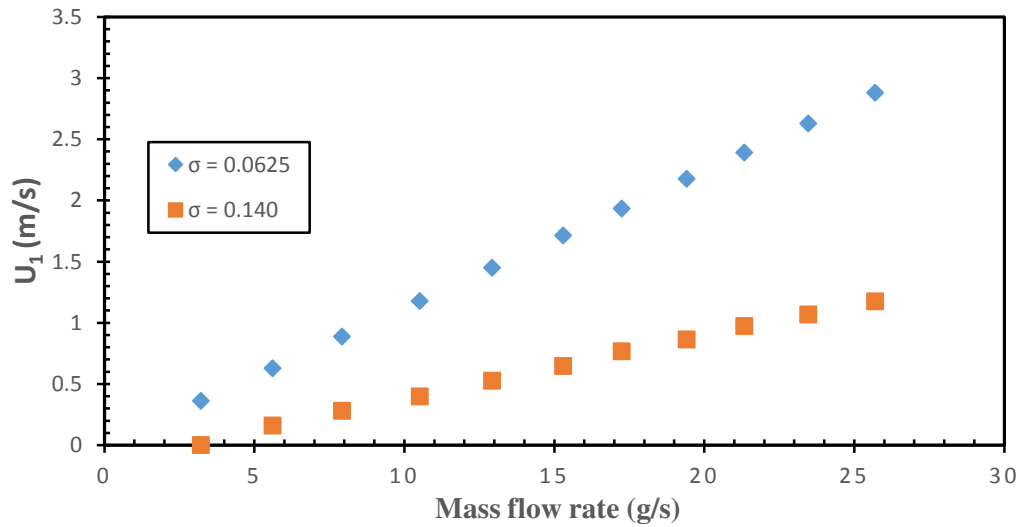
Figure 73. *Impact of variation of area ratio on downstream velocity for a channel with sudden area contraction*
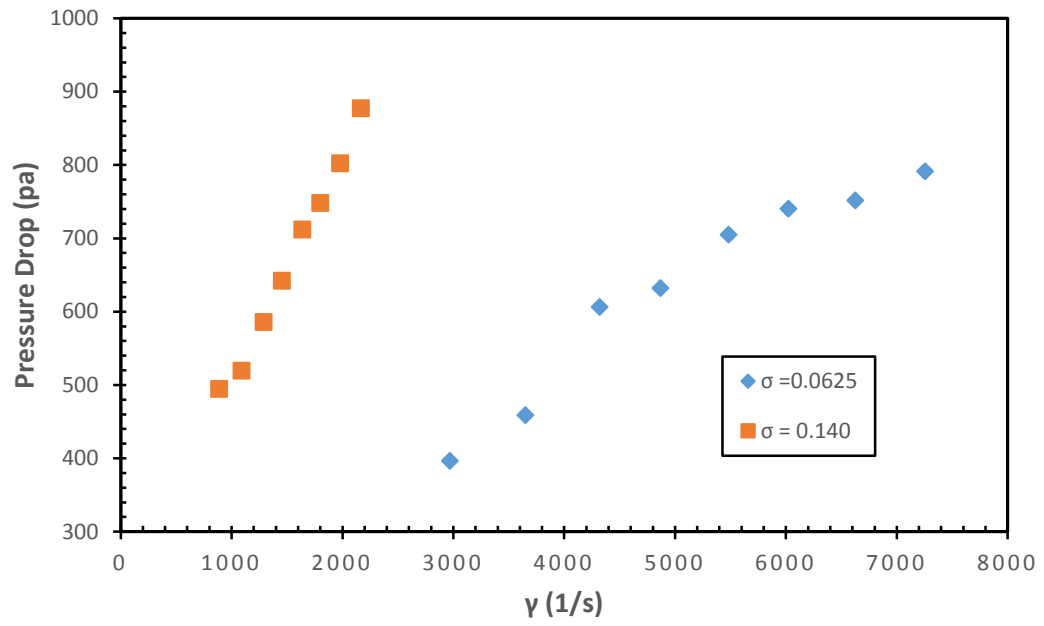
Figure 74. *Impact of variation of area on silicon dioxide nanofluid
pressure drop calculated from loss coefficient results for
channel with sudden area contraction*

CHAPTER V

CONCLUSIONS AND RECOMMENDATIONS

In this chapter, key conclusions are drawn from the results of theoretical and experimental investigation of water and 9.58% silicon dioxide nanofluid flow in channels with sudden area expansion and contraction. Moreover, some improvements and further work are suggested in order to make this work more suitable for intended applications.

5.1 Water Flow

5.1.1 Water Flow in Channel with Sudden Area Expansion ($\sigma = 0.0625$)

The following expression was derived from momentum analysis and was used to quantify the experimental loss coefficient at various Reynolds numbers.

$$K_e = \frac{\Delta P_{eo} - \frac{1}{2}\rho U_1^2(\sigma^2 - 1)}{\frac{1}{2}\rho U_1^2} = \frac{\Delta P_{e0}}{\frac{1}{2}\rho U_1^2} - (\sigma^2 - 1)$$

The experimental investigation, aimed at measuring static pressure at various mass flow rates, was done at ambient conditions with distilled water as the working fluid. The mass flow rates measured range from 5 to 30 g/s. These equate to Reynolds numbers that range from 2257 to 13261. Static pressure data were plotted against the axial length of the channel, and pressure drop at singularity ΔP_{e0} was obtained by doing linear extrapolation. The results show, that singularity pressure drop is negative because the flow slows down in the downstream region nearby the singularity which results in the rise of static pressure.

98

It was also found that the magnitude of pressure drop at singularity increases with increasing Reynolds numbers.

Furthermore, loss coefficient due sudden expansion increases with increasing flow rates and reaches an optimum value that is in the neighborhood of 0.85. This was seen as an evidence, that a fully turbulent flow was reached. All results fall in the range of 0.65-0.87 with a maximum of ±8.10% based on 95% confidence level uncertainty analysis. Carnot equation could not predict our experimental results, because loss coefficient varies with the flow rate. The followings correlations were developed in order to predict the varying loss coefficient for a single phase fluid flowing is channel with sudden area expansion.

$$K_e = (1 - \sigma)^2 + 2\sigma[0.4619 \ln(R_{e1}) + 1.37885\sigma - 4.5721]$$

The above correlation is recommended for σ < 0.3 and Re < 7000. The correlation below is recommended for σ < 0.4 and 7000 < Re < 120 000.

$$K_e = (1 - \sigma)^2 + 2\sigma[0.1185 \ln(R_{e1}) + 0.1689\sigma - 1.4666]$$

5.1.2 Sudden Area Contraction (σ = 0.0625)

Similarly to sudden area expansion, static pressure data for sudden area contraction were measured at ambient conditions for Reynolds numbers ranging from 3227 to 13261. The following expression was derived for the loss coefficient:

$$K_c = \frac{\Delta P_{c0} - \frac{1}{2}\rho U_1^2(1 - \sigma^2)}{\frac{1}{2}\rho U_1^2} = \frac{\Delta P_{c0}}{\frac{1}{2}\rho U_1^2} - (1 - \sigma^2)$$

Unlike sudden area expansion, for sudden area contraction, pressure drop at singularity was positive as the result of the gradual decrease in static pressure downstream. The results of loss coefficient show, that the experimental loss coefficient decreases with

increasing area ratio. This trend was explained by the increase in corrected dynamic pressure which decreases the overall pressure drop due to sudden contraction.

5.2 Silicon Dioxide (9.58%) Nanofluid Flow

5.2.1 Sudden Area Expansion

Static pressure measurements, aiming at analyzing the behavior of 9.58% nanofluid at varying flow rate, were taken for the channels with sudden area expansion ($\sigma = 0.0625$ and 0.140). The results showed that static pressure smoothly decrease with the axial length of the channel. The impact of sudden area change was observed at downstream, where the fluid slows down and accelerates, as it moves away from the singularity. The increase of the flow rate resulted in increase of static pressure. Also the increase in area ratio caused the static pressure to increase due to the decrease of fluid velocity. The impact was greatly observed in the region nearby the singularity.

Furthermore, the equations used to quantify loss coefficient and pressure drop for water, can also be used for this type of nanofluid. The results showed that loss coefficient due to sudden expansion decreases with increasing flow rate and decreases with increasing flow rate. For 0.0625 channel area ratio, loss coefficient results are higher for nanofluid than water at lower flow rate. The difference in loss coefficient results for both fluids was greatly reduced as the flow reached turbulent. This trend was also observed in pressure drop results ($\sigma = 0.0625$). For the lowest flow rate measured ($\dot{m} = 7.92$ g/s or $\gamma = 2236.5$ 1/s), there was pressure drop due to sudden area expansion for silicon dioxide nanofluid was 129% higher compared to pressure drop for water. However, this percentage increase

was reduced to 16.4% at the highest flow rate ($\dot{m} = 25.7$ g/s or $\gamma = 7255$ 1/s). This behavior was attributed to the increase in turbulence at higher flow rates.

5.2.2 Sudden Area Contraction

Two flow channels ($\sigma = 0.0625$ and 0.140) were used for the flow with sudden area contraction. Unlike sudden area expansion, the impact of area ratio change on static pressure profile was not observed at upstream. Downstream of the singularity, static pressure gradually decreases with increasing axial length of the channel and increasing area ratio for a certain flow rate. The increase in flow rate resulted in increase of static pressure due to the decrease of flow velocity.

The results further show that loss coefficient decreases with increasing flow rate and increases with increasing area ratio. The comparative analysis proved that loss coefficient is higher for nanofluid than water for the same channel area ratio and flow rate. The percentage increase in loss coefficient due to the addition of silicon dioxide nanoparticles in water drops drastically at higher flow rates.

This was seen as the evidence of the dominance of eddy viscosity. For $\sigma = 0.0625$, loss coefficient increased by 94.38% at $\dot{m} = 10.51$ g/s or $\gamma = 2668.9$ 1/s. This percentage drops to 16.48% at 25.7 g/s or $\gamma = 72255.5$ 1/s.

Moreover, pressure drop due to sudden contraction increased with increasing flow rate and area ratio.

For practical applications, it is recommended that this type of nanofluid be used for systems that require higher flow rates (turbulent flow), because pressure drop due to sudden area change for water and for silicon dioxide tend to be closer at higher flow rates.

This may result in heat transfer enhancement with less increase in pressure drop or pumping power.

There are number of ways this work can be improved in order to make sure, that the subjects covered meet well intended practical applications. In order to gain more insight on silicon dioxide nanofluid thermal performance, there is a desire to investigate heat transfer in channels with sudden area change. The results of the heat transfer investigation can be compared with the results of pressure drop provided by this work. Moreover, silicon dioxide nanofluid with lower nanoparticles concentration should be experimented in order to understand more the effect of nanoparticles addition on thermal performance.

Static Pressure Raw Data for Water in Channels with Sudden Area Change

Table 6. Static pressure raw data for water flow in channel with sudden area   expansion ($\sigma = 0.0625$)

X (in)	30 (g/s)	27.5 (g/s)	25 (g/s)	22.5 (g/s)	20 (g/s)	17.5 (g/s)	15 (g/s)	12.5 (g/s)	10 (g/s)	7.5 (g/s)	5.0 (g/s)
-5	137.18	115.89	98.39	82.75	67.99	54.51	42.66	32.14	23.18	15.53	11.18
-4	135.75	115.20	97.59	82.04	67.34	53.95	42.18	31.76	22.88	15.33	11.01
-3	132.96	113.17	96.01	80.71	66.28	53.23	41.70	31.47	22.71	15.29	11.03
-2	131.44	112.32	95.13	79.90	65.65	52.71	41.35	31.18	22.50	15.15	10.92
-1	129.94	111.39	94.31	79.14	65.14	52.32	41.05	30.97	22.37	15.09	10.93
1	129.24	110.74	93.74	78.68	64.73	52.01	40.78	30.77	22.24	15.03	10.90
2	130.12	111.14	94.10	79.07	64.93	52.15	40.92	30.86	22.29	15.07	10.93
3	130.51	111.05	94.18	79.11	64.93	52.20	40.88	30.87	22.29	15.06	10.94
4	130.76	110.97	94.09	79.10	64.99	52.19	40.89	30.87	22.32	15.05	10.95
5	131.21	110.86	94.08	79.06	64.96	52.21	40.88	30.84	22.32	15.03	10.94

X: Axial length along the channel defined from singularity

Table 7. Static pressure raw data for water flow in channel with sudden area contraction (σ = 0.0625)

X (in)	30 (g/s)	27.5 (g/s)	25 (g/s)	22.5 (g/s)	20 (g/s)	17.5 (g/s)	15 (g/s)	12.5 (g/s)	10 (g/s)	7.5 (g/s)	5.0 (g/s)
-5	147.24	124.56	105.18	88.60	72.57	58.05	48.34	36.73	26.73	18.25	14.68
-4	147.02	124.58	105.09	88.57	72.64	58.05	48.34	36.74	26.75	18.23	14.68
-3	146.13	124.62	105.20	88.52	72.55	58.05	48.35	36.74	26.73	18.18	14.68
-2	145.96	124.68	105.19	88.41	72.53	58.06	48.33	36.74	26.74	18.19	14.64
-1	145.85	124.66	105.16	88.43	72.55	58.03	48.31	36.79	26.76	18.24	14.69
1	135.89	116.27	98.21	82.74	68.02	54.53	45.45	34.72	25.16	17.42	14.14
2	135.10	115.20	97.32	81.95	67.35	54.06	45.08	34.40	25.08	17.27	14.03
3	133.25	113.75	96.16	81.10	66.58	53.44	44.60	34.04	24.93	17.13	13.94
4	133.18	112.92	95.39	80.58	66.20	53.09	44.28	33.82	24.80	17.06	13.88
5	131.04	110.93	93.80	79.19	64.99	52.17	43.54	33.25	24.40	16.87	13.73

X: Axial length along the channel defined from singularity

APPENDIX B

Static Pressure Raw Data for Silicon Dioxide Nanofluid in Channels with Sudden Area Change

Table 8. Static pressure raw data for 9.58% Silicon dioxide nanofluid flow in channel with sudden area expansion ($\sigma = 0.0625$)

X (in)	3.2 (g/s)	5.6 (g/s)	7.90 (g/s)	10.5 (g/s)	12.9 (g/s)	15.3 (g/s)	17.2 (g/s)	19.4 (g/s)	21.3 (g/s)	23.5 (g/s)	25.7 (g/s)
-5	11.61	16.49	22.13	29.26	36.06	45.60	53.65	65.75	76.05	90.66	103.55
-4	11.69	16.73	22.03	29.03	35.77	45.29	53.29	65.04	75.33	89.80	102.17
-3	11.63	16.73	21.81	28.84	35.53	44.77	52.75	64.51	74.61	88.57	101.12
-2	11.58	16.62	21.73	28.66	35.33	44.18	52.40	63.87	73.97	87.65	100.63
-1	11.59	16.56	21.68	28.48	35.14	43.53	51.92	63.10	73.24	86.95	99.87
1	11.17	16.05	21.22	27.92	34.59	42.87	51.22	62.62	72.39	85.95	98.79
2	11.12	16.02	21.14	28.02	34.66	43.30	51.25	62.72	72.71	86.24	99.01
3	11.14	16.07	21.16	27.99	34.63	43.49	51.31	62.77	72.73	86.47	98.63
4	11.14	16.04	21.18	27.92	34.52	43.59	51.30	62.67	72.66	86.73	98.57
5	11.16	15.96	21.23	27.85	34.48	43.49	50.92	62.59	72.56	86.65	98.75

X: Axial length along the channel defined from singularity

Table 9. Static pressure raw data for 9.58% Silicon dioxide nanofluid flow in channel with sudden area expansion (σ = 0.140)

X (in)	3.2 (g/s)	5.6 (g/s)	7.9 (g/s)	10.5 (g/s)	12.9 (g/s)	15.3 (g/s)	17.2 (g/s)	19.4 (g/s)	21.3 (g/s)	23.5 (g/s)	25.7 (g/s)
-5	12.10	17.20	22.75	29.84	37.01	44.21	53.58	62.88	74.86	87.79	103.37
-4	12.00	17.13	22.68	30.11	36.73	43.77	53.29	62.76	74.40	87.14	103.76
-3	12.03	17.12	22.69	30.11	36.28	43.72	53.19	62.49	74.13	85.90	103.43
-2	12.07	17.09	22.68	30.04	36.18	43.62	53.01	62.49	74.10	85.71	103.06
-1	12.08	17.16	22.68	29.81	36.03	43.48	52.79	62.21	74.10	85.61	103.09
1	11.66	16.72	22.26	29.34	35.59	42.98	52.31	61.69	73.59	84.79	102.65
2	11.66	16.62	22.23	29.56	35.72	43.11	52.55	61.98	73.60	85.08	102.57
3	11.61	16.63	22.21	29.58	35.77	43.16	52.63	61.90	73.55	84.81	102.79
4	11.56	16.63	22.16	29.52	36.13	43.11	52.61	62.00	73.66	86.59	102.90
5	11.64	16.66	22.16	29.20	36.30	43.41	52.73	61.93	74.85	87.34	102.19

X: Axial length along the channel defined from singularity

Table 10. Static pressure raw data for 9.58% Silicon dioxide nanofluid flow in channel with sudden area contraction (σ = 0.0625)

X (in)	3.2 (g/s)	5.6 (g/s)	7.9 (g/s)	10.5 (g/s)	12.9 (g/s)	15.3 (g/s)	17.2 (g/s)	19.4 (g/s)	21.3 (g/s)	23.5 (g/s)	25.7 (g/s)
-5	11.94	16.74	22.51	29.47	36.74	44.63	55.48	67.02	77.79	93.41	108.44
-4	11.70	16.79	22.43	29.85	37.22	45.20	56.46	67.13	77.89	93.63	108.86
-3	11.37	16.60	22.45	29.33	36.68	45.26	56.53	67.39	77.69	93.84	108.31
-2	11.20	16.45	22.51	29.72	37.11	45.35	56.57	67.28	77.61	94.21	108.67
-1	11.46	16.66	22.62	30.00	37.21	45.76	56.41	67.59	77.61	94.19	108.72
1	11.40	16.36	21.89	28.57	35.27	43.15	53.29	63.62	73.03	88.58	102.01
2	11.34	16.09	21.65	28.11	34.88	42.52	52.95	62.77	72.30	87.72	101.04
3	11.26	15.91	21.40	27.79	34.58	42.02	52.33	61.81	71.60	86.42	99.63
4	11.20	15.81	21.12	27.67	34.35	41.64	51.92	61.46	71.32	85.60	99.41
5	11.13	15.62	20.77	27.32	33.85	40.78	50.57	60.47	69.98	83.94	97.13

X: Axial length along the channel defined from singularity

Table 11. Static pressure raw data for 9.58% Silicon dioxide nanofluid flow in channel with sudden area contraction (σ = 0.140)

X (in)	3.2 (g/s)	5.6 (g/s)	7.9 (g/s)	10.5 (g/s)	12.9 (g/s)	15.3 (g/s)	17.2 (g/s)	19.4 (g/s)	21.3 (g/s)	23.5 (g/s)	25.7 (g/s)
-5	12.00	17.02	23.02	29.14	36.76	46.07	56.34	66.45	79.41	91.66	108.27
-4	12.01	17.08	22.97	29.23	36.86	45.80	55.98	66.55	78.93	92.00	108.98
-3	12.02	17.07	22.97	29.28	36.95	45.65	56.02	66.47	79.11	92.40	109.15
-2	12.03	17.09	22.93	29.33	37.16	45.62	55.92	66.38	79.74	92.95	108.54
-1	12.03	17.11	22.92	29.41	37.18	45.61	55.88	66.47	79.57	93.63	108.41
1	11.63	16.64	22.35	28.74	36.38	44.64	54.72	65.15	78.06	91.90	106.44
2	11.61	16.58	22.33	28.60	36.28	44.55	54.69	64.91	78.06	91.02	106.36
3	11.60	16.56	22.34	28.49	36.01	44.51	54.64	64.87	77.28	90.34	106.71
4	11.57	16.55	22.31	28.41	35.88	44.59	54.54	64.86	76.99	89.66	106.46
5	11.55	16.47	22.31	28.30	35.72	44.77	54.79	64.67	77.32	88.90	105.51

X: Axial length along the channel defined from singularity

APPENDIX C

Uncertainty in Results of loss coefficient for Water in channels with Sudden Area Change

Table 12. Results of uncertainty in loss coefficient values for water flow in channel with sudden area expansion ($\sigma = 0.0625$)

$\dot{m}$(g/s)	U_1(m/s)	Re	σ_{st}	Ke	$\pm\Delta$	$\%U_{ke}$
5	0.64	2257.65	0.04	0.66	0.05	8.10
7.5	0.95	3227.04	0.04	0.80	0.05	6.56
10	1.27	4306.90	0.04	0.87	0.05	5.96
12.5	1.58	5377.00	0.03	0.87	0.04	5.00
15	1.91	6960.00	0.03	0.86	0.04	4.52
17.5	2.22	8155.00	0.03	0.85	0.04	4.49
20	2.55	9331.63	0.03	0.84	0.04	4.81
22.5	2.86	10474.28	0.03	0.84	0.04	4.44
25	3.18	11050.61	0.03	0.85	0.04	4.50
27.5	3.50	12814.00	0.03	0.85	0.04	4.39
30	3.82	13260.73	0.03	0.83	0.04	4.36

$\pm\Delta$: Uncertainty in loss coefficient results based on 95% confidence level

Ke $\pm\Delta$: AccepTable range of values of loss coefficient

σ_{st} : Standard deviation

$\%U_{ke}$: Percentage of uncertainty in loss coefficients results

$$\pm\Delta = \frac{\sigma_{st}T}{\sqrt{n}}$$

Table 13. Results of uncertainty in loss coefficient values for water flow in channel with sudden area contraction ($\sigma = 0.0625$)

$\dot{m}$(g/s)	U_1(m/s)	Re	σ_{st}	Kc	$\pm\Delta$	%U_{kc}
7.5	0.95	3227.04	0.02	0.31	0.03	8.34
10	1.27	4306.90	0.02	0.28	0.02	8.48
12.5	1.58	5377.00	0.01	0.22	0.01	5.98
15	1.91	6960.00	0.01	0.18	0.01	6.04
17.5	2.22	8155.00	0.01	0.18	0.01	5.30
20	2.55	9331.63	0.01	0.16	0.01	5.43
22.5	2.86	10474.28	0.01	0.15	0.01	5.59
25	3.18	11050.61	0.01	0.15	0.01	5.82
27.5	3.50	12814.00	0.01	0.15	0.01	6.29
30	3.82	13260.73	0.00	0.12	0.01	5.84

$\pm\Delta$: Uncertainty in loss coefficient results based on 95% confidence level

Kc $\pm\Delta$: AccepTable range of values of loss coefficient

σ_{st} : Standard deviation

%U_{kc} : Percentage of uncertainty in loss coefficients results

$$\pm\Delta = \frac{\sigma_{st}T}{\sqrt{n}}$$

REFERENCES

Abdelall, F., Hahn, G., Ghiaasiaan, S., Abdel-Khalik, S., Jeter, S., Yoda, M. (2004). Pressure drop caused by abrupt flow area changes in small channels. *Experimental Thermal and Fluid Science*, *29*, pp.425–434.

Balakhrisna, T., Ghosh, S., & Das, P. (2010). Oil–water flows through sudden contraction and expansion in a horizontal pipe – Phase distribution and pressure drop. *International Journal of Multiphase Flow, 36*, pp.13-24.

Bear J. (1972), Dynamics of Fluids in Porous Media, Dover Publications, INC. New York.

Bengtson, H., & Stonecypher, L. (2010). Pipe Flow Calculations 2: Reynolds Number and Laminar & Turbulent Flow. Retrieved December 8, 2014, from http://www.brighthubengineering.com/hydraulics-civil-engineering/55053-pipe-flow-calculations-2-reynolds-number-and-laminar-and-turbulent-flow/

BP Systems, Mixing & Process Technology. Batch Mixers- High Shear Batch Mixers. Retrieved August 13, 2014, from http://bpsystems-eu.com/batch-mixers/

Casey, N., & Klepfer, N. (2013). Small Scale Geothermal. Retrieved December 8, 2014, from https://wiki.uiowa.edu/display/greenergy/Small Scale Geothermal

Chalfi, T. Y., & Ghiaasiaan, S. (2008). Pressure drop caused by flow area changes in capillaries under low flow conditions. *International Journal of Multiphase Flow*, *34*, pp.2-12.

Chandrasekar, M., S. Suresh and A. Chandra Bose (2010). Experimental studies on heat transfer and friction factor characteristics of Al2O3/water nanofluid in a circular pipe under laminar flow with wire coil inserts, *Experimental Thermal and Fluid Science*, 34(2), pp.122-130.

Chen, I. Y., Chu, M., Liaw, J., & Wang, C. (2008). Two-phase flow characteristics across sudden contraction in small rectangular channels. *Experimental Thermal and Fluid Science*, *32*, pp.1609–1619.

Cheng, L. (2009). Nanofluid Heat Transfer Technologies. *Bentham Science Publishers Ltd.*, pp.1-7.

Chisholm, D. (1983). Two-phase flow in pipelines and heat exchangers. London: G. Godwin in association with Institution of Chemical Engineers.

Choi, S. U. S. (1995). Enhancing thermal conductivity of fluids with nanoparticles. ASME FED, Vol. 231, pp. 99–105.

Duangthongs, W., & Wongwises, S. (2009). An experimental study on the heat transfer performance and pressure drop of TiO2-water nanofluids flowing under a turbulent flow regime. *International Journal of Thermal Sciences,* pp.*53*, 334–344.

Duangthongs, W., & Wongwises, S. (2008). Heat transfer enhancement and pressure drop characteristics of TiO2–water nanofluid in a double-channel counter flow heat exchanger. *International Journal of Heat and Mass Transfer, 52*, pp.2059–2067.

Elger D.F, Williams B.C, Crowe G.T, Robertson J.A, (2012). *Engineering Fluid Mechanics,* John Wiley& Sons Inc, Hoboken, NJ, USA, Chap. 10.

Emerson Process Management. Rosemount 3051S Series of Instrumentation Scalable pressure, flow, and level solutions. Retrieved August 19, 2014, from http://www2.emersonprocess.com/siteadmincenter/pm_rosemount_documents/00813-0100-4801.pdf

Escher, W., Brunschwiler, T., Shalkevich, N., Shalkevich, A., Burgi, T., Michel, B., & Poulikakos, D. (2011). On the Cooling of Electronics With Nanofluids. *JOURNAL OF HEAT TRANSFER, 133*, pp.45-62.

Geiger, G.E., (1964). Sudden Contraction Losses in Single and Two-phase Flow, PhD Thesis, University of Pittsburgh.

Gültekin, G. G., Karagoz, S., Manay, E., & Sahin, B. (2013). "Experimental investigation of heat transfer and pressure drop characteristics of al2o3–water nanofluid. *Experimental Thermal and Fluid Science*.

Guo, H., Wang, L., Yu, J., Ye, F., Ma, C., & Li, Z. (2009). Local resistance of fluid flow across sudden contraction in small channels. *Higher Education Press and Springer-Verlag, 2*, pp.149-154.

Haddad, Z., Abid, C., Oztop, H. F., & Mataoui, A. (2014). A review on how the researchers prepare their nanofluids. *International Journal of Thermal Sciences*, *76*, 168-189.

He, Y., Jin, Y., Chen, H., Ding, Y., Cang, D., & Lu, H. (2006). Heat transfer and flow behaviour of aqueous suspensions of TiO2 nanoparticles (nanofluids) flowing upward through a vertical pipe. *International Journal of Heat and Mass Transfer, 50*, pp.2272–2281.

Heo, K., Ko, G., Lee, K., Kim, D., Kim, C., Sohn, Y., & Choi, M. (2007). An experimental study on the pressure drop of nanofluids containing carbon nanotubes in a horizontal tube. *International Journal of Heat and Mass Transfer, 50*(23-24), pp.4749–4753.

Ijam, A., Saidur, R., & Ganesan, P. (2012). Cooling of minichannel heat sink using nanofluids.*International Journal of Heat and Mass Transfer, 39*, pp.1188–1194.

Kays. M.A. (1949). Loss coefficients for abrupt changes in flow cross section with low Reynolds number flow in single and multiple channel systems. *Transactions of the ASME*. 72. pp.1067–1074.

Kostic, M.M., (2013). Friction and Heat Transfer Characteristics of Silica and CNT Nanofluids in a Channel Flow. *The 8th International conference of Energy & Environment*. Recent Advances in Energy and Environmental Management. Rhodes Island, Greece.

Liquiflo Chemical Processing Pumps. Model 35F Standard Duty Gear Pump. Retrieved July 23, 2014, from http://www.liquiflo.com/v2/gears/3/35f.htm

Liu, M., Hu, M., Lin, J., & Wang, C. (2009). Performance Augmentation of a Water Chiller System Using Nanofluids. *115*(1), pp.581-581.

Manay, E., Sahin, B., Yilmaz, M., & Gelis, K. (2012). Experimental Studies on Heat Transfer and Friction Factor Characteristics of Al2O3/Water Nanofluid in a Circular Pipe Under Transition Flow With Wire Coil Inserts. *World Academy of Science, Engineering and Technology,* 67.

Mehrabian, M. Khoramabadi, (2007). Application of numerical methods to study the effect of variable fluid viscosity on the performance of plate heat exchangers. *International Journal of Numerical Methods for Heat & Fluid Flow*, Vol. 17 Iss: 1, pp.94 – 107

Mendler, O.J., (1963). Sudden Expansion Losses in Single and Two-phase Flow, PhD Thesis, University of Pittsburgh.

Nguyen C.T., G.Roy, Christian Gauthier, N.Galinis, (2007). Temperature and particle-size dependent viscosity data for water-based nanofluids – Hysteresis phenomenon, *Int. J. Heat and Fluid Flow*, 28, pp.1492–1506.

Northern Lights Solar Solutions. Solar Pool Heat Exchangers. Retrieved August 14, 2014, from http://www.solartubs.com/solar-pool-heat-exchanger.html

Omega. Quick Disconnect Thermocouples with Miniature Connectors. Retrieved August 18, 2014, from http://www.omega.com/ppt/pptsc_right.asp?ref=JMQSS&subsection=A04&book=Temperature

Omegadyne. PX409 Series Gage and Absolute Pressure Transmitters. Retrieved August 21, 2014, from http://www.omegadyne.com/ppt/prod.html?ref=PX409_Series

Park, B.C. and Y.I. Cho (1998). Hydrodynamic and heat transfer study of dispersed fluids with submicron metallic dioxide particles, *Journal of Experimental Heat transfer*, 11, pp.151-163.

Pinho, F., & Whitelaw, J. (1990). Flow of Non-Newtonian Fluids in a Pipe. *Journal of Non-Newtonian Fluid Mechanics, 34*(1990), pp.129-144.

Rudman, M., Graham, L., Blackburn, H., & Pullm, L. (2002). Non-Newtonian Turbulent and Transitional Pipe Flow.

Sahin, B., Gültekin, G., Manay, E., & Karagoz, S. (2013). Experimental investigation of heat transfer and pressure drop characteristics of Al2O3–water nanofluid. *Experimental Thermal and Fluid Science, 50*, pp.21-28.

Sajadi, A., & Hazemi, M. (2011). Investigation of turbulent convective heat transfer and pressure drop of TiO2/water nanofluid in circular tube. *International Communications in Heat and Mass Transfer, 38*, pp.1474–1478.

Schutt, H.C. (1929). Losses of Pressure Head due Sudden Enlargement of Flow Cross Section. Trans. ASME. 51, pp. 83-87.

Selvakumar, P., & Suresh, S. (2012). Convective performance of CuO/water nanofluid in an electronic heat sink. *Experimental Thermal and Fluid Science, 40*, pp.57-63.

Sonawane, S., Patankar, K., Fogla, A., Puranik, B., Bhandarkar, U., & Kumar, S. (2011). An experimental investigation of thermo-physical properties and heat transfer performance of Al2O3-Aviation Turbine Fuel nanofluids. *Applied Thermal Engineering, 31*, pp.2841-2849.

Tiwari, S. (2012). Evaluation of Thermophysical Properties, Friction factor, Heat Transfer of Alumina Nanofluid flow in Channels, Master thesis, University of North Dakota, Grand Forks, ND.

Williams, W., Buongiorno, J., Hu, L.W. (2008). Experimental Investigation of Turbulent Convective Heat Transfer and Pressure Loss of Alumina/Water and Zirconia/Water Nanoparticle Colloids (Nanofluids) in Horizontal Channels, *ASME Journal of Heat Transfer*, 130, pp. 1-7.

Xuan, Y., & Li, Q. (2003). Investigation on Convective Heat Transfer and Flow Features of Nanofluids. *Journal of Heat Transfer, 125*, pp.151-165.